Modelling wave damping by fluid mud

Derivation of a dispersion equation and an energy dissipation term and implementation into SWAN

Wouter Kranenburg

MSc. Thesis

February 2008

Graduation Committee:

Prof.dr.ir. G.S. Stelling
dr.ir. J.C. Winterwerp*
dr.sc. A. Metrikine
ir. J.M. Cornelisse
dr.ir. M. Zijlema
ir. G.J. de Boer*

(* 'daily supervisors')

Modelling wave damping by fluid mud

Derivation of a dispersion equation and an energy dissipation term and implementation into SWAN

Wouter Kranenburg

MSc. Thesis

February 2008

Preface

The following pages form my MSc. Thesis on the subject 'Modelling wave damping by fluid mud'. I worked on this project from March 2007 to January 2008, mainly at WL | Delft Hydraulics (presently Deltares).

Excuse me for the fact that I need so many pages to explain what I did. Probably it tells you more about me and my inclination to be too complete and to explain things that are clear already, than it tells you about the amount of work. Perhaps I could have reduced the number of words. But I am convinced that it would not be an improvement to economize on the number of chapters. We even miss one chapter: the calibration of the model on a practical case. What I like about this project is that – except for the calibration – the complete development is investigated from a simple mathematical model to an implementation that can be used in engineering environment. This development is clearly reflected in the structure of this report. I consider passing through all stages involved not only as instructive to myself, but also as a valuable contribution to the discussion in literature on this subject, because it underlines the importance of consistency between the various parts of the model. It is also for that reason that I am especially content with the derivation of the energy dissipation term (chapter 6). When my supervisors frowned their brows at my rather naïvely made remark on the influence of the pressure term on the energy dissipation, I realized that there was a challenging task for me in the derivation of an energy dissipation term that is consistent with the used dispersion equation.

At the end of this project, I would like to take the opportunity to thank the people that contributed to both my pleasure and my results during this project.

I would like to thank Han for his very accurate reading of both text and formula's. Also his purposive approach and ability to present plans and results positive and convincing are a great motivation. The offered possibility to do a part of my work in Brasil contributed for sure to my enthousiasm. Next, thanks to Gerben for his essential practical assistance in the 'daily work' of programming and post-processing, his ideas for finding a useful function for the starting value and his general role as sparring-partner. I also would like to thank the other members of my graduation committee. Although less closely associated to my project, they all made a positive contribution. Let me mention e.g. the introduction in Fortran by John Cornelisse the modifications in the SWAN infrastructure by Marcel Zijlema that enabled me to implement dispersion equation and energy dissipation term, the fundamental questions on wave mechanics and suggestions for methods by Andrei Metrikine and the financial support by professor Stelling for writing an article in the coming months.

Thanks also to Susana, for the supervision during my time in Brasil and the opportunity to join the fieldwork near Cassino. I am sorry I didn't finalize the calibration yet, but I am sure it will be done soon. Thanks to my friend Saulo and the other MSc. and PhD. students in Brasil, both Rio de Janeiro and Rio Grande. Saulo was not only the first student-colleague that didn't get tired of conversations on the subject, but was also a funny roommate and a great guide in both culturale and natural wilderness of Rio. Thanks to the student-colleagues at WL | Delft Hydraulics. I am convinced we together form the most pleasant department of

WL | Delft Hydraulics. I would be honoured if you would carry on the tradition of cookie-time I introduced.

Thanks to my family for their interest in my work and well being, for their morale and financial support and for their patient listening to my considerations in the processes of making choices. Thanks to my girlfriend Ditske, whose cheerfull character wipes out even my most peevish mood. Your enthousiasm, confidence and perseverance are a great inspiration to me. Finally, I would like to give thanks to the Lord, for his blessings and care, for the health and strength he gave me to do my work. I am called to do my work and live my life to honour him. Therefore I would like to do it good, in a positive mood, with sincere interest for the people around me and the world I am living in and gratefullness towards my Lord.

Wouter Kranenburg
February 2008

Abstract

At numerous locations in the world mud occurs in front of the coast close to river mouths. This mud can be transported to these place in fluid state or can become fluid under certain wave conditions. Fluid mud may have a strong damping effect on surface waves. This study presents modelling of wave damping by fluid mud.

After studying various two-layer models described in literature, one schematization is chosen to describe the water-mud-system (Figure 1). In this schematization, the upper layer represents the water and is non-hydrostatic and non-viscous. The lower layer represents the mud and is quasi-hydrostatic and viscous. Based on this schematization a complex dispersion equation is derived and compared with other dispersion equations from literature. A numerical procedure is formulated in Fortran to solve this implicit dispersion equation for the wave number. The function for the initial approximation in the iteration depends on the relative water depth and is assembled from the limit of the dispersion equation for shallow water with mud and the limit for intermediate and deep water without mud. When the wave number is known, information on the damping is given by the imaginary part, while the real part is associated with the wave length and the propagation velocity of energy.

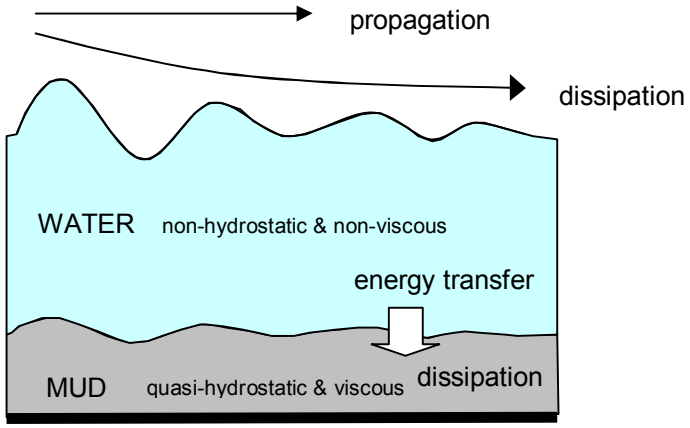

Figure 1 viscous two-layer model

To compute wave damping for situations in practice, the influence of mud is incorporated in the wave model SWAN. First, an energy dissipation term is derived that represents the mud-induced dissipation. The derivation is based on the used viscous two-layer model and consistent with the dispersion equation. This term is added as a sink term to the energy balance in SWAN. By making the mud-adjusted wave number available through the whole code, also influence of fluid mud on energy propagation is included in the model. The performance of the model for both energy dissipation and energy propagation is validated for some simple cases.

The final result of this study is a modified version of SWAN which allows to model the decrease of energy during the propagation of a wave field over fluid mud. The model is ready for use in engineering applications by specialists. Further improvement of the solving procedure to calculate the wave number and calibration of the model on a practical case are the main recommendations.

Samenvatting

Op vele plaatsen in de wereld is voor de kust modder te vinden. Meestal vinden we de modder in de buurt van mondingen van rivieren of estuaria. Deze modder kan hier terecht komen doordat ze als vloeibare modder naar deze plaatsen wordt getransporteerd. Het kan ook zo zijn dat eerder afgezette modder vloeibaar wordt onder invloed van golven. Hoe het ook zij, vloeibare modder kan een grote dempende werking hebben op oppervlaktegolven. In deze studie is onderzocht hoe de demping van golven door vloeibare modder kan worden gemodelleerd.

De basis van de modellering is een tweelagenmodel (Figure 2. De bovenste laag stelt het water voor. De druk in deze waterlaag is niet-hydrostatisch en er wordt verondersteld dat het water niet viskeus is. De onderste laag stelt de vloeibare modder voor. In deze laag is de drukverdeling hydrostatisch. Daarnaast is de vloeibare modder viskeus. Op basis van deze schematizatie is een dispersierelatie afgeleid. Door de aanwezigheid van demping, wordt deze dispersierelatie complex. Om deze dispersierelatie op te lossen voor het golfgetal, is een numerieke oplosroutine gebruikt. Daarbij is veel aandacht besteed aan een eerste schatting van het golfgetal. Deze schatting wordt gebruikt als startwaarde voor de iteratie. Wanneer het complexe golfgetal is gevonden, geeft het imaginare deel informatie over de demping. Het reële deel geeft informatie over de golflengte en over de voortplantingssnelheid van de golfenergie.

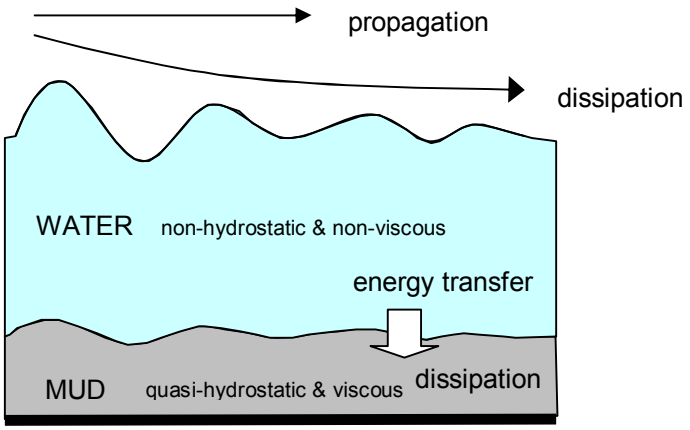

Figure 2 Tweelagenmodel

Om de demping van golven door vloeibare modder te berekenen voor praktische situaties (Figure 3), zijn aanpassingen gedaan aan het bestaande golf model SWAN. Allereerst is ingebouwd dat het golfgetal berekend wordt via de eerder afgeleide dispersierelatie. Vervolgens is een uitdrukking afgeleid die de energiedissipatie door vloeibare modder beschrijft en die consistent is met de dispersierelatie. Deze term is toegevoegd aan de energiebalans in SWAN. In de volgende stap is het programma zo aangepast, dat het door de modder beïnvloede golfgetal ook gebruikt wordt voor de berekening van andere processen, zoals golfvoortplanting (propagatie). Middels een aantal eenvoudige testen en vergelijking

met analytische berekeningen is het model zowel voor dissipatie als voor propagatie gevalideerd.

Het uiteindelijke resultaat van deze studie is een aangepaste versie van SWAN, waarmee het mogelijk is de demping van golven door vloeibare modder te modelleren. Het model is klaar voor gebruik.

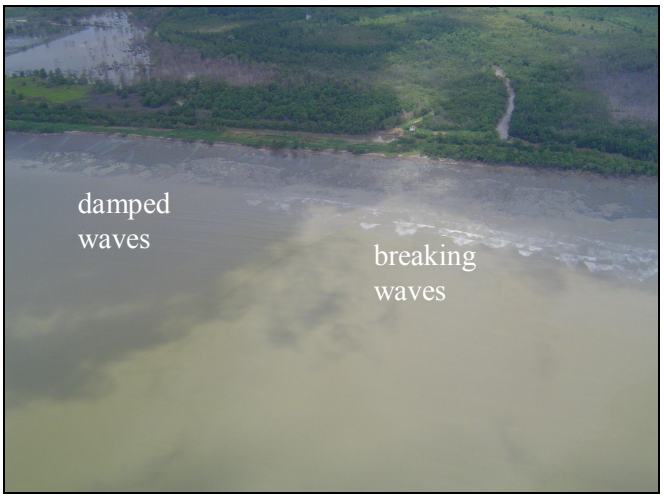

Figure 3 Luchtfoto van breking en demping van golven, Demerara Coast, Guyana

Contents

1 Introduction

1.1 General background

At various places in the world mud has been deposited in front of the coast close to river mouths or estuaries. These mud deposits can be liquefied under incoming waves when the waves cause stresses in the mud above a certain limit (De Wit, 1995). Liquefied mud may damp waves very effectively (Gade, 1958). At the same time, wave-induced currents can cause transport of the liquefied mud, sometimes even resulting in mud deposits on the shore.

The liquefaction of muddy bottoms, the mud-induced wave damping and the transport of mud are phenomena of practical importance, because they can have implications for e.g. constructing, dredging, ecology and coastal protection. These phenomena can influence wave loads on structures, wave refraction, soil motions, also around structures and pipelines, and the accessibility of the shore.

The practical importance is reason to study these phenomena, among others with the use of process based models. This project focuses on the stand-alone modelling of the damping of waves by fluid mud. This is schematically presented in the figure below.

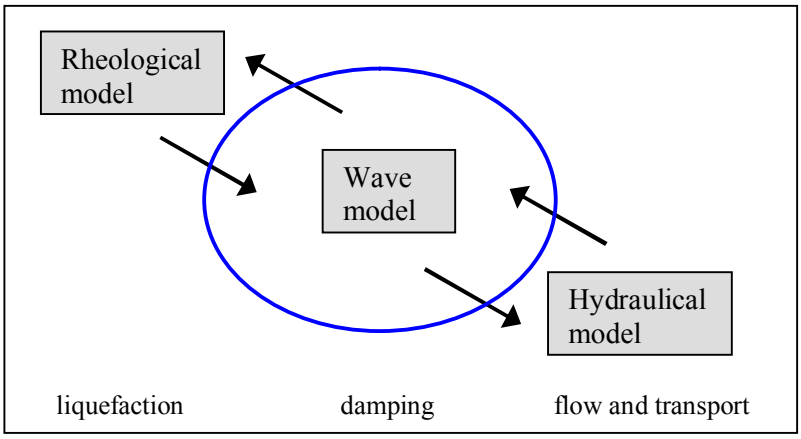

Figure 4 Schematic presentation of the context of the project with indication of the current focus

1.2 Problem analysis

In literature often a two layer approach is used to model the surface-bottom interaction in the case of wave propagation over muddy bottoms. Various schematizations, each focusing on different properties of the mud, have been examined to investigate the deformation of the bottom. It is argued in literature (o.a. Dalrymple 1978) that after liquefaction of the mud, viscosity is the most important property to deal with.

The schematization of Gade (1958) is a schematization that assumes both layers to be hydrostatic and takes into account only the viscosity of the lower layer. This schematization

has been used earlier to assess the dissipation of energy by liquefied mud. A procedure based on this schematization has been build in the SWAN spectral wave model and calculations have been performed for wave attenuation in the Guyana coastal system (Winterwerp *et al.*, 2007). Although the model shows quite well that energy is dissipated by the mud layer, an extension of the model is proposed to give a better account of the dissipation of non-shallow water waves.

Schematizations that take also into account non-shallow water waves lead to quite complex dispersion relations. The first problem is that the dispersion relations in literature are not free of typing or derivation errors. Another problem is that the more complex dispersion relations do not give an explicit or analytical solution for the wave number.

In practical cases, waves with various frequencies and wave heights approach from various directions over a bed with changing bathymetry. Also the thickness of the mud layers can change in space. To make it possible to model the wave propagation over mud in practical cases, the non-shallow water schematization(s) has to be applied on various frequencies and directions in a practical applicable spectral wave model. Problems in this part of the project are the translation of the dispersion relation into a dissipation term that can be applied in the wave model, the parallel application on different frequencies in a spectrum and the change in the propagation velocity of energy.

1.3 Framework

ONR, the Office of Naval Research (USA), is the initiator and financier of a series of projects on the interaction between waves and mud. Some of the projects focus on field measurements or real-time monitoring, other on further research on the dissipation mechanisms. Numerical modeling of the processes presently known is also a greater task in a part of the projects. The locations of the field experiments are the coast of Louisiana, USA, and Cassino Beach in Southern Brazil. The projects are executed by universities and institutes mainly in the United States and Brazil. WL|Delft Hydraulics is also involved as a participant in the Cassino Beach project. The contribution of WL|Delft Hydraulics mainly exists of numerical modeling with the use of the WL-product DELFT3D and the open source spectral wave energy model SWAN.

1.4 Project objectives

The main objective of this MSc. Thesis project is the development and testing of an adaptation to SWAN with which it is possible to model the decrease of wave energy during the propagation of a wave field over fluid mud.

This implementation has to be:

- applicable for shallow and non-shallow water
- consistent

- efficient
- reliable
- validated

Several sub objectives can be distinguished. These sub objectives form steps in the project.

1. Study of the short-wave energy dissipation mechanism in two layer systems and comparison of the dispersion relations for the various schematizations in literature
2. Search for an efficient and reliable solving routine to determine the wave number from the dispersion relation
3. Determination of a mud-induced energy dissipation term that can be used in SWAN, implementation of this term and validation of the model for a simple 1D case
4. Extension of the model with influence of mud on the propagation velocity of energy, validation of the implementation for simple propagation tests (1D/2D)
5. Calibration of the model by application on a practical case: Cassino Beach, Brazil

1.5 Reading guide

In this chapter the objective of this MSc. Thesis project was shortly described after a short analysis of the problem of wave damping by fluid mud.

The chapters 2, 3 and 4 concern with dispersion equations and wave numbers. Chapter 2 discusses various models that describe the response of a non-rigid bed to progressive waves, mainly focussing on viscous bed models. Chapter 3 describes the derivation of the 'DELFT' dispersion equation. In chapter 4 the dispersion equation is solved for the complex wave number. The results of the calculations are compared to results for other dispersion equations and results obtained with a different method.

The chapters 5, 6, 7 and 8 mainly study the influence of mud on waves in terms of wave energy. Chapter 5 gives a brief introduction on wave models, focussing on SWAN, and studies recent implementations of viscous bed models in wave models described in literature. Chapter 6 gives the derivation of an energy dissipation term consistent with the 'DELFT' dispersion equation. Chapter 7 describes the implementation of dispersion equation and energy dissipation term into SWAN and shows the results of a few simple tests. Chapter 8 discusses the inclusion in the SWAN-mud model of the influence of fluid mud on energy propagation. Also this extended model is tested for some discriminating cases.

Conclusions and recommandations of this project are discussed in chapter 9. The content of this report is schematically presented in Figure 5.

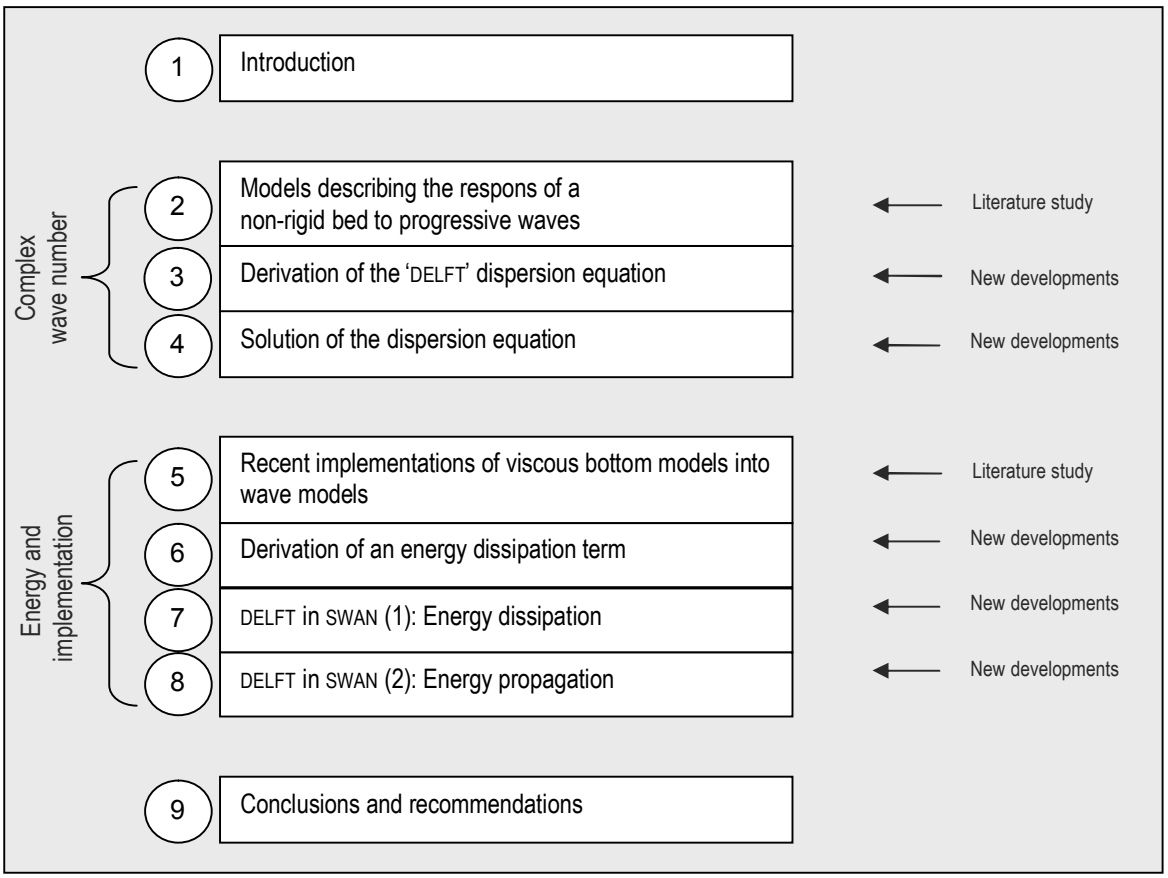

Figure 5 Schematic presentation of the content of this report

2 Models describing the response of a non-rigid bed to progressive waves

2.1 Introduction

Various models exist to describe the response of a non-rigid bed to progressive waves. This chapter discusses the models described in literature. A classification of various types of models is given in section 2.2. Viscous models to describe wave damping by fluid mud are extensively studied in section 2.4. Because the investigated viscous models are all two layer models, a short introduction to wave propagation in stratified flows is given in section 2.3. This chapter is concluded with a discussion (section 2.5). This discussion indicates which schematizations can be used in the adaptation to SWAN and what problems have to be accounted for while comparing the various schematizations.

2.2 Classification of various types of models

The various models that describe the response of a non-rigid bed to progressive waves use various rheological models and constitutive equations to describe the mechanical properties of the non-rigid bed. De Wit (1995) gives an overview of the models presented in literature and divides the models in five groups based on rheology.

The first group of models consideres waves over an **ideal elastic bed**. The influence of pore water is incorporated in the **poro-elastic models**. These two groups of models can be used to calculate the maximum wave pressure induced shear stress in the bed. These models are thoroughly studied by De Wit, because the results of these models might be used to estimate the onset of liquefaction when the yield stress of the mud is known. The application of the first group of models is limited to non-fluid, highly consolidated cohesive beds. The second group of models can also be applied to relatively thin layers of unconsolidated mud. These models cannot calculate wave damping, because dissipation is not incorporated.

When the bed consists of a mud layer that is fluid, wave damping occurs. Fluid mud in general has viscous, viscoelastic or viscoplastic properties. Based on these characteristics, De Wit distinguishes **viscous models** (group three), **viscoplastic models** (group four) and **viscoelastic models** (group five). De Wit states that the viscoplastic description is not suitable to model the response of a mud bed to waves, because '*in the field the shearing of mud due to wave action is oscillatory and the rheological response to oscillatory shearing shows that the mud then behaves more like an viscoelastic material.*' (p.62). The viscoelastic models probably represent the rheological properties of soft mud in the best way, but application of these models is rather complex. De Wit gives a number of reasons, most of which are connected to the determination of the viscoelastic properties and the fact that these parameters depend nonlinearly on depth, oscillatory strain amplitude and consolidation time. In the viscous models the fluid mud is considered as a Newtonian fluid. Although these models only partly represent the rheological properties of the mud, these

models can be used to estimate the wave damping and the wave-induced velocities in a fluid-mud layer.

2.3 Introduction to wave propagation in stratified fluids

2.3.1 External and internal waves

The viscous models studied in section 2.4 are all two-layer models, describing the system of water and fluid mud as two layers of fluid with a clear interface and different density and viscosity. As an introduction to the study of these models a few remarks are made on the propagation of waves in stratified, non-viscous fluids, as presented for long waves in C.Kranenburg (1998).

Assuming no viscosity, small density differences between the layers, and long, linear surface waves, two types of waves can be distinguished, namely **external** (or surface) long waves and **internal** long waves**.**

For the external wave, both layers behave in fact as one layer. The propagation velocity of the external wave is close to the propagation velocity in a one layer system. The ratio between the amplitude on the interface and the amplitude on the surface is the same as the ratio between the thickness of the lower layer and the total depth. For long external waves, the velocity of the current induced by the disturbance is the same in both layers.

Internal waves mainly disturb the interface. The surface is much less affected. The propagation velocity of internal waves is much smaller than the propagation speed of the external waves. For systems of salt and fresh water, the amplitude of the surface is an order smaller than the amplitude of the interface. The velocities in the two layers are opposite, in such a way that the total discharge is zero.

C.Kranenburg illustrates the theory with some simple sketches (Figure 6).

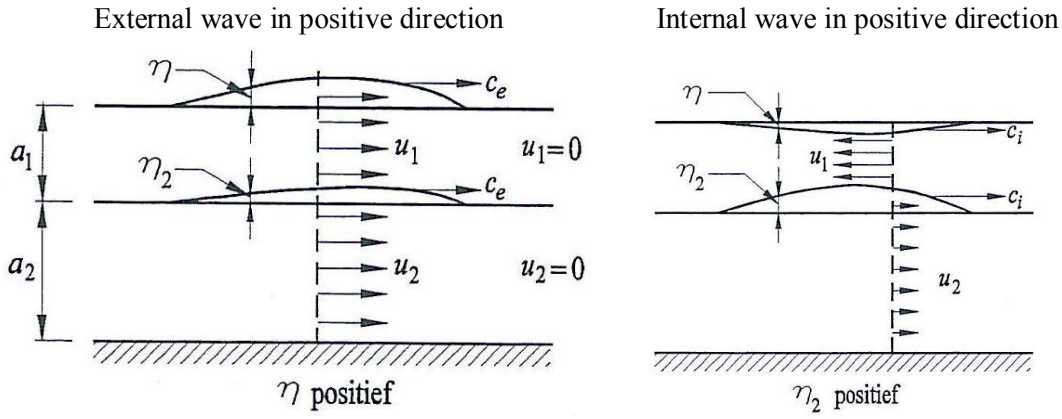

Figure 6 Schematic presentation of two-layer system with external (left) and internal long wave, taken from C.Kranenburg (1998). The positive direction is defined to the right.

where we define:

c_e =	propagation speed external wave	u_1 =	velocity in upper layer
c_i =	propagation speed internal wave	u_2 =	velocity in lower layer
η =	elevation of the surface	a_1 =	thickness of upper layer
η_2 =	elevation of the interface	a_2 =	thickness of lower layer

Considering an *x*-*z*-plane, both type of waves can travel in positive (to the right) and negative *x*-direction. So four waves can be distinguished. The propagation velocities can be found by writing the continuity equation and momentum equation of the two layers in a homogeneos matrix notation and determining the four eigenvalues of this matrix. The four eigenvalues for this case are all included in the expression:

$$c = \pm\left(\frac{ga \pm \sqrt{(ga)^2 - 4g^2 a_1 a_2 \varepsilon}}{2}\right)^{1/2} \tag{1}$$

where $\varepsilon = \frac{\rho_2 - \rho_1}{\rho_2} \ll 1$ and $a = a_1 + a_2$

To facilitate discussion, names are assigned to the four waves in the table below.

type of wave	**traveling direction**	**Signs of roots**	**Name**
external wave	positive direction	+ & +	EWpos
external wave	negative direction	- & +	EWneg
internal wave	positive direction	+ & -	IWpos
internal wave	negative direction	- & -	IWneg

Table 1 Overview of the four waves with type, traveling direction, signs of the roots and a name attributed to each wave. This table is given here to facilitate interpretation in the remainder of this study.

Following C.Kranenburg's example, the characteristics of the waves are collected in Table 2.

Type of wave	Waves in positive direction	Waves in negative direction
External	$c_{e+} = \frac{\omega}{k_{e+}} \approx \sqrt{ga}$	$c_{e-} = \frac{\omega}{k_{e-}} \approx -\sqrt{ga}$
	$\eta_{2e+} = \frac{a_2}{a}\eta_{e+}$	$\eta_{2e-} = \frac{a_2}{a}\eta_{e-}$
	$u_{1e+} = \frac{c_e}{a}\eta_{e+}$	$u_{1e-} = \frac{c_{e-}}{a}\eta_{e-}$
	$u_{2e+} = \frac{c_e}{a}\eta_{e+}$	$u_{2e-} = \frac{c_{e-}}{a}\eta_{e-}$
Internal	$c_{i+} = \frac{\omega}{k_{i+}} \approx \sqrt{\varepsilon g \frac{a_1 a_2}{a}}$	$c_{i-} = \frac{\omega}{k_{i-}} \approx -\sqrt{\varepsilon g \frac{a_1 a_2}{a}}$
	$\eta_{i+} = -\varepsilon \frac{a_2}{a}\eta_{2i+}$	$\eta_{i-} = -\varepsilon \frac{a_2}{a}\eta_{2i-}$
	$u_{1e+} = -\frac{c_{i+}}{a_1}\eta_{2i+}$	$u_{1e-} = -\frac{c_{i-}}{a_1}\eta_{2i-}$
	$u_{2i+} = \frac{c_{i+}}{a_2}\eta_{2i+}$	$u_{2i-} = \frac{c_{i-}}{a_2}\eta_{2i-}$

Table 2 Overview of the characteristics (propagation velocity, surface and interface elevation en layer velocity) of external and internal waves in positive and negative directions

where η_i and η_e are the elevation of the surface as a consequence of the internal respectively the external wave.

2.3.2 Relevant waves for this study

Although wave damping by viscous dissipation was not included, the explanation of the theory for long waves in stratified fluids in section 2.3.1 shows that in a two-layer model four waves are playing a role. Every disturbance can be seen as a linear combination of these four waves. The aim of this study is to determine the influence of a mud layer on the surface elevation. In the models in literature this is studied in a half-infinite space extending in the positive direction. Therefore only waves propagation in positive direction have to be taken into account. The influence of the internal wave to the surface elevation is small. So also damping of this wave will hardly affect the surface elevation. Therefore it can be concluded that the relevant wave for this study on wave damping is the **external wave traveling in positive direction** (EWpos). This is merely the ordinary surface wave, the effects of which extend down to the interface and cause a smaller disturbance in the lower layer (Gade, 1958).

2.4 Viscous two-layer models

2.4.1 Introduction

This section discusses non-rigid bottom models of the category of viscous models. In these models the system is schematized as a two layer system, the upper layer being a non or low viscous water layer and the lower layer a layer consisting of fluid mud. This lower layer is viscous and has a high density. The general schematization for viscous models is shown in the picture below.

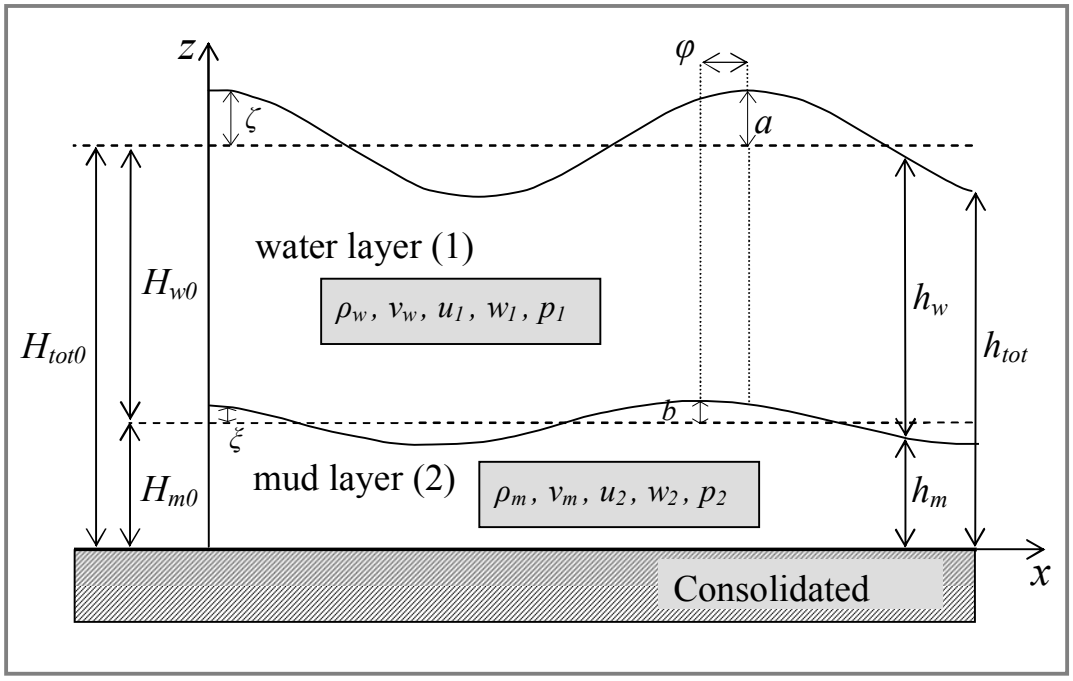

Figure 7 Schematic presentation of two-layer fluid mud system, with definitions

Symbol	*f (par.)*	Description	Units	Alternative name
H_{w0}	constant	Equilibrium height of water layer	m	
H_{m0}	constant	Equilibrium height of mud layer	m	D, D_{m0}
H_{tot0}	constant	Equilibrium height of total system	m	
h_w	*(x, t)*	Height of water layer	m	h_1
h_m	*(x, t)*	Height of mud layer	m	h_2 , d_m
h_{tot}	*(x, t)*	Height of total system	m	
a	constant	Amplitude of water surface displacement	m	
ζ	*(x, t)*	Displacement of water surface (ref. = eq.)	m	
b	constant	Amplitude of interface displacement	m	
φ	constant	Phase difference between surface and interface	rad	
ξ_0	constant	(complex) amplitude of interface displacement	m, rad	
ξ	*(x, t)*	Displacement of interface (ref. = eq.)	m	
ρ_w	constant	Density of water	kg / m^3	ρ_1
ρ_m	constant	Density of mud	kg / m^3	ρ_2
ν_w	constant	Kinematic viscosity of water	m^2 / s	ν_1
ν_m	constant	Kinematic viscosity of mud	m^2 / s	ν_2

u	(x, z, t)	Horizontal orbital velocity in x-direction	m / s	
w	(x, z, t)	Vertical orbital velocity in z-direction	m / s	
p	(x, z, t)	Pressure	N / m^2	
ω		Wave (angular) frequency (2π / T)	rad / s	σ
k	(all par.)	Wave number	rad / m	

Table 3 Definition of parameters in the two-layer models

Assumptions

Gade (1958) was the first who studied the modification of waves by fluid mud with a two layer approach. He gives a thorough overview of the assumptions in his model. Some of these assumptions are used in all the models discussed in this section:

1) viscosity is assumed to be constant over a layer
2) density is assumed to be constant over a layer
3) the fluid in both layers is assumed to be incompressible
4) the fluid mud is assumed to be a Newtonian fluid
5) the interface is assumed to be stable, no interfacial mixing is present
6) the lower layer is assumed to rest on a rigid horizontal stratum at which no motion exists (we assume this to be a consolidated bed that is not liquefied by the waves)
7) the fluid layers are considered to be of infinite horizontal extent
8) the wave is of sinusoidal form
9) only plane waves are considered
10) the wave amplitude is considered small compared with depth
11) the disturbance of the upper fluid is not directly associated with any driving or dissipative shearing forces. (The wave is a free wave which gives us the possibility to determine a dispersion relation.)
12) variations of surface pressure are neglected
13) motions of both fluids are free of divergence
14) it is assumed that the mean current is zero
15) effects of earth rotation are neglected

Equations

If we ignore the possible effects of advection, turbulence and earth rotation and assume a small disturbance, the fluid system can be described with the continuity equation and the linearized momentum equations for each layer i (where i can be 1 or 2):

$$\frac{\partial u_i}{\partial x} + \frac{\partial w_i}{\partial z} = 0 \tag{2}$$

$$\frac{\partial u_i}{\partial t} + \frac{1}{\rho_i}\frac{\partial p_i}{\partial x} - \nu_{x,i}\frac{\partial^2 u_i}{\partial x^2} - \nu_{z,i}\frac{\partial^2 u_i}{\partial z^2} = 0 \tag{3}$$

$$\frac{\partial w_i}{\partial t}+\frac{1}{\rho_i}\frac{\partial p_i}{\partial z}-\nu_{x,i}\frac{\partial^2 w_i}{\partial x^2}-\nu_{z,i}\frac{\partial^2 w_i}{\partial z^2}=-g \tag{4}$$

In these equations, p is the total pressure. This pressure contains in fact three terms. One term is directly connected to the orbital motion. The second term is the hydrostatic part, determined by the distance to the equilibrium surface or interface. The third term is the ambient pressure, consisting of the pressure at the surface or interface.

$$p_1 = p_1^{orb} + \rho_1 g(H_{tot0} - z) + 0 \tag{5}$$

$$p_2 = p_2^{orb} + \rho_2 g(H_{m0} - z) + \rho_1 g H_{w0} \tag{6}$$

The displacement of the free surface and the interface with reference to the equilibrium levels are described by:

$$\zeta(x,t) = a e^{i(kx-\omega t)} \tag{7}$$

$$\xi(x,t) = \xi_0 e^{i(kx-\omega t)} = b e^{i\varphi} e^{i(kx-\omega t)} \tag{8}$$

where k is the complex wave number with $k = k_r + ik_i$.

The amplitude of the interface displacement ξ_0 is complex to account for a phase shift between surface and interface displacement. This complex amplitude is a priori unknown. Note that with this notation for the phase of waves (kx-ωt), used in all viscous models treated in this section, the phase angle appears to become negative with growing t. Therefore a negative value for the phase shift φ implies an interface elevation that is ahead of the surface elevation.

Boundary conditions

To complete the description of the system, boundary conditions are required. The conditions used in the various models are all simplifications or subsets of the list below.

At $z = 0$, the location of the fixed bed, slip and penetration are not allowed:

$$u_2(x,0,t) = 0 \tag{9}$$

$$w_2(x,0,t) = 0 \tag{10}$$

At $z = h_m$, the location of the interface, velocities and stresses have to be continuous over the interface (kinematic and dynamic boundary conditions respectively). Additional information about the vertical velocity can be derived from the fact that particles on the interface have to follow the interface.

$$u_2(x,h_m,t) = u_1(x,h_m,t) \quad \text{(only used in complete continuous description)} \tag{11}$$

$$w_2(x,h_m,t) = w_1(x,h_m,t) \tag{12}$$

$$w_2(x,h_m,t) = \frac{D\xi(x,t)}{Dt} \tag{13}$$

$$\sigma_{zz2}(x,h_m,t) = \sigma_{zz1}(x,h_m,t) \tag{14}$$

$$\tau_{xz2}(x,h_m,t) = \tau_{xz1}(x,h_m,t) \tag{15}$$

At $z = h_{\text{tot}}$, the location of the free surface, particles have to follow the surface as well. Dynamic boundary conditions require the imposition of zero normal and tangential stresses.

$$w_1(x,h_{tot},t) = \frac{D\zeta(x,t)}{Dt} \tag{16}$$

$$\sigma_{zz1}(x,h_{tot},t) = 0 \tag{17}$$

$$\tau_{xz1}(x,h_{tot},t) = 0 \tag{18}$$

Simplifications of the equations above in the various models are introduced through extra assumptions in the various schematizations or through considering the problem as linear.

2.4.2 Gade

Gade (1958) was the first who used a viscous model to study the effects of a non rigid, impermeable bottom on plane surface waves. In his mathematical model, the upper layer is inviscid. For both layers, a shallow water approximation was used. Gade assumes the pressure to be hydrostatic, neglects the vertical accelerations in both layers and assumes the horizontal velocity in the upper layer to be independent of depth.

These assumptions lead to simplification of the differential equations and the boundary conditions. By substitution of an assumed harmonic solution for each variable that is separable in time and x-direction, a dispersion relation can be derived. This derivation is described in detail in his article.

The dispersion relation for Gade's schematization is:

$$k = \pm\omega\left\{\frac{\left(1+\Gamma\frac{H_{m0}}{H_{w0}}\right)\pm\sqrt{\left(1+\Gamma\frac{H_{m0}}{H_{w0}}\right)^2-4\gamma\Gamma\frac{H_{m0}}{H_{w0}}}}{2\gamma g\Gamma H_{m0}}\right\}^{1/2} \tag{19}$$

where

$$\Gamma = 1-\frac{\tanh\left(mH_{m0}\right)}{mH_{m0}} \quad , \qquad m = (1-i)\sqrt{\frac{\omega}{2\nu}} \quad \& \qquad \gamma = \frac{\rho_2-\rho_1}{\rho_2} \tag{20}$$

Gade's dispersion relation gives four solutions. As explained in section 2.3.2, the relevant solution is the solution for the external wave traveling in positive direction (EWpos). This is the solution with a plus sign for the first root and a minus sign for the second root. (The smallest positive value of k gives the highest propagation speed, which is the external wave.) Gade's dispersion relation gives an explicit expression for the wave number k, which can be calculated analytically.

Gade presented his results in graphs of the normalized real and imaginary wave number as function of the normalized mud layer thickness. The wave number is normalized with the shallow water wave number for one water layer only. The mud layer thickness is normalized with the wave boundary layer thickness in the mud layer. The dimensionless parameters are:

$$\mathrm{Re}\left(\frac{k^2}{\omega^2}H_{w0}g\right),\ \ \mathrm{Im}\left(\frac{k^2}{\omega^2}H_{w0}g\right) \tag{21}$$

$$H_{m0}\left(\sqrt{\frac{\omega}{2\nu}}\right) \tag{22}$$

A consequence of this normalization is that the normalized real wave number will approach one when the mud layer thickness approaches zero. The imaginary wave number will approach to zero in this situation, because without a mud layer, there is no damping. Gade's model is based on shallow water approximations. Therefore Gade limits the applicability of his model to cases where $H' / L \leq 1/20$, with H' a certain 'effective depth'. For the fixed value of viscosity, densities, period and water layer thickness this results in an upper limit for the normalized mud layer thickness beyond which the solution is not valid.

$$H_{m0}\left(\sqrt{\frac{\omega}{2\nu}}\right) \leq 1.6815 \tag{23}$$

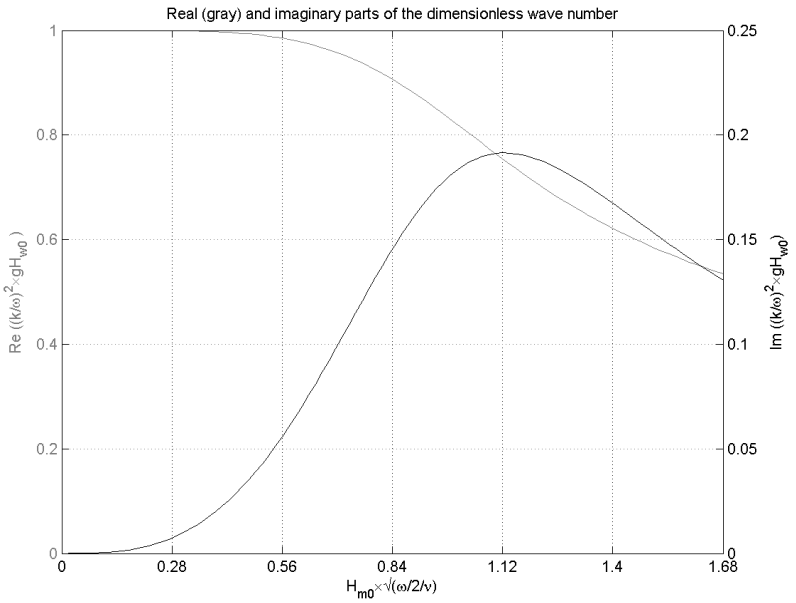

Figure 8 Real and imaginary parts of the dimensionless wave number versus the dimensionless mud layer thickness as shown in Gade (1958), figure 2.

Gade found that the wave height decays exponentially with travelled distance as long as the imaginary wave number k_i is constant. According to Gade, the rate of decay has a maximum value when the normalized mud layer thickness has a value of 1.2 [*sic*].

2.4.3 De Wit

De Wit (1995) modified Gade's model for the situation of a non-hydrostatic inviscid water layer over a viscous mud layer that is thin compared to the wave length. For the upper layer, the vertical acceleration was taken into account in the vertical momentum equation. The lower layer was still assumed to be quasi-hydrostatic: no vertical acceleration is taken into account in the lower layer vertical momentum equation. The vertical velocity can than be computed with the continuity equation.

Again, the relevant model assumptions lead to specific forms of the differential equations and the boundary conditions and again, the variables are substituted by assumed solutions that are separable and periodic in time and x-direction. First the amplitudes of the variables as function of the vertical position z are determined via the differential equations. Subsequently the expressions for the variables are substituted in the boundary conditions. This set of equations can be written in a homogeneous matrix equation. In order to have non-trivial solutions, the coefficient matrix should be singular. The non-trivial solution is found by equating the coefficient determinant of the matrix to zero. This gives an equation in which the wave number k is the only unknown variable, i.e. the dispersion relation. De Wit gives:

$$\left[-1+\frac{\rho_2-\rho_1}{\rho_2}\frac{gk}{\omega^2}\left(kH_{m0}-\frac{k}{m}\tanh\left(mH_{m0}\right)\right)\right]\left[\frac{gk}{\omega^2}\tanh\left(kH_{w0}\right)-1\right] \qquad (24)$$
$$-\frac{\rho_1}{\rho_2}\left[kH_{m0}-\frac{k}{m}\tanh\left(mH_{m0}\right)\right]\left[\frac{gk}{\omega^2}-\tanh\left(kH_{w0}\right)\right]=0$$

De Wit explains his method carefully, but typing errors occur in the formulation of the amplitudes of the variables and the substitution into the boundary conditions. A dispersion equation is presented, but the details of the derivation are not given. In an attempt to reproduce his dispersion equation starting from his schematization, a new dispersion equation has been derived (the 'DELFT' dispersion equation, further disussed in chapter 3). Reproduction of De Wit's dispersion equation was only possible by making some additional simplifications (discussed in chapter 3 and appendix B).

The dispersion equation which is found using the schematization of De Wit is an implicit expression for the wave number k. In contrast to Gade, an iteration method is needed to find the value of k for which the determinant is zero.

2.4.4 Gade+

Another extension of Gade's model was presented by Cornelisse and Verbeek (1994). In this extension both layers can be non-hydrostatic. Therefore the vertical accelerations are taken into account in the vertical momentum equation of both layers. Only the lower layer is viscous with the same viscosity in x- and z-direction.

The dispersion equation resulting from this schematization is given by Cornelisse as:

$$g\gamma + \frac{\omega^2\left(\omega^2\tanh(kh_w) - gk\right)}{k\left(\omega^2 - gk\tanh(kh_w)\right)} - \nu_m^2\left(k^2+\lambda^2\right)\frac{2k\lambda + \left(k^2+\lambda^2\right)\left(S_{kh_m}S_{\lambda h_m} - \frac{\lambda}{k}C_{kh_m}C_{\lambda h_m}\right)}{\lambda S_{kh_m}C_{\lambda h_m} - kC_{kh_m}S_{\lambda h_m}}$$
$$+ 2\nu_m^2 k\lambda\frac{2k^2\left(C_{kh_m}C_{\lambda h_m} - \frac{\lambda}{k}S_{kh_m}S_{\lambda h_m}\right) - \left(k^2+\lambda^2\right)}{\lambda S_{kh_m}C_{\lambda h_m} - kC_{kh_m}S_{\lambda h_m}} = 0 \qquad (25)$$

where

$$S_x = \sinh(x)\ , \qquad C_x = \cosh(x) \qquad \& \qquad \lambda^2 = k^2 - i\frac{\omega}{\nu_m} \qquad (26)$$

This dispersion equation yields also an implicit expression for the wave number *k*. So also in this case, an iteration method is needed to find a solution. The derivation of this method is given in detail in Cornelisse *et al.* (1994), together with derivations of Gade and Dalrymple (1a).

2.4.5 Dalrymple and Liu 'complete models'

In Dalrymple and Liu (1978) three models are developed (called here 1a, 1b and 2). Model 1a and 1b are the subject of this section. In the article, these models are called the 'complete models'.

'These 'complete models' are developed to be valid for any depth upper layer and both deep and shallow lower fluid layers, thus extending Gade's results to deeper water. These models also include the viscous effects in the upper layer for completeness, although the damping effects there are quite small when compared to the lower, more viscous layer' (Dalrymple and Liu, 1978, p.1121).

In Dalrymple and Liu (1978) the equations of motion are almost the same as in the introduction section. Differences are that Dalrymple and Liu assume the viscosity to be the same in *x*- and *z*-direction and that they directly cancel out the gravitational acceleration against the hydrostatic part of the pressure in the vertical momentum equations.

Dalrymple and Liu introduces a simplification in **model 1a**, which implies a constraint for the validity of the results, related to the parameter λ, where

$$\lambda^2 = k^2 - i\frac{\omega}{\nu_m} \qquad (27)$$

They state that *'for most problems ν_i is quite small with respect to k by several orders of magnitude. Consequently, the λ_i are quite large and in fact represent the viscosity-dominated flow in the vicinity of boundaries. Away from the boundaries, i.e. outside any boundary layers, the viscous terms are negligible.*' (ibid. p.1122) For this reason they assume a solution for the amplitudes *W(z)* with viscous terms near the boundaries and without viscous terms away from the boundaries. This assumption restricts the validity of the model to cases where the lower layer is thick compared to the viscous boundary layer δ_{BL}:

$$H_{m0} \gg O(\delta_{BL}), \quad \text{with } \delta_{BL} = \sqrt{\frac{2\nu_m}{\omega}} \tag{28}$$

Model 1b, described in appendix B of Dalrymple and Liu (1978), focusses on the case where the lower layer is thin, of the same order of magnitude as the boundary layers within the region, i.e. where

$$H_{m0} = O(\delta_{BL}) \qquad \text{with } \delta_{BL} = \sqrt{\frac{2\nu_m}{\omega}} \tag{29}$$

This model differs from model 1a in the assumed solution for the amplitude $W(z)$. Now viscosity is present over the entire layer.

The procedure in both models 1a and 1b is the same as in De Wit: after determination of the amplitudes of the variables via the differential equations, the expressions for the variables are substituted in the boundary conditions. A coefficient matrix is obtained by writing these equations in a homogeneous matrix notation. Equation the determinant of this matrix to zero, gives a dispersion equation that is an implicit expression for k which has to be solved with the help of an iteration technique. Dalrymple and Liu (1978) mention this procedure, but do not elaborate it in detail in their article.

2.4.6 Dalrymple and Liu 'boundary layer approximation'

In appendix C of their article, Dalrymple and Liu also present a boundary layer approximation for large values of $H_{m0}(\omega/2\nu_m)^{1/2}$. This approximation is a further simplification of model 1a. The basic assumption is that the energy dissipation mainly takes place in the boundary layers near the solid bottom and the interface, and that the core of the layers can be treated as inviscid. As a consequence the velocity field can be divided into a rotational part and a potential part. The rotational velocity is significant only near the solid bottom and the interface. Dalrymple first solves the potential velocity (which gives the same solution as the two-layer model for non-hydrostatic water layers without damping in the theory of density currents, see C.Kranenburg, 1998) and subsequently adds a rotational velocity in the boundary layers, which is solved with the use of adapted boundary conditions. Finally expressions are given for the time-averaged wave energy density and for the energy dissipation in the boundary layers near the bottom, under the interface and above the interface and substituted into an energy balance:

$$\frac{\mathrm{d}\overline{E}}{\mathrm{d}t} = \frac{\mathrm{d}\omega}{\mathrm{d}k}\frac{\mathrm{d}\overline{E}}{\mathrm{d}x} = -\overline{P}_d \tag{30}$$

where E is the time-averaged wave energy density. The total rate of change of energy while following the wave front makes it possible to estimate the wave damping.

Dalrymple gives as constraints for the validity of this approximation

$$H_{m0} \gg O(\delta_{BL}), \quad \text{with } \delta_{BL} = \sqrt{\frac{2\nu_m}{\omega}} \qquad \cap \qquad \frac{\omega^2}{g}\left(\frac{\nu_m}{\omega}\right)^{1/2} \ll 1 \tag{31}$$

and states that this approach yields explicit solutions for the wave damping when

$$kH_{w0} \ll 1 \qquad \cap \qquad kH_{m0} \ll 1 \tag{32}$$

The boundary layer approximation is compared with the 'complete models' in Dalrymple and Liu (1978) figure 2, here presented in Figure 9.

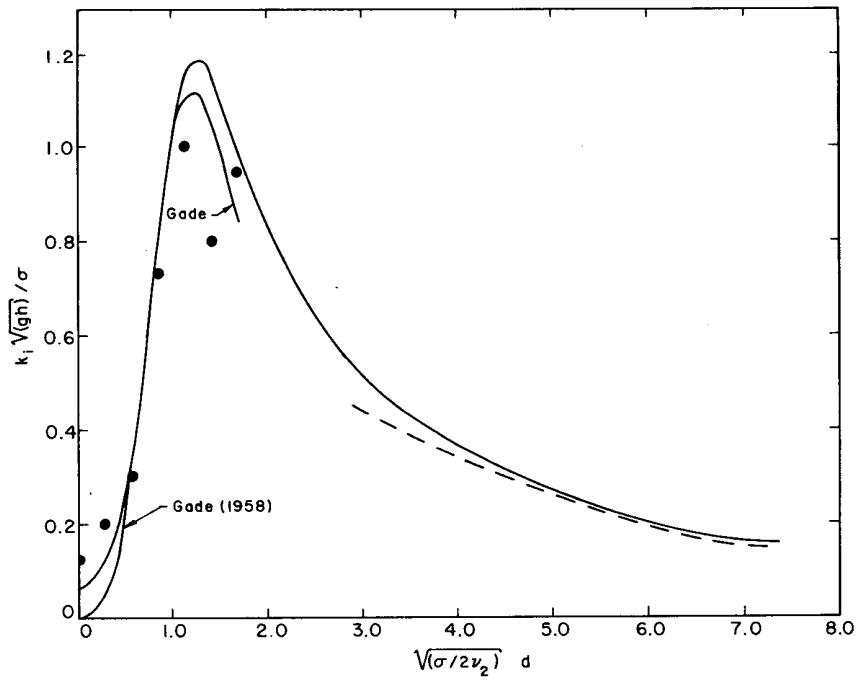

FIG. 2. Comparison of dimensionless damping coefficient k_i (the complex part of the wavenumber) versus dimensionless lower layer depth d as calculated by the complete models. The data points correspond to Gade's (1957) experiment and the dashed line is the result of the boundary layer model developed in Appendix C. The characteristics of the fluids and wave are $T = 1.4$ s, $h = 3.81 \times 10^{-2}$ m, $\nu_1 = 2.42 \times 10^{-6}$ m^2 s^{-1}, $\nu_2 = 2.6 \times 10^{-3}$ m^2 s^{-1}, $\rho_1 = 859.3$ kg m^{-3}, $\rho_2 = 1504$ kg m^{-3}.

Figure 9 Comparison of the boundary layer approximation of Dalrymple and Liu (1978) with their 'complete models'. On the horizontal axis the relative mud layer thickness $H_{m0}/(2\nu/\omega)^{1/2}$, on the vertical axis the normalized imaginary wave number $k_i/(\omega/(gH_{w0})^{1/2})$.

2.4.7 Ng 'boundary layer approximation'

Ng (2000) "*provides an analytical limit to the complete model of Dalrymple (1978) when the mud layer is comparable in thickness to the Stokes' boundary layer, and much thinner than the overlying water layer*" (Ng, 2000, p. 236), so Ng is an approximation of model 1b of Dalrymple.

The key assumption is that both the mud layer thickness H_{m0} and the boundary layer thickness are of the same order of magnitude as the wave amplitude a, which is much smaller than the wavelengh. These assumptions result in an ordening parameter ε, where:

$$\varepsilon \equiv ka \sim kH_{m0} \sim k\delta_{BL} \ll 1 \tag{33}$$

Because of the shallowness, the wave-induced motion of mud is dominated by viscosity throughout the layer. This means that the boundary layer equations are the governing equations in the mud layer and the water layer close to the interface. Ng uses the ordening

parameter ε to indicate relative order to determine which terms can be kept out of consideration.

For the water layer, Ng determines expressions for velocity valid inside the boundary layer close to the interface and valid inside the boundary layer close to the surface (where damping is assumed to be small compared to all the other boundary layers, resulting in a potential solution). These two expressions are asymptotically matched. This asymptotic matching allows the determination of the complex eigenvalue for the wave number k.

The dispersion relation according to Ng is:

$$\frac{\omega^2}{gk} = \frac{\tanh(kH_{w0}) + B}{1 + B\tanh(kH_{w0})} \tag{34}$$

where B is a complex parameter following from the asymptotically matching. The wave number k can be expanded in terms of different order n, where $k_n = O(k\delta_{BL})^{n-1}$. The first term k_1 is real and dominated by the normal single layer non-shallow water dispersion relation. The next order k_2 is complex and given by:

$$k_2 = -\frac{Bk_1}{\sinh(k_1H_{w0}) + \cosh(k_1H_{w0}) + k_1H_{w0}} \tag{35}$$

The imaginary part of this expression gives the wave attenuation rate due to dissipation in the fluid mud layer and can explicitely be calculated when k_1 and B are known.

Ng (2000) thoroughly investigates the effects of varying viscosity and density ratio's between the layers and the shape of the graph of the wave number k as function of the normalized mud layer thickness H_{m0} . In his graphs, '*the effect of mud on the wave damping is most pronounced when (I) the mud is highly viscous, (II) the mud layer is approximately 1.5 times as thick as its Stokes' boundary layer and (III) the mud is not too much denser than water*' (Ng, 2000, p.229).

2.4.8 Jain 'full semi-analytical solution'

Jain (in review) compares the dispersion relation according to Ng and according to Dalrymple and Liu (not clearly stated which one, I suppose model 1a) with her own 'full semi-analytical solution'. This full semi-analytical solution is firstly derived for the first order problem and later extended to a second order solution. First the wave amplitude is assumed to be small compared to the wave length. This makes it possible to linearize. Except for the fact that she strictly holds on to the first order approximation (and the gravitational acceleration is again canceled out against the hydrostatic part of the pressure in the vertical momentum equation), she does not add any constraint in the equations in section 2.4.1. The method of substituting an assumed solution for each variable separable and periodic in time and x-direction, has been followed here as well. Jain does not give her dispersion equation, but it is evident that this is an implicit relation which needs an iteration procedure to be solved.

Jain assumes that the modification of surface wave profiles will be more significant for muddy beds than for rigid bottoms. She also assumes that damping can be quite different for non-sinusoidal wave profiles. That is why she extends her solution to a second order solution by a perturbation approach in terms of wave steepness. The Stokes expansion she uses is only valid if the series converges. The rate of convergence is related to the so called Ursell number, a measure for the ratio between wave length L, wave height ($2a$) and water depth H. For a valid expansion, the Ursell number is bound to:

$$Ur \equiv \frac{L^2 2a}{H_0^3} < 25 \tag{36}$$

Comparing Ng and Dalrymple and Liu with her full semi-analytical solution of the first order, Jain concludes that Ng's solution is a very good approximation as long as the mud thickness is less than the Stokes' boundary layer thickness. For depths a little larger than the boundary layer thickness, Ng's solution starts to deviate. Jain shows pictures of a case of intermediate water depth and of a shallow water scenario. In the first case, Ng's solution shows a lower, in the second case a higher wave attenuation coefficient than Jain's full semi-analytical solution of the first order. Dalrymple and Liu's solution starts to deviate from Jain's solution when the normalized mud layer thickness is less than 2.5. A noteworthy observation is that Dalrymple and Liu's solution predicts a high wave attenuation in case of intermediate water depth even when the mud layer thickness approaches to zero.

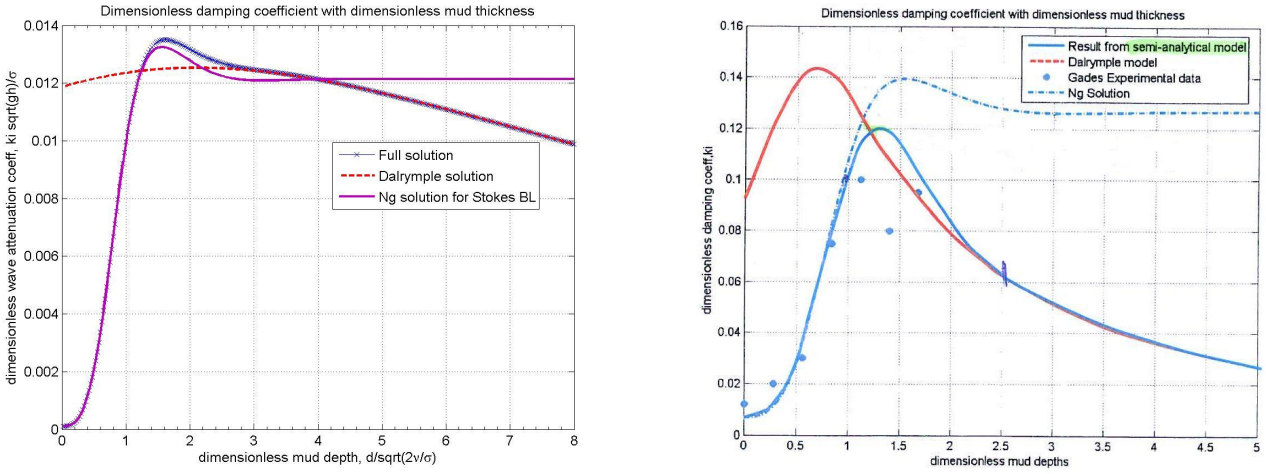

Figure 10 Comparison of the normalized imaginary wave number as function of the dimensionless mud layer thickness for the case of intermediate water depth (left) and shallow water depth (right) as obtained with the Ng-model, a Dalrymple model (probably the boundary layer approximation) and the 'full semi-analytical solution' according to Jain.

Jain also compares the peak of the wave attenuation in the different models. In Ng's solution the peak dissipation always occurs when the mud layer thickness is 1.55 times the boundary layer thickness. Jain's solution shows peaks at lower values of the normalized mud layer thickness. This is especially the case for shallow water scenario's. This also agrees better with Gade's calculation for the shallow water case, that showed a peak dissipation at a normalized mud layer thickness of 1.2, and Gades experimental data that showed peaks in the range 1.3 δ_{BL} - 1.5 δ_{BL}.

2.4.9 Overview

An overview of the terms taken into account in the various dispersion relations in literature is given in Table 4. The table also mentions if a dispersion equation is presented by the authors, and if the equation is implicit or explicit for the wave number k. The last column gives constraints on the domain of application resulting from assumptions in the derivations.

Name	Mom. eq. lower layer			Mom. eq. lower layer			Disp. eq. given	Impl / Expl	Constraints on the domain
	dw_1/dt	v_{x1}	v_{z1}	dw_2/dt	v_{x2}	v_{z2}			
Gade	-	-	-	-	-	+	Yes	Expl	shallow water, thin mud
De Wit	+	-	-	-	-	+	Yes	Impl	thin mud layer ($kH_{m0} \ll 1$)
Gade+	+	-	-	+	-	+	Yes	Impl	not specified
Dalrymple&Liu									
1a, complete model	+	$v_{x1} =$	v_{z1}	+	$v_{x2} =$	v_{z2}	No	Impl	$H_{m0} \gg \sqrt{2\nu_m/\omega}$
1b, complete model	+	$v_{x1} =$	v_{z1}	+	$v_{x2} =$	v_{z2}	No	Impl	$H_{m0} = O\left(\sqrt{2\nu_m/\omega}\right)$
2, boundary layer approximation	+	$v_{x1} =$	v_{z1}	+	$v_{x2} =$	v_{z2}	Yes	Expl	$H_{m0} \gg \sqrt{2\nu_m/\omega}$, $\frac{\omega^2}{g}\left(\frac{\nu_m}{\omega}\right)^{1/2} \ll 1$
Ng boundary layer approximation	- / +	-	+	-	-	+	Yes	Expl	$H_{m0} = O\left(\sqrt{2\nu_m/\omega}\right)$, $H_{w0} \gg H_{m0}$
Jain semi-anal. full solution	+	$v_{x1} =$	v_{z1}	+	$v_{x2} =$	v_{z2}	No	Impl	not specified

Table 4 Overview of terms taken into account in the momentum equations and constraints on the domain of application for the various dispersion equations discussed in this section.

2.5 Discussion and conclusions

This discussion indicates which schematizations can be used in the adaptation to SWAN and what kind of problems has to be accounted for while comparing the various schematizations.

2.5.1 Issues concerning comparison

Normalization

Many parameters are involved in the computation of the wave number k with the dispersion equations discussed in section 2.4 (viz. ρ_w, ρ_m, H_{w0}, H_{m0}, ω, (ν_w), ν_m, g). To compare the various dispersion relations in a useful way, normalization is needed. At present all authors follow Gade in his parameter normalization. (The wave number is normalized with the shallow water wave number for one water layer only and the mud layer thickness is normalized with the Stokes visous boundary layer thickness δ_{BL}. See eq. 21 & 22). Because most authors extend the domain to non-shallow water cases, it seems more logical to normalize the wave number with the normal non-shallow water wave number that can be calculated from:

$$\omega^2 = gk\tanh(kH) \tag{37}$$

With this normalization, the normalized real wave number k_r should approach 1 for all dispersion equations and parameter settings in case the mud layer thickness approaches zero.

The normalization with the Stokes viscous boundary layer thickness δ_{BL} reduces the number of parameters and has a clear physical meaning. However, it is not fully clear if this normalization gives a summary of the results. It is suggested in Rogers and Holland (in review) that the boundary layer thickness might not be the best parameter to compare results or define the limits of a domain. Rogers and Holland suggest to use H_{w0} as normalization parameter as well. In case of normalization with the boundary layer thickness each value of H_{w0} gives a separate line in the graph. The normalization of parameters is subject to further considerions in chapter 4.

Domains

When comparing the various dispersion relations, it is important to note for which part of the domain these relations have been derived. Jain (in review) compared Ng, Dalrymple and Liu (model 1a) and her own semi-analytical full solution and suggested to distinguish three parts in the range of normalized mud layer thicknesses:

$$H_{m0}\sqrt{\frac{\omega}{2\nu_m}} < 1, \qquad 1 \le H_{m0}\sqrt{\frac{\omega}{2\nu_m}} < 2.5 \qquad 2.5 \le H_{m0}\sqrt{\frac{\omega}{2\nu_m}} \tag{38}$$

(thus indicating the domains (1) where here dispersion equation gives the same results as Ng, (2) where here dispersion equation does not coincide with another considerd in here comparison, and (3) where here dispersion equation coincides with result from Dalrymple and Liu (model 1a), see Figure 10).

It is also important to determine which part of each graph represents the shallow water situation. This is not evident in the graphical presentation as used in the articles describing the various dispersion relations.

Peaks

A feature that might discriminate dispersion relations is the location and the height of the peak of the (normalized) imaginary wave number as a function of other normalized parameters. Gade found that the rate of decay has a maximum value when the relative mud depth has a value of 1.2 [*sic*]. Ng states that the attenuation rate is maximum when the relative mud depth equals 1.55. Dalrymple and Liu (1978) show values for the peak in between, but Jain shows peaks for Dalrymple and Liu (1a) at relative mud depths less then 1.0 (see Figure 10). This makes clear that various dispersion equations and various computations with the same dispersion equation show maximum wave attenuation at different values of the normalized mud layer thickness. Especially the latter indicates the need for a better normalization.

Special cases

To check the correctness and validity of various dispersion relations, investigation of their behaviour for special cases can be helpful. The first one is the limit of mud layer thickness H_{m0} approaching zero. If there is no mud layer, the real wave number is expected to approach the normal (non-shallow water) wave number, and the imaginary wave number is expected to approach zero, or at least low values, because the viscosity of the water layer is much less than the viscosity of the mud layer. Also for ν_m approaching zero while $\rho_m = \rho_w$, the normal non-shallow water wave number should be obtained, where $H = H_{tot0}$. A third case that can be investigated is the limit of ν_m approaching 0 while $\rho_m \neq \rho_w$. For the case of non-shallow layers this case should approach the two layer dispersion relation for short waves as derived in C.Kranenburg (1998).

2.5.2 Criteria for further work

Although an elaborated comparison of results for all dispersion relations discussed in section 2.4 would certainly give much insight in the behaviour of the functions and the consequences of various assumptions, a preselection is made here to determine which dispersion relations are most relevant for this project.

The aim of this project is to model the energy loss during propagation over a mudlayer by implementing a dispersion relation into the wave energy model SWAN. This introduces a number of criteria. First, the model should be valid and consistent for practical cases. It is clear that in reality the water layer above the fluid mud can not always be considered as shallow. Especially higher frequency waves fall outside the shallow water domain. In most marine environments the mud layer is typically much thinner than the overlying water layer (Mei and Liu, 1987). Therefore a dispersion relation has to be applied that covers these

practical situations. Secondly, it is required to calculate the proper wave number in a reliable way from a dispersion equation that is clear and fully understood.

The schematization of De Wit is a suitable candidate, because it is valid in the most interesting domain: shallow and non-shallow water and thin mud layers. The schematization for this relation is simple and the assumptions are clear. The domain overlaps the domain of Gade's analytical relation, so the results of the model can be checked easily. Therefore it is decided to derive anew the dispersion equation from the schematization of De Wit, to investigate this function and to compare results to results for Gade. (Model 1a of Dalymple and Liu is also enclosed in the comparison, because in literature it is considered as the most complete equation and because it is available from previous studies).

The next step would be to investigate the analytical solutions of the boundary layer approximations of Ng and Dalrymple and Liu (model 2), because these solutions are explicit and their wave numbers can be calculated much faster. Because in a wave model the wave number has to be calculated quite often, this would save much computer time. Especially the dispersion relation of Ng is interesting, because it covers the domain of a non-shallow water layer over a thin mud layer. Note that the constraints for Ng are stronger than for De Wit. For Ng the mud layer has to be thin compared to the wave length, but also compared to the water layer thickness. The latter constraint is not the case for the schematization of De Wit. Furthermore, Jain showed that Ng already started to deviate from a more complete solution at a relative mud layer thickness $H_{m0}/(2\nu/\omega)^{1/2} < 1$ (see Figure 10).

3 Derivation of the 'DELFT' dispersion equation

3.1 Introduction

In chapter 2 various viscous two-layer models have been discussed. It was concluded that the schematization of De Wit covers the water and mud layer thicknesses that occur in reality, and is a suitable candidate for implementation into the wave model SWAN. Therefore it was decided to elaborate the dispersion equation from the schematization of De Wit and to compare it to results of Gade (and Dalrymple and Liu as extra). This chapter describes step by step the derivation of the dispersion equation belonging to the schematization of the system as a two-layer system. The upper layer is considered non-viscous and no constrictions are imposed on the layer thickness. The lower layer is considered viscous and shallow compared to the wave length. (For a drawing and more details of the schematization and the assumptions, see section 2.4.1 and 2.4.3).

The clear derivation of a well understood dispersion equation for a relevant schematization is an important contribution to the development of SWAN-mud models. Therefore it is presented in the main text of this report. The last section of this chapter (3.9) summarizes the conclusions. Those not interested in the derivation can limit themselves to the conclusions without losing the thread of the story.

Section 3.2 gives the differential equations describing the system. Section 3.3 mentions the assumed forms of the solutions for the unknown (fluctuating) parameters. Expressions for the amplitudes of these fluctuations are determined in section 3.4. The next step of the derivation is formed by the formulation of the boundary conditions (section 3.5). Notation of these equations in terms of a (reduced) homogeneous matrix equation gives a coefficient matrix (section 3.6). The determinant of the matrix gives the dispersion equation when equated to zero (section 3.7). A verification of the dispersion equation is carried out in section 3.8 with two basic tests. The conclusions are summarized in section 3.9.

The symbolic mathematical computer program MAPLE has been used in the derivation. Results are inserted as formulae in MAPLE output format to avoid typing errors.

3.2 Differential equations

The system is described by a horizontal (*a*) and vertical (*b*) momentum equation and a continuity equation (*c*) for each layer (*1&2*) (compare with section 2.4.1).

$$verg1a := \left(\frac{\partial}{\partial t} u1(x, z, t) \right) + \frac{\frac{\partial}{\partial x} p1(x, z, t)}{\rho 1} = 0 \tag{39}$$

$$verg1b := \left(\frac{\partial}{\partial t} w1(x, z, t) \right) + \frac{\frac{\partial}{\partial z} p1(x, z, t)}{\rho 1} + g = 0 \tag{40}$$

$$verg1c := \left(\frac{\partial}{\partial x} u1(x, z, t) \right) + \left(\frac{\partial}{\partial z} w1(x, z, t) \right) = 0 \tag{41}$$

$$verg2a := \left(\frac{\partial}{\partial t} u2(x, z, t) \right) + \frac{\frac{\partial}{\partial x} p2(x, z, t)}{\rho 2} = \nu \left(\frac{\partial^2}{\partial z^2} u2(x, z, t) \right) \tag{42}$$

$$verg2b := \frac{\frac{\partial}{\partial z} p2(x, z, t)}{\rho 2} + g = 0 \tag{43}$$

$$verg2c := \left(\frac{\partial}{\partial x} u2(x, z, t) \right) + \left(\frac{\partial}{\partial z} w2(x, z, t) \right) = 0 \tag{44}$$

3.3 Assumed solutions

The solutions for horizontal and vertical velocity and pressure are assumed to be of the following form:

$$u1(x, z, t) := U1(z)\, \mathbf{e}^{(I\,(k\,x - \omega\,t))} \tag{45}$$

$$u2(x, z, t) := U2(z)\, \mathbf{e}^{(I\,(k\,x - \omega\,t))} \tag{46}$$

$$w1(x, z, t) := W1(z)\, \mathbf{e}^{(I\,(k\,x - \omega\,t))} \tag{47}$$

$$w2(x, z, t) := W2(z)\, \mathbf{e}^{(I\,(k\,x - \omega\,t))} \tag{48}$$

$$p1(x, z, t) := P1(z)\, \mathbf{e}^{(I\,(k\,x - \omega\,t))} + \rho 1\, g\, (Htot0 - z) \tag{49}$$

$$p2(x, z, t) := P2(z)\, \mathbf{e}^{(I\,(k\,x - \omega\,t))} + \rho 1\, g\, (Htot0 - Hm0) + \rho 2\, g\, (Hm0 - z) \tag{50}$$

3.4 Expressions for the z-amplitudes

Water layer

By substituting the assumed solutions for *u1(x,z,t)* and *p1(x,z,t)* in equation (39), $P1(z)$ can be expressed in terms of $U1(z)$. When this result is substituted in equation (40), also $W1(z)$ can be expressed in terms of $U1(z)$.

$$P1(z) := \frac{U1(z)\ \omega\ \rho 1}{k} \tag{51}$$

$$W1(z) := -\frac{I\left(\frac{d}{dz} U1(z)\right)}{k} \tag{52}$$

Substitution of expression (52) in the continuity equation (41) results in an ordinary differential equation in terms of $U1(z)$.

$$ODE\_U1 := \frac{I\, e^{(I\,(k\,x - \omega\,t))}\left(U1(z)\,k^2 - \left(\frac{d^2}{dz^2} U1(z)\right)\right)}{k} = 0 \tag{53}$$

When this differential equation is solved, expressions for $U1(z)$, $W1(z)$ and $P1(z)$ are found. It is chosen to work with trigonometric notations (rather than exponential).

$$U1(z) := C1\ \sinh(k\ z) + C2\ \cosh(k\ z) \tag{54}$$

$$W1(z) := -I\ (C1\ \cosh(k\ z) + C2\ \sinh(k\ z)) \tag{55}$$

$$P1(z) := \frac{\omega\ \rho 1\ (C1\ \sinh(k\ z) + C2\ \cosh(k\ z))}{k} \tag{56}$$

Mud layer

Also for the mud layer, first an expression for $P2(z)$ is determined by substituting the assumed solution of *p2(x,z,t)* (eq. 50) in the vertical momentum equation (43). This shows that $P2(z)$ has to be a constant (here named E):

$$verg2b := \frac{\left(\frac{d}{dz} P2(z)\right) e^{(I\,(k\,x - \omega\,t))} - \rho 2\ g}{\rho 2} + g = 0 \tag{57}$$

$$P2(z) := E \tag{58}$$

Substitution of this expression for $P2(z)$ and the assumed solution for *u2(x,z,t)* (equation 46) in the horizontal momentum equation (42), leads to an ordinary differential equation in terms of $U2(z)$:

$$ODE\_U2 := \frac{I\, e^{(I\,(k\,x - \omega\,t))}\,(-U2(z)\ \omega\ \rho 2 + E\ k)}{\rho 2} = \nu\left(\frac{d^2}{dz^2} U2(z)\right) e^{(I\,(k\,x - \omega\,t))} \tag{59}$$

The solution of this ODE is:

$$U2(z) := \sin\left(\frac{\left(\frac{1}{2}+\frac{1}{2}I\right)\sqrt{2}\sqrt{\omega}\,z}{\sqrt{\nu}}\right) C4 + \cos\left(\frac{\left(\frac{1}{2}+\frac{1}{2}I\right)\sqrt{2}\sqrt{\omega}\,z}{\sqrt{\nu}}\right) C3 + \frac{E\,k}{\omega\,\rho 2} \tag{60}$$

(This solution is obtained with MAPLE. This step in the derivation is elaborated in appendix A).

With the continuity equation for the mud layer, eq. (44), an expression for $W2(z)$ can be found:

$$w2 = -\int \frac{\partial u2}{\partial x} dz \tag{61}$$

When we introduce the variable m (as introduced by Gade):

$$(1-I)\frac{\sqrt{\omega}}{\sqrt{2\nu}} = m \tag{62}$$

and make use of the facts that

$$1 + I = I(1-I) \tag{63}$$

$$\sin(Imz) = I\sinh(mz) \tag{64}$$

$$\cos(Imz) = \cosh(mz)$$

the solutions for $U2(z)$, $W2(z)$ and $P2(z)$ can be written as:

$$U2(z) := C3\cosh(m\,z) + I\,C4\sinh(m\,z) + \frac{E\,k}{\omega\,\rho 2} \tag{65}$$

$$W2(z) := -\frac{I\,k\,C3\sinh(m\,z)}{m} + \frac{k\,C4\cosh(m\,z)}{m} - \frac{I\,k^2\,z\,E}{\omega\,\rho 2} + C5 \tag{66}$$

$$P2(z) := E \tag{67}$$

3.5 Boundary conditions

The displacement of the free surface and the interface with respect to the equilibrium levels are described by:

$$\zeta(x,t) = ae^{i(kx-\omega t)} \tag{68}$$

$$\xi(x,t) = \xi_0 e^{i(kx-\omega t)} = be^{i\varphi}e^{i(kx-\omega t)} \tag{69}$$

Note that the amplitude of the interface displacement ξ_0 is complex to account for a phase shift between surface and interface displacement. This complex amplitude is a priori unknown. The height of the free surface and interface become:

$$h_{tot}(x,t) = H_{tot0} + ae^{i(kx-\omega t)} \tag{70}$$

$$h_m(x,t) = H_{m0} + \xi_0 e^{i(kx-\omega t)} \tag{71}$$

At $z = h_{\text{tot}}$, the location of the free surface, particles have to follow the surface (kinematic boundary condition, BC I). Dynamic boundary conditions require that the normal stress is zero (atmospheric pressure is not taken into account, BC II).

BC I:
$$w_1(x,h_{tot},t) = \frac{D\zeta(x,t)}{Dt} \tag{72}$$

BC II:
$$\sigma_{zz1}(x,h_{tot},t) = 0 \quad \Rightarrow \quad p_1(x,h_{tot},t) = 0 \tag{73}$$

At $z = h_{\text{m}}$, the location of the interface, the vertical velocity can be derived from the fact that particles have to follow the interface (kinematic boundary condition, BC IV). Moreover vertical velocities (BC III) and tangential (BC V) and normal (BC VI) stresses have to be continuous over the interface (kinematic and dynamic boundary conditions respectively).

BC III:
$$w_2(x,h_m,t) = w_1(x,h_m,t) \tag{74}$$

BC IV:
$$w_2(x,h_m,t) = \frac{D\zeta(x,t)}{Dt} \tag{75}$$

BC V:
$$\tau_{xz2}(x,h_m,t) = \tau_{xz1}(x,h_m,t) \tag{76}$$

BC VI:
$$\sigma_{zz2}(x,h_m,t) = \sigma_{zz1}(x,h_m,t) \tag{77}$$

At $z = 0$, the location of the fixed bed, slip (BC VII) and penetration (BC VIII) are not allowed:

BC VII:
$$u_2(x,0,t) = 0 \tag{78}$$

BC VIII:
$$w_2(x,0,t) = 0 \tag{79}$$

In the viscous lower layer, the presence of viscosity causes extra terms for normal and shear stresses:

$$\text{contribution of viscosity to normal stress} = -2\rho\nu\frac{\partial w}{\partial z} \tag{80}$$

$$\text{contribution of viscosity to shear stress} = \rho\nu\left(\frac{\partial u}{\partial z} + \frac{\partial w}{\partial x}\right) \tag{81}$$

Expressions for the boundary conditions are found by linearizing the equations. This is done by using the Taylor approximations around the equilibrium level of the surface and the interface. Dingemans makes some remarks about the order of approximation in personal communication with Winterwerp:

"We suppose the perturbations of the free surface and the intermediate layer to be small quantities as is usual in water wave mechanics for which the linear approximation is valid. We suppose that $|\zeta| = a$ and $|\xi| = |\xi_0| = b$ (small adaptation WK) are of equal order of magnitude. The velocities in the upper layer are typically of $O\{a\}$ and those in the lower layer are of $O\{b\}$. In the Taylor approximations we will account for terms linear in ζ and ξ, thus of terms of $O\{a,b\}$. That means that terms of (ζ or,WK) ξ which are multiplied by a derivative of a velocity are of second order and are therefore ignored. The situation is different for the pressure. (…), the pressure is composed of a hydrostatic part, which is of order one, and a perturbation, which is of order a. Thus $p = O\{1\}$." (M.Dingemans; a two layer fluid-flow model, version March 8, 2007, p.2, communication with Winterwerp).

This means that we get the following boundary conditions:

At $z = H_{tot0}$:

BC I:
$$w_1(x,H_{tot0},t) = \frac{\partial \zeta(x,t)}{\partial t} \tag{82}$$

BC II:
$$p_1\left(x,H_{tot0},t\right) + \zeta \frac{\partial p_1}{\partial z}|_{z=H_{tot0}} = 0 \tag{83}$$

At $z = H_{m0}$:

BC III:
$$w_1(x,H_{m0},t) = \frac{\partial \zeta(x,t)}{\partial t} \tag{84}$$

BC IV:
$$w_2(x,H_{m0},t) = \frac{\partial \zeta(x,t)}{\partial t} \tag{85}$$

BC V:
$$\frac{\partial u_2}{\partial z}|_{z=H_{m0}} = 0 \tag{86}$$

BC VI:
$$p_1\left(x,H_{m0},t\right) + \xi \frac{\partial p_1}{\partial z}|_{z=H_{m0}} = p_2\left(x,H_{m0},t\right) + \xi \frac{\partial p_2}{\partial z}|_{z=H_{m0}} - 2\rho_2 \nu_2 \frac{\partial w_2}{\partial z}|_{z=H_{m0}} \tag{87}$$

At $z = 0$:

BC VII:
$$u_2(x,0,t) = 0 \tag{88}$$

BC VIII:
$$w_2(x,0,t) = 0 \tag{89}$$

3.6 The coefficient matrix

The expressions for the z-amplitudes $U_i(z)$, $W_i(z)$ and $P_i(z)$, derived in section 3.4, are substituted in the assumed solutions of section 3.3. These assumed solutions are substituted in the boundary conditions.

$$BC1 := -1.\, I\,(C1\,\cosh(k\,Htot0) + C2\,\sinh(k\,Htot0))\,\mathbf{e}^{(1.\,I\,(k\,x\,-\,1.\,\omega\,t))} + 1.\, I\, a\, \omega\, \mathbf{e}^{(1.\,I\,(k\,x\,-\,1.\,\omega\,t))} = 0 \tag{90}$$

$$BC2 := \frac{\omega\,\rho 1\,(C1\,\sinh(k\,Htot0) + C2\,\cosh(k\,Htot0))\,\mathbf{e}^{(I\,(k\,x\,-\,\omega\,t))}}{k} \tag{91}$$

$$+ a\, e^{(I(kx-\omega t))}\left(\frac{\omega\,\rho 1\,(C1\cosh(k\,Htot0)\,k + C2\sinh(k\,Htot0)\,k)\,e^{(I(kx-\omega t))}}{k} - \rho 1\,g\right) = 0$$

$$BC3 := -I\,(C1\cosh(k\,Hm0) + C2\sinh(k\,Hm0))\,e^{(I(kx-\omega t))} + I\,\xi 0\,\omega\,e^{(I(kx-\omega t))} = 0 \quad (92)$$

$$BC4 := \left(-\frac{I\,k\,C3\sinh(m\,Hm0)}{m} + \frac{k\,C4\cosh(m\,Hm0)}{m} - \frac{I\,k^2\,Hm0\,E}{\omega\,\rho 2} + C5\right)e^{(I(kx-\omega t))} + I\,\xi 0\,\omega\,e^{(I(kx-\omega t))} = 0 \quad (93)$$

$$BC5 := (C3\sinh(m\,Hm0)\,m + I\,C4\cosh(m\,Hm0)\,m)\,e^{(I(kx-\omega t))} = 0 \quad (94)$$

$$BC6 := \frac{\omega\,\rho 1\,(C1\sinh(k\,Hm0) + C2\cosh(k\,Hm0))\,e^{(I(kx-\omega t))}}{k} \quad (95)$$

$$+ \xi 0\,e^{(I(kx-\omega t))}\left(\frac{\omega\,\rho 1\,(C1\cosh(k\,Hm0)\,k + C2\sinh(k\,Hm0)\,k)\,e^{(I(kx-\omega t))}}{k} - \rho 1\,g\right) - E\,e^{(I(kx-\omega t))}$$

$$+ \xi 0\,e^{(I(kx-\omega t))}\,\rho 2\,g + 2\,\nu\,\rho 2\left(-I\,k\,C3\cosh(m\,Hm0) + k\,C4\sinh(m\,Hm0) - \frac{I\,k^2\,E}{\omega\,\rho 2}\right)e^{(I(kx-\omega t))} = 0$$

$$BC7 := \left(C3 + \frac{E\,k}{\omega\,\rho 2}\right)e^{(I(kx-\omega t))} = 0 \quad (96)$$

$$BC8 := \left(\frac{k\,C4}{m} + C5\right)e^{(I(kx-\omega t))} = 0 \quad (97)$$

These equations can be written in a more convenient way in a matrix notation. Before doing so, a closer look is given to BC2 and BC6. These equations contain the products aC1 and aC2 or ξ_0C1 and ξ_0C2 respectively. These products are introduced by the Taylor –term

$$\zeta \frac{\partial p_1}{\partial z}\Big|_{z=H_{tot0}} \quad (98)$$

or its equivalent at the interface. We would like to state here the following:
If terms of ζ or ξ which are multiplied by a derivative of a velocity are of second order and therefore can be ignored, then terms of ζ or ξ which are multiplied by the derivative of the perturbation part of the pressure can be ignored as well. After all it is a multiplication of $O\{\xi_0\}$ with $O\{\xi_0\}$ and is therefore negligible. This is not the case for the ζ- or ξ-terms multiplied by the derivative of the hydrostatic part of the pressure. Therefore these terms (containing $\rho_1 g a$, $\rho_1 g \xi_0$ and $\rho_2 g \xi_0$) are taken into account while building the coefficient matrix.

The dispersion relation will be determined by equating the determinant of the coefficient matrix to zero. If aC1-products would be kept in the boundary conditions, coefficients with the wave height a arise in the matrix. In that case, the wave height a is of influence in the determination of the complex wave number k. In a one dimensional test case, it would make a difference if k_i is calculated at the beginning or half way the mud patch. The damping will never have the form of

$$H_s(x) = H_s(0)\exp(-k_i x) \tag{99}$$

This non-linearity is outside the scope of this project. As long as the wave amplitude is considered small compared to the depth, this assumption is justified.

The boundary conditions above represent a system of 8 equations and 8 unknowns. Boundary condition VII and VIII allow a direct reduction of the 8x8-matrix tot a 6x6-matrix. For reasons of simplicity some rows are multiplicated with certain factors. This will not affect the determinant of the matrix nor the parameters in the vector. With only the linear terms from the boundary conditions, the following matrix is obtained:

$$\begin{bmatrix}
\cosh(k\,Htot0) & \sinh(k\,Htot0) & 0 & 0 & -\omega & 0 \\
\sinh(k\,Htot0) & \cosh(k\,Htot0) & 0 & 0 & -\frac{g\,k}{\omega} & 0 \\
\cosh(k\,Hm0) & \sinh(k\,Hm0) & 0 & 0 & 0 & -\omega \\
0 & 0 & \frac{k\,(-\sinh(m\,Hm0)+m\,Hm0)}{m} & -\frac{I\,k\,(\cosh(m\,Hm0)-1)}{m} & 0 & \omega \\
0 & 0 & \sinh(m\,Hm0) & I\cosh(m\,Hm0) & 0 & 0 \\
\frac{\omega\sinh(k\,Hm0)}{k} & \frac{\omega\cosh(k\,Hm0)}{k} & -\frac{\rho 2\,(-\omega+2\,I\,\nu\,k^2\cosh(m\,Hm0)-2\,I\,\nu\,k^2)}{k\,\rho 1} & \frac{2\,\nu\,\rho 2\,k\sinh(m\,Hm0)}{\rho 1} & 0 & \frac{g\,(\rho 2-\rho 1)}{\rho 1}
\end{bmatrix} \tag{100}$$

Matrix 1: coefficient matrix, belonging to the vector with the constants [C1, C2, C3, C4, a, ξ_0]

In a parallel derivation by Winterwerp, $U2(z)$ was written in a different way:

$$U2(z) = C_{Wi}\sinh(mz) + D_{Wi}\cosh(mz) + \frac{k}{\omega\rho_2}E \tag{101}$$

That means that the relation between the constants is:

$$C_{Wi} = I * C4 \tag{102}$$
$$D_{Wi} = C3$$

The matrix belonging to these constants is obtained by dividing the fourth column by I and swapping the third and the fourth column:

$$\begin{bmatrix}
\cosh(k\,Htot0) & \sinh(k\,Htot0) & 0 & 0 & -\omega & 0 \\
\sinh(k\,Htot0) & \cosh(k\,Htot0) & 0 & 0 & -\frac{g\,k}{\omega} & 0 \\
\cosh(k\,Hm0) & \sinh(k\,Hm0) & 0 & 0 & 0 & -\omega \\
0 & 0 & -\frac{k\,(\cosh(m\,Hm0)-1)}{m} & \frac{k\,(-\sinh(m\,Hm0)+m\,Hm0)}{m} & 0 & \omega \\
0 & 0 & \cosh(m\,Hm0) & \sinh(m\,Hm0) & 0 & 0 \\
\frac{\omega\sinh(k\,Hm0)}{k} & \frac{\omega\cosh(k\,Hm0)}{k} & -\frac{2\,I\,\nu\,\rho 2\,k\sinh(m\,Hm0)}{\rho 1} & -\frac{\rho 2\,(-\omega+2\,I\,\nu\,k^2\cosh(m\,Hm0)-2\,I\,\nu\,k^2)}{k\,\rho 1} & 0 & \frac{g\,(\rho 2-\rho 1)}{\rho 1}
\end{bmatrix} \tag{103}$$

Matrix 2: coefficient matrix, belonging to the vector with the constants [C1, C2, I*C4, C3, a, ξ0]

As a consequence the whole determinant is divided by I. This does not have any consequences for the value of k where the determinant is zero.

3.7 The dispersion equation

The dispersion equation is obtained by equating the determinant of the matrix with zero. For reasons of overview the equation is multiplied by $\omega\rho_1$ and written as a polynomial of ω. The equation is considerably shortened by using the equations:

$$\begin{aligned}\sinh(kH_{w0}) &= \sinh(kH_{tot0})*\cosh(kH_{m0}) - \cosh(kH_{tot0})*\sinh(kH_{m0}) \\ \cosh(kH_{w0}) &= \cosh(kH_{tot0})*\cosh(kH_{m0}) - \sinh(kH_{tot0})*\sinh(kH_{m0})\end{aligned} \tag{104}$$

The resulting dispersion equation itself is given by:

$$\begin{aligned}Disprel :=& \left(\frac{\cosh(m\,Hm0)\,\rho2\cosh(k\,Hw0)}{k} - \frac{\rho1\sinh(k\,Hw0)\sinh(m\,Hm0)}{m} + \rho1\sinh(k\,Hw0)\cosh(m\,Hm0)\,Hm0 \right)\omega^4 \\ &+ (-2\,I\,k\,\rho2\,\nu\cosh(m\,Hm0)^2\cosh(k\,Hw0) + 2\,I\,k\,\nu\,\rho2\sinh(m\,Hm0)^2\cosh(k\,Hw0) + 2\,I\,k\,\rho2\,\nu\cosh(m\,Hm0)\cosh(k\,Hw0))\,\omega^3 \\ &+ \left(\frac{\rho2\,g\,k\cosh(k\,Hw0)\sinh(m\,Hm0)}{m} - \rho2\,g\,k\cosh(k\,Hw0)\cosh(m\,Hm0)\,Hm0 - \rho2\,g\cosh(m\,Hm0)\sinh(k\,Hw0) \right)\omega^2 \\ &+ (2\,I\,k^2\,\rho2\,\nu\,g\sinh(k\,Hw0)\cosh(m\,Hm0)^2 - 2\,I\,k^2\,\rho2\,\nu\,g\sinh(k\,Hw0)\sinh(m\,Hm0)^2 - 2\,I\,k^2\,\rho2\,\nu\,g\sinh(k\,Hw0)\cosh(m\,Hm0))\,\omega \\ &+ \frac{k^2\,g^2\sinh(k\,Hw0)\sinh(m\,Hm0)\,\rho1}{m} - k^2\,g^2\sinh(k\,Hw0)\,\rho1\cosh(m\,Hm0)\,Hm0 + k^2\,g^2\sinh(k\,Hw0)\cosh(m\,Hm0)\,Hm0\,\rho2 \\ &- \frac{k^2\,g^2\sinh(k\,Hw0)\sinh(m\,Hm0)\,\rho2}{m} = 0\end{aligned} \tag{105}$$

Formula (105): the DELFT dispersion equation

In the remainder of this report this dispersion equation is named the DELFT dispersion equation. The various people playing a role in the origine of this expression are all presently or formerly connected to WL|Delft Hydraulics or Delft University of Technology.

3.8 Verification

Two simple checks are carried out to check whether the DELFT dispersion relation (105) can be correct. The first one is the limit for the absence of mud when $H_{m0} \rightarrow 0$ and $\rho_2 \rightarrow \rho_1$. For this case the dispersion equation reduces to:

$$DispRelwater := \frac{\rho1\cosh(k\,Hw0)\,\omega^4}{k} - \rho1\,g\sinh(k\,Hw0)\,\omega^2 = 0 \tag{106}$$

which is the regular dispersion relation

$$\omega^2 = gk \tanh\left(kH_{w0}\right) \tag{107}$$

The second check only concerns the presence of I in the dispersion equation. It follows out of the matrix that the factor I can only be present in the determinant in combination with ω^0 or ω^2. This can be deduced when we realize that terms of the determinant are assembled by multipliing six position out of the matrix, chosen in such a way that all rows and columns are represented. After multiplication with $\omega\rho_1$, I can only be present in the dispersion equation in combination with ω^1 or ω^3. This is the case.

Finally, the newly derived dispersion equation is compared with the original dispersion equation of De Wit (1995). Although it is a question whether you verify the equation of De Wit with the DELFT dispersion equation or the other way around, comparison can take away confusion and doubt. This comparison is described in appendix B. It shows that the original dispersion equation of De Wit can only be reproduced by making some additional simplifications, that cause the disappearance of the odd powers of ω from the DELFT dispersion equation (105).

3.9 Conclusions

This chapter describes the derivation of a dispersion equation. This dispersion equation is derived using the schematization of De Wit (see 2.4.3), assuming a non-hydrostatic, non-viscous water layer and a quasi-hydrostatic, viscous mud layer. The result of the derivation is given in equation (108):

$$\begin{aligned}
Disprel :=& \left(\frac{\cosh(m\,Hm0)\,\rho2\cosh(k\,Hw0)}{k} - \frac{\rho1\sinh(k\,Hw0)\sinh(m\,Hm0)}{m} + \rho1\sinh(k\,Hw0)\cosh(m\,Hm0)\,Hm0 \right) \omega^4 \\
&+ (-2\,I\,k\,\rho2\,\nu\cosh(m\,Hm0)^2\cosh(k\,Hw0) + 2\,I\,k\,\nu\,\rho2\sinh(m\,Hm0)^2\cosh(k\,Hw0) + 2\,I\,k\,\rho2\,\nu\cosh(m\,Hm0)\cosh(k\,Hw0))\,\omega^3 \\
&+ \left(\frac{\rho2\,g\,k\cosh(k\,Hw0)\sinh(m\,Hm0)}{m} - \rho2\,g\,k\cosh(k\,Hw0)\cosh(m\,Hm0)\,Hm0 - \rho2\,g\cosh(m\,Hm0)\sinh(k\,Hw0) \right) \omega^2 \\
&+ (2\,I\,k^2\,\rho2\,\nu\,g\sinh(k\,Hw0)\cosh(m\,Hm0)^2 - 2\,I\,k^2\,\rho2\,\nu\,g\sinh(k\,Hw0)\sinh(m\,Hm0)^2 - 2\,I\,k^2\,\rho2\,\nu\,g\sinh(k\,Hw0)\cosh(m\,Hm0))\,\omega \\
&+ \frac{k^2\,g^2\sinh(k\,Hw0)\sinh(m\,Hm0)\,\rho1}{m} - k^2\,g^2\sinh(k\,Hw0)\,\rho1\cosh(m\,Hm0)\,Hm0 + k^2\,g^2\sinh(k\,Hw0)\cosh(m\,Hm0)\,Hm0\,\rho2 \\
&- \frac{k^2\,g^2\sinh(k\,Hw0)\sinh(m\,Hm0)\,\rho2}{m} = 0
\end{aligned}$$

Formula (108): DELFT dispersion equation (108)

where

H_{w0} = Equilibrium height of water layer
H_{m0} = Equilibrium height of mud layer
ν = Kinematic viscosity of mud
ρ_1 = Density of water
ρ_2 = Density of mud
ω = Wave (angular) frequency (2π / T)
k = (complex) wave number
I = Imaginary unit i
g = Gravitational acceleration

$$m = (1 - I)\frac{\sqrt{\omega}}{\sqrt{2\nu}}$$

In the remainder of this report this dispersion equation is named the DELFT dispersion equation. This equation is the one that is numerically investigated and implemented in SWAN during this study.

4 Solution of the dispersion equation

4.1 Introduction

Chapter 3 described the derivation of the DELFT dispersion equation. This chapter deals with the solution of this equation for the complex wave number. An iteration procedure is needed to solve the equation. Section 4.2 describes the iteration method and starting value developed in this study. A separate part of this section gives a description of the process that led to the described solving routine. Section 4.3 describes the normalization that is used to investigate results obtained with the solving routine of section 4.2. The results itself are given in section 4.4. As a test, these results are compared with the results obtained with an alternative method: Argand diagrams (section 4.5). This chapter is finalized with a discussion, containing conclusions and recommendations (section 4.6).

4.2 Description of the solving routine

4.2.1 General remarks

The DELFT dispersion equation, like all the other dispersion equations describing wave damping, is a complex equation. Both its real and imaginary part are functions of both the real and the imaginary part of the wave number k and a list of other parameters:

$$F_{re} = f\left(k_{re}, k_{im}, \nu_w, \nu_m, \rho_w, \rho_m, H_{m0}, H_{w0}, \omega\right) \tag{109}$$

$$F_{im} = f\left(k_{re}, k_{im}, \nu_w, \nu_m, \rho_w, \rho_m, H_{m0}, H_{w0}, \omega\right) \tag{110}$$

If we assume all the other parameters to be constants, F_{re} and F_{im} can be seen as curved surfaces with a (z-)value representing the height above the horizontal k_{re}- k_{im}-plain. Both surfaces can cross the horizontal plain more than once, for each function resulting in secants where the value of the function is zero. At the points of intersections of secants of F_{re} and F_{im}, both functions are zero. These crossing points are solutions for the dispersion equation.

The DELFT dispersion equation is also an implicit equation for the wave number k. Therefore a numerical iteration procedure is needed to find the solutions. Section 4.2.2 describes this iteration method, while section 4.2.3 focusses on the starting value for the iterations. Starting value and iteration procedure together form the routine used to solve the dispersion equation.

4.2.2 The iteration method

The method of iteration employed in this study is the **ZANLY / DZANLY routine** for complex functions. This routine is available from the Fortran IMSL library (Visual Numerics, 1997) .

This method makes use of Muller's method (see: Burden and Faires, 2001, p. 67-99), which is a generalization of the Secant Method.

In the most simple iteration routines, the new approximation p_n of the zero crossing is determined out of the old one p_{n-1} with

$$p_n = p_{n-1} - \frac{f(p_{n-1})}{f'(p_{n-1})} \tag{111}$$

where n is the counter of the iterations.

The Secant Method avoids the evaluation of the derivative by using an approximation based on the assumption that the function is approximately linear in the region of interest:

$$p_n = p_{n-1} - \frac{f(p_{n-1})}{\left(\frac{f(p_{n-1}) - f(p_{n-2})}{p_{n-1} - p_{n-2}}\right)} \tag{112}$$

In Muller's Method the Secant Method is generalized for less linear cases by using a quadratic 3-point interpolation. This method is adapted for complex functions and used in the ZANLY / DZANLY routine.

4.2.3 Starting values for the iteration

The starting value for the iteration is computed from two analytical functions. These two functions each deal with a different limit of the dispersion equation. The weight of the contribution of each function depends on the relative water depth kH_{w0}.

For low values of kH_{w0}, the DELFT dispersion equation is expected to give a result for the wave number close to Gade. This expectation is based on the fact that Gade's schematization represents a subdomain of the schematization of De Wit, namely the shallow water case.

For higher values of kH_{w0}, the water can be considered as deep. This implies that the effect of the (muddy) bottom on the waves will be less. In case no influence of mud is present, the regula dispersion relation $\omega^2 = gk \tanh(kH)$ can be used to calculate the (real) wave number. This function is an implicit function itself. To avoid the necessity of iterations, the regular dispersion equation is approximated with the explicit approximation of Guo (2002). (See Fenton, 2006, for an investigation of the quality of this approximation.) Although there is no damping in deep water, a positive imaginary part is added to this starting value to make sure that the iteration procedure converges to non-negative solutions.

These considerations result in two analytical functions for starting values:

$$k_{SV1} = +\omega \left\{ \frac{\left(1+\Gamma\frac{H_{m0}}{H_{w0}}\right) - \sqrt{\left(1+\Gamma\frac{H_{m0}}{H_{w0}}\right)^2 - 4\gamma\Gamma\frac{H_{m0}}{H_{w0}}}}{2\gamma g\Gamma H_{m0}} \right\}^{1/2} \tag{113}$$

Starting Value 1: Gade's analytical dispersion equation

with

$$\Gamma = 1 - \frac{\tanh\left(mH_{m0}\right)}{mH_{m0}} \quad , \qquad m = (1-i)\sqrt{\frac{\omega}{2\nu}} \quad \& \qquad \gamma = \frac{\rho_2 - \rho_1}{\rho_2} \tag{114}$$

and

$$k_{SV2} = \frac{\omega^2}{g}\left(1 - \exp^{-\left(\omega\sqrt{H_{w0}/g}\right)^{5/2}}\right)^{-2/5} + \frac{1}{10}\mathrm{Im}\left(k_{SV1}\right) \tag{115}$$

Starting Value 2: Guo's approximation of the normal dispersion equation plus a small imaginary part resulting from Gade's dispersion equation (113)

The starting value for the wave number used in the iteration procedures (k_{SV}) is a weighted superposition of these two functions. The superposition is computed from these functions using the weights f_1 and f_2:

$$k_{SV} = f_1 * k_{SV1} + f_2 * k_{SV2} \tag{116}$$

$$f_1 = 1 - f_2 \tag{117}$$

$$f_2 = \frac{\tanh\left(a\left(kH_{w0} - c\right)\right) + 1}{2}$$

The parameter c denotes the value of kH_{w0} where both function contribute with the same weight to the starting value. The parameter a is a measure for the width of the zone where the two functions are merged to compute a starting value. Using $\tanh(x) \approx 1$ for $x \geq 3$, the width of the merging zone can be computed with width = $6/a$. Applied values for a and c are:

$$c = 1.5 \tag{118}$$

$$a = 1.2 \tag{119}$$

Figure 11 shows the weights for the two functions used to calculate the Starting Value of the iteration, as function of the relative water depth kH_{w0}.

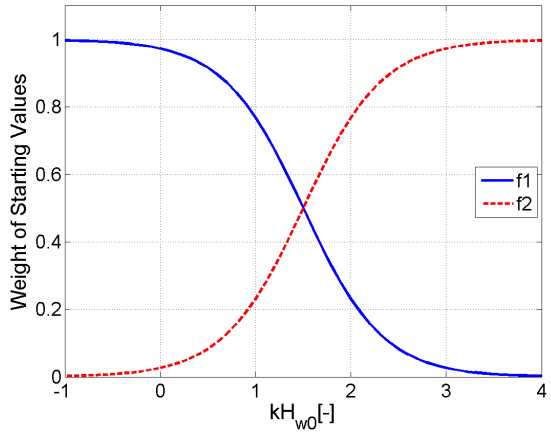

Figure 11 Graph of the weights of the two functions used to compute the Starting Value of the iteration procedure, plotted as function of the relative water depth kH_{w0}

4.2.4 Justification of choices concerning solving routine

The previous sections described the solving routine used to calculate the wave number. This section gives a justification of the choices concerning iteration method and starting value by roughly describing the process that led to the present solving routine. The computation of a starting value out of a combination of limits has a clear physical meaning and seems quite trivial. But to investigate the performance of a routine, to make sure that the relative water depth kH_{w0} is the normative dimensionless parameter and to determine a good combined starting value is not that trivial. The process of development during this project can be split in the following steps, which are shortly discussed in the sections below.

1. Choice of iteration method
6. Choice of a preliminary starting value
7. Normalization
8. Visualization
9. Evaluation of the preliminary results
10. Investigation of other possible starting values
11. Assembling of a function to compute the Starting Value

Step 1: Choice of iteration method

In previous projects at WL|Delft Hydraulics, Groenewegen and Cornellisse have applied a Newton and a DZANLY solver, respectively, to solve the wave number in complex implicit dispersion relations. A main problem was that these applications did not always find a proper solution. As explained in section 2.3, each dispersion relation has more than one solution for the wave number. In the previous attempts a small change in input parameters could lead to a totally different solution, probably one of the other roots. In some cases no solution was found at all. Globally comparing the performance of the various methods, the DZANLY method seemed to converge succesfully in more cases and from greater distances to a solution that could be the proper root. This better convergens and more robust performance can be explained by the more sophisticated character of the procedure. Because

no good approximations for the starting value were available at that moment, a robust procedure was needed. Therefore it was decided to investigate the DELFT dispersion relation with the DZANLY iteration method.

Step 2: Choice of a preliminary starting value

The DELFT dispersion equation is an extension of Gade. Therefore it was decided to start the investigation with the analytical expression of Gade as preliminary starting value.

Step 3: Normalization

To evaluate the behaviour of the solving routine and the behaviour of the function, the results have to be presented in an informative and orderly way. In literature, most of the time the real and imaginary wave numbers are plotted while only one parameter is variable and all others are kept at the same value. Following Gade (1958), most authors use a normalization in which the wave number is divided by the shallow water wave number and the mud layer thickness by the wave boundary layer thickness of the viscous sublayer. By evaluating the results in this way, it is possible to distinguish a value for the running parameter or for the dimensionless parameter on the x-axis where the function or the iteration procedure does not function well. But as soon as the value of one of the other parameters changes, the value of the running (normalized) parameter where the results show erroneous values changes as well. Summarizing, the presentation of the (dimensionless) results as function of one (dimensionless) parameter is not sufficient to determine where in the parameter domain errors occur. Obvious reason for this is that many parameters are present in the dispersion equation.

A new normalization is carried out to determine physically meaningful dimensionless parameters that span the parameter domain. These dimensionless parameters are used in the visualization and are used to identify the location of the erroneous results. Because of the importance of this step, the normalization and the results are more thoroughly discussed in section 4.3.

Step 4: Visualization

Based on the normalization, contour plots could be made that show the normalized wave number against the normalized mud layer thickness $H_{m0}/(2\nu/\omega)^{1/2}$, the ratio of the mud and water layer thicknesses H_{m0}/H_{w0}, and the relative water depth kH_{w0}.

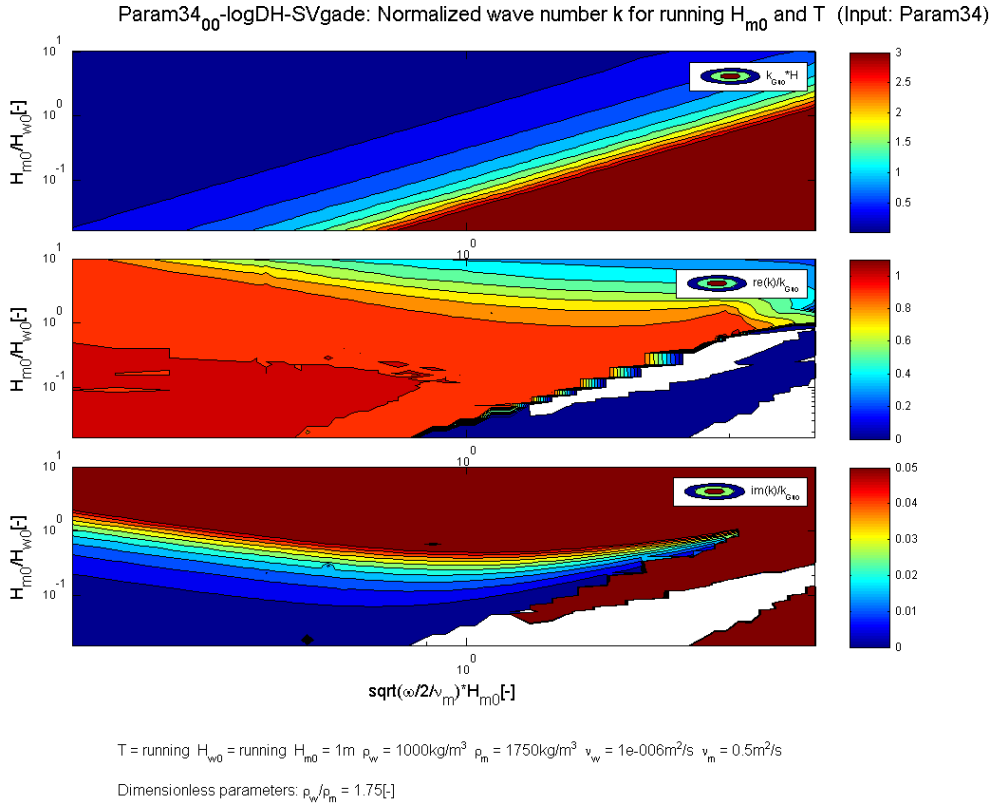

Figure 12 Contour plot of the real (middle panel) and imaginary (bottom panel) wave number normalized with the wave number for cases without mud. The wave number is plotted as function of the normalized mud layer thickness and the ratio of layer thicknesses. The upper panel shows the relative water depth kH_{w0}. The white areas indicate areas where the solving routine does not give a solution.

Step 5: Evaluation of the preliminary results

Two issues were subject of the evaluation: the behaviour of the solving routine and the behaviour of the dispersion equation itself. It was assumed that the DELFT dispersion equation would show the same kind of behaviour with respect to the imaginary wave number as Gade: a smooth function, a maximum in the damping at values for the normalized mud layer thickness of the order 1, and values for the imaginary wave number of the same order or one order lower or higher. In that case the peaks and the areas of unexpected high or low values or no results at all could be attributed to malfunctioning of the solving routine.

Investigation of the results with visualizations as discussed under step 4, clearly indicated that the bigger part of the erroneous results occurred at higher values of kH_{w0}. Therefore, an other starting value had to be found for this part of the domain.

Step 6: Investigation of other possible starting values

A possible other starting values is the solution for the wave number in the situation of two non-viscous layers with different densities. For small density differences, an explicit

expression is given in C. Kranenburg (1998). But for small density differences and equal current velocity in both layers, the external propagation velocity in a system of two non-viscous layers is the same as in a one layer system. The expression for higher density differences is implicit for the wave number k (C. Kranenburg, 1998). Therefore the wave number for systems of one layer of intermediate or deep water depth was chosen as second starting value to investigate. This is the regular dispersion equation for waves in water, which is implicit for the wave number as well, but for which various explicit approximations exist (Fenton, 2006). Based on Fenton's investigation of the quality of various approximations it was chosen to work with the approximation of Guo (2002).

The results obtained with this starting value where investigated in the same way as the results obtained with Gade as starting value. For higher values of the relative water depth kH_{w0} the results where much better: a smooth curve without peaks or unexpected high or low values. On the other hand, for low values of kH_{w0} the results where less positive: area's with no solution appeared in this part of the domain.

Step 7: Assembling the function to compute the Starting Value

The two functions where merged to acquire a function that determines a suitable starting value for the whole domain. At low values of kH_{w0}, Gade is dominant in the determination of the starting value. At high values of kH_{w0}, Guo is dominant. The contribution of each function for kH_{w0}-values in between is determined with a hyperbolic tangent. (The result is described in formulae in 4.2.3). The kH_{w0}-value of equal contributions of Gade and Guo, the constant c in (117), is determined as follows:

First it is tried to identify a dividing line between the area where Gade gives good results and the area where Guo gives good results. This is done by plotting the difference between the two outcomes as a function of kH_{w0} (see Figure 13).

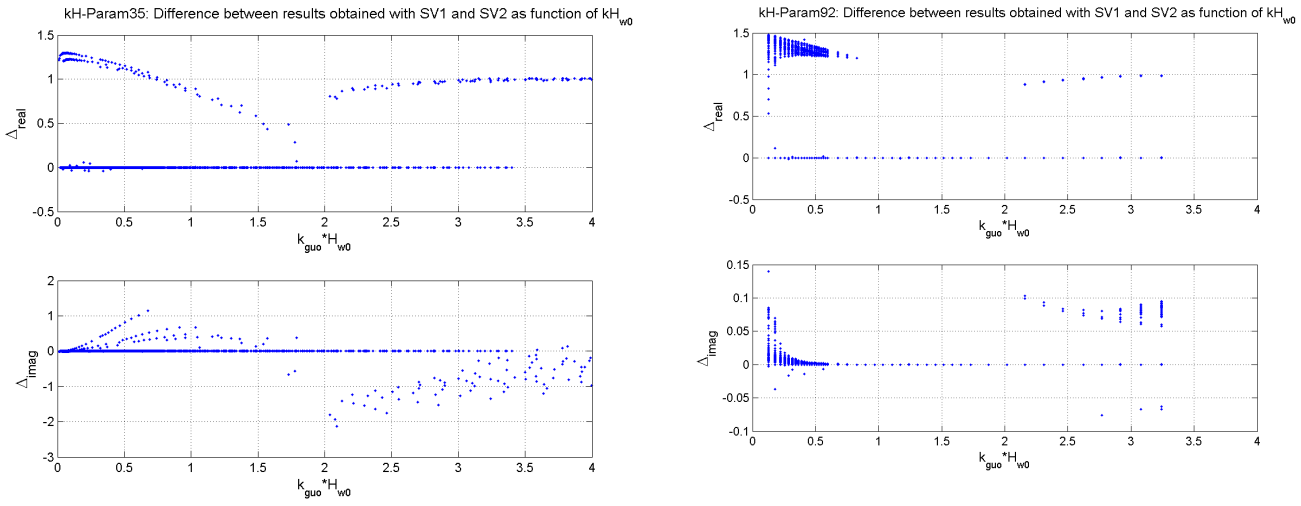

Figure 13 Plot of the difference between the results for DELFT dispersion equation obtained with Starting Value I: Gade-analytical and obtained with Starting Value II: Guo, as function of kH_{w0}. This plot shows results for two parameter sets (left, right) and shows the result for the real (top) and the imaginary (bottom) wave number.

Figure 13 shows the difference in the results obtained with the two starting values. The results are compared with each other with:

$$\Delta_{\text{real}} = \frac{\text{Re}(k)_{\text{obtained with SV2}} - \text{Re}(k)_{\text{obtained with SV1}}}{\text{Re}(k_{\text{SV2}})} \quad (120)$$

$$\Delta_{\text{imag}} = \text{Im}(k)_{\text{obtained with SV2}} - \text{Im}(k)_{\text{obtained with SV1}} \quad (121)$$

In the area where almost all points are on the zero line, both starting values interate towards the same solution. The various pictures show that this is the case at kH_{w0} is around 1.5 to 1.7. Sometimes the area of identical results is very small (left graph), sometimes it is much wider (right).

The parameter a, determining the widht of the 'merging-zone', is choosen by fitting a graph of the new starting value by trial and error over the results of the previous calculations for various parameter sets.

4.3 Normalization

The DELFT dispersion equation resulting from the schematization of De Wit contains a high number of variables. A reduction of the parameters involved is needed to get some insight in the behaviour of the function and to present the results clearly. A dimensional analysis is carried out to reduce the parameters and also to get more insight in physical relevant combinations of parameters.

4.3.1 Dimensional analysis

The **Buckingham Π theorem**, a key theorem in dimensional analysis, forms the basis of this analysis.

The Buckingham Π theorem states that, if we have a meaningful equation such as

$$f(q_1, q_2, \ldots q_n) = 0 \quad (122)$$

where the q_i are the n physical variables, and they are expressed in terms of k independent physical units, then the above equation can be restated as

$$F(\pi_1, \pi_2, \ldots \pi_p) = 0 \quad (123)$$

where the π_i are dimensionless parameters constructed from the q_i by $p = n - k$ equations of the form

$$\pi_i = q_1^{m_1} q_2^{m_2} \ldots q_n^{m_n} \quad (124)$$

where the exponents m_i are rational numbers (http://en.wikipedia.org/wiki/Buckingham).

The DELFT dispersion equation can be written as

$$f(\omega, H_{w0}, H_{m0}, \rho_w, \rho_m, \nu_m, g, k) = 0 \quad (125)$$

In this equation the viscosity of water is not taken into consideration according to the assumptions of the schematization. The gravitational acceleration g is taken into account, because this is a dimensional parameter (although not variable in our problem). The number of physical variables n becomes eight. The dimensional matrix looks as follows:

	quantity	Omega	Hw0	Hm0	rhow	rhom	num	g	k
quantity	unit	1/s	m	m	kg/m3	kg/m3	m2/s	m/s2	1/m
M	kg	0	0	0	1	1	0	0	0
L	m	0	1	1	-3	-3	2	1	-1
t	s	-1	0	0	0	0	-1	-2	0

Table 5 Dimensional Matrix of the DELFT dispersion equation

Only three independent physical units are present ($k = 3$). This means that the number p of dimensionless parameters π with which the problem can be restated, is 5 ($p = n - k = 8 - 3 = 5$).

The Buckingham Π theorem does not state anything about how the dimensionless parameters can be constructed and which set of dimensionless parameters is a relevant set to describe the problem. A plausible criterium in answering the last question is that all the original variables should be present in the final set of five dimensionless parameters. Furthermore, dimensionless parameters with sound physical meanings are preferred.

There are many ways to determine dimensionless variables. The most simple methods are to use repeaters or primary variables. In the first method k combinations of original variables each with the dimension of one different physical unit are used to make all other parameters dimensionless (see De Vriend, course material River Dynamics, part Scale Models). In the second method a set of k primary variables is choosen from the original variables in such a way that all k physical units are present. (More precise is the criterium that the determinant of the dimensional matrix of these k primary variables has to be non-zero. This does not allow to use one parameter containing two physical units twice, or to use two variables with the same dimensions, like ρ_w and ρ_m). Again, the primary variables can be used to make all the other parameters dimensionless (see Finlayson *et al.*, 1997, p.3-89).

If we apply the method of primary variables on our problem, sets of primary variables can be found by taking one variable out of each row below. This ensures that all k physical units are present in a set of primary variables.

$$\begin{aligned} &\text{kg:} && \rho_w, \rho_m \\ &\text{m:} && H_{w0}, H_{m0}, \nu_m, g, k \\ &\text{s:} && \omega, \nu_m, g \end{aligned} \tag{126}$$

Choosing one parameter twice is not allowed. When v_m is chosen from row 2, the choice in row three is restricted to ω or g, otherwise the determinant of the dimensional matrix of the three primary variables would be zero.

The (sets of) dimensionless parameters that can be generated are thoroughly investigated with the various methods. Finally the most obvious primary variables turn out to give the physically most interesting dimensionless parameters.

$$\text{A:}\quad \rho_w, H_{w0}, \omega \rightarrow \left(\pi_1 = \frac{H_{m0}}{H_{w0}},\ \pi_2 = \frac{\rho_m}{\rho_w},\ \pi_3 = \frac{\nu_m}{\omega H_{w0}^2},\ \pi_4 = \frac{g}{\omega^2 H_{w0}},\ \pi_5 = kH_{w0} \right) \tag{127}$$

$$\text{B:}\quad \rho_w, H_{m0}, \omega \rightarrow \left(\pi_1 = \frac{H_{w0}}{H_{m0}},\ \pi_2 = \frac{\rho_m}{\rho_w},\ \pi_3 = \frac{\nu_m}{\omega H_{m0}^2},\ \pi_4 = \frac{g}{\omega^2 H_{m0}},\ \pi_5 = kH_{m0} \right) \tag{128}$$

4.3.2 Physical meanings of dimensionless parameters

In set A and B π_1 and π_2 are ratios of the thickness or the density of the two layers. In set B π_3 is directly related to ratio of the mud layer thickness and the Stokes boundary layer thickness of the mud layer:

$$\left(2\pi_3\right)^{-1/2} = \sqrt{\frac{\omega}{2\nu_m}} H_{m0} \tag{129}$$

This is the parameter often used in the visualizations in literature. π_3 of set A does not really have a sound physical meaning. It relates the water layer thickness to the viscous boundary layer thickness of the mud layer. π_5 in set A is a ratio between water depth and wave length, often used to discriminate between shallow (low values), intermediate and deep water. Although the real wave number will be affected by the mud, the value is dominated by the 'normal' real wave number (Ng, 2000). This is especially true for deep water, because in deep water the wave is not affected by the (muddy) bottom, so k_{mud} and $k_{\text{no mud}}$ will be the same. Therefore the unadjusted wave number calculated via the normal dispersion relation will be a suitable parameter to characterize the waterdepth. Combinations of π_4 and π_5 from set A also give interesting parameters. For the situation without mud we know:

$$\begin{aligned} &\omega^2 = gk \tanh\left(kH_{w0}\right) \qquad (130)\\ &\rightarrow \quad \text{if } \left(kH_{w0}\right) \ll 1 \quad \rightarrow\ \omega^2 = gk\left(kH_{w0}\right) \quad \rightarrow \quad k = \omega / \sqrt{gH_{w0}} \quad \text{(shallow)}\\ &\rightarrow \quad \text{if } \left(kH_{w0}\right) > \pm 3 \quad \rightarrow\ \omega^2 = gk \qquad\quad \rightarrow \quad k = \omega^2 / g \qquad \text{(deep)} \end{aligned}$$

Combining π_4 and π_5 from set A results in the following interesting parameters:

$$\pi_5 \sqrt{\pi_4} = kH_{w0} \sqrt{\frac{g}{\omega^2 H_{w0}}} = k \sqrt{\frac{gH_{w0}}{\omega^2}} = k / k_{\text{no mud, shallow}} \tag{131}$$

$$\pi_5 \pi_4 = kH_{w0} \frac{g}{\omega^2 H_{w0}} = k \frac{g}{\omega^2} = k / k_{\text{no mud, deep}} \tag{132}$$

Of course it is also possible to relate the wave number for the mud affected situation with the wave number for intermediate water depth without mud. This becomes clear when we

use the approximation formula of Guo (Guo 2002, Fenton 2006) for the normal dispersion relation:

$$kH_{w0} = \frac{\omega^2 H_{w0}}{g}\left(1-\exp^{-\left(\omega\sqrt{H_{w0}/g}\right)^{5/2}}\right)^{-2/5} \tag{133}$$

in which kH_{w0} is completely determined by π_4. So

$$\pi_5 f\left(\pi_4\right)^{-1} = k / k_{\text{no mud, intermediate water depth}} \tag{134}$$

The considerations above are the basis for the presentation of the results in graphs of the wave number normalized with the unaffected wave number for intermediate water depth ($\pi_{5A} f(\pi_{4A})$) as a function of Stokes layer normalized mud layer thickness ($f(\pi_{3B})$) and the ratio of the layer thicknesses (π_1) while the density ratio (π_2) is kept constant:

$$\pi_{5A} f\left(\pi_{4A}\right)^{-1} = f\left(\pi_{1A}, \pi_{2A}, \pi_{3B}\right) \tag{135}$$

4.4 Results for the wave number

4.4.1 Introduction

The wave number according to the DELFT dispersion equation (chapter 3) has been computed using the solving routine presented in section 4.2 and can be plotted using the normalization discussed in section 4.3. This section presents results for the wave number and gives an evaluation. This evaluation discussed both the behaviour of the solving routine and the behaviour of the function itself. To make this possible, the results are compared with results obtained for other dispersion equations. A representative subset of the results is presented in Figure 14 and Figure 15.

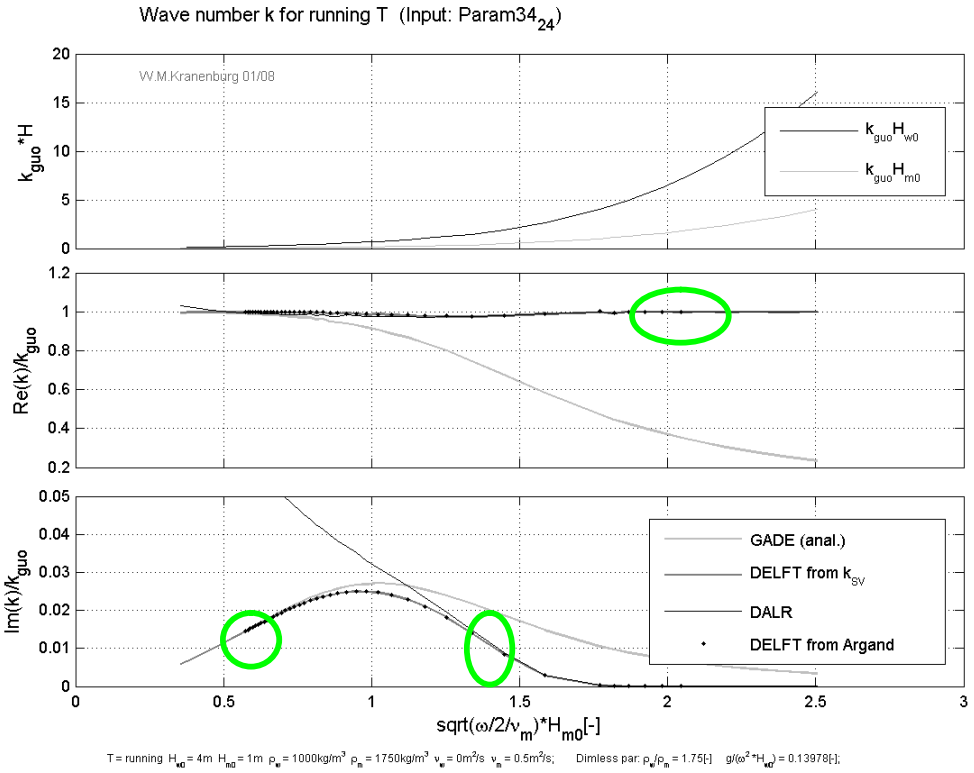

Figure 14 Plots of the normalized real (middle panel) and imaginary (bottom panel) wave number as function of the normalized mud layer thickness for the dispersion equations Gade, DELFT and Dalrymple and Liu (1a). The kH_{w0}- and kH_{m0}-values are given in the top panel.

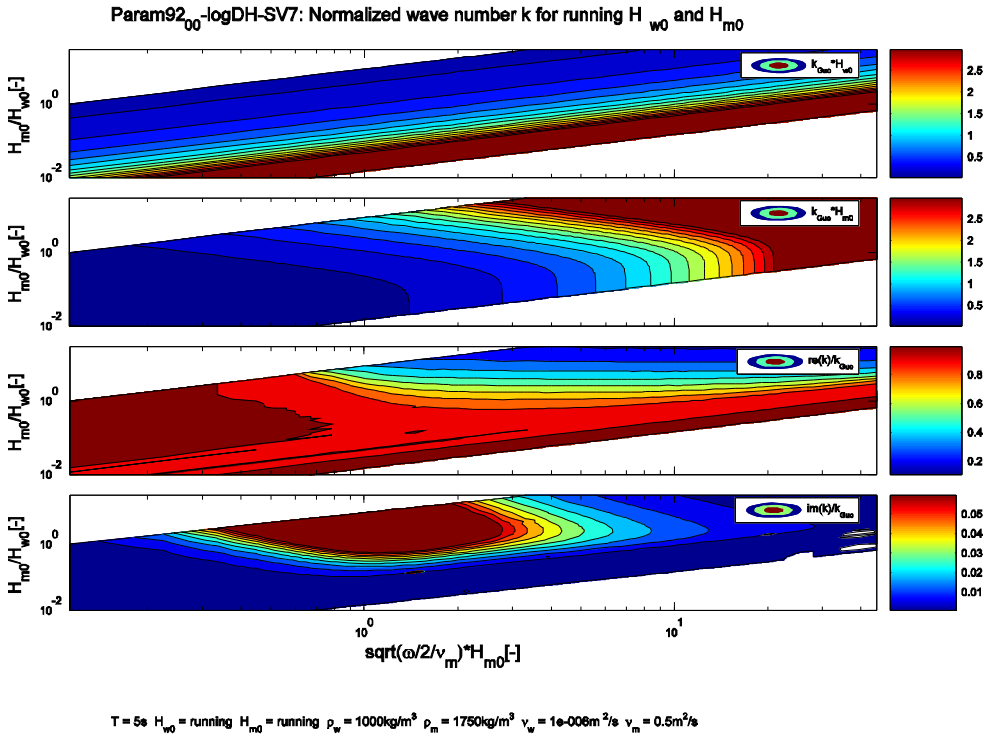

Figure 15 Contour plot of the real (panel 3) and imaginary (panel 4) wave number as function of the normalized mud layer thickness and the ratio of water and mud layer thickness. Panel 1 and panel 2 show kH_{w0}- and kH_{m0}-values. This graph is obtained with the starting value described in section 4.2.3.

4.4.2 Evaluation of behaviour of solving routine

In evaluating the solving routine, three kinds of errors are distinguished:
1. Occasional errors
12. More persistent errors
13. No (positive) results at all

In case of errors of the first kind, the iteration procedure fails on a certain point in the domain, while around this point the procedure works well. These errors are indicated by dots, smudges or occasional anomalies in a contour that in the rest is smooth. The more serious errors of the second category are indicated by irregular contours, sharp edges in contours that are in the rest gradually bending, and bigger patches of different colours. These characteristics indicate that the iterations converge to another solution. When areas in a picture are not filled at all, this is an indication of non-convergence of the iteration.

With this distinction it was possible to asses the various starting values as well as the merged starting value function. Figure 15 shows a smooth contour for the wave number both for low and high values of kH_{w0}. This indicates that the solving routine functions well for all water depths. Simulations for other parameter sets give the same results, although occasional errors still occur.

In this investigation, the routine is run with thight criteria for the iteration. Therefore, many iterations are carried out before a solution is returned. A consequence is that this routine is quite time consuming.

4.4.3 Evaluation of behaviour of the function

The evaluation of the behaviour of the function itself is mainly based on Figure 14. At cases comparable with the cases investigated by GADE (shallow water, low values for kH_{w0}), the DELFT dispersion equation shows the same behaviour as GADE (circle). The more a certain parameter combination represents shallow water, the better coincides DELFT with GADE.

For higher frequencies, the relative water depth is larger. Also the normalized mud layer thickness is larger. In this case, the behaviour of DELFT is similar to Dalrymple and Liu (1a) (vertical oval), which has as basic assumption that the mud layer thickness is large compared to the Stokes boundary layer thickness.

Very high frequencies imply a large value for the relative mud layer thickness and a large value for kH_{w0}. In this case, the real wave number seems to be hardly affected by the mud (horizontal oval). This is a clear difference with the result for GADE, what can be explained by the fact that GADE is not valid for this case of deep water.

4.5 Alternative method: Argand diagrams for increasing viscosity

4.5.1 Description of the method

As a test of the solving routine, the wave number according to the DELFT dispersion equation is computed with an alternative method. This more extended approach is taken from dynamic stability analysis in mechanics of structures. Examples can be found in Païdoussis (1998), where the method is applied to pipes conveying fluid.

The method works as follows: First, the situation without damping is investigated (mud viscosity $\nu_m = 0$). This comes down to determination of the zero crossings of a real function of the real wave number k. Iterations with the presented DELFT dispersion equation do not give answers for $\nu_m = 0$ (because of divisions by zero). Therefore the DELFT dispersion equation is reduced to a real function belonging to the situation without damping by elimination of the terms related to damping. This reduction together with some basic checks of the result is presented in appendix C. The zero crossings of DELFT-reduced are found by walking along the k-axis and computing the function for each step. If the sign of the answer changes between two values of k, the k-value of the zero crossing is assumed to be in the middle of these values.

When the real wave numbers k are found that belong to the situation without damping, the viscosity ν_m is increased in small steps. The values of k_{re} and k_{im} for which the complex DELFT dispersion equation is zero are determined with the iteration method DZANLY, with the (real) wave number for the situation without damping as starting value of the first iteration. The (complex) outcome of the iteration is used as input for the next iteration, in which ν_m is increased again. This procedure is continued untill ν_m has reached his proper value.

The advantage of this approach is that a starting value is used that is relevant and close to the proper solution. It is possible to gain insight in the development of all the wave numbers k for increasing values of ν_m. Because of the fact that it is possible to follow the wave numbers starting from the situation where $\nu_m = 0$, both the physical meaning and the number of solutions are clear. An easy way to present the results, is to plot the results of each iteration step in the complex plain. Such plots are also called **Argand diagrams**.

4.5.2 Situation without viscosity

Figure 16 shows the reduced function for a situation without damping for three arbitrary parameter sets. The picture shows clearly that there are two zero crossings at each site of the y-axis. When we connect the zero-crossings for various values of omega, a graph of the dispersion relation for the situation without damping is achieved (plotted in Figure 17 as function of wave angular frequency ω and of the wave period T for the positive solutions only). These values for the real wave number k_{real} are used as starting point for the iterations with increasing viscosity.

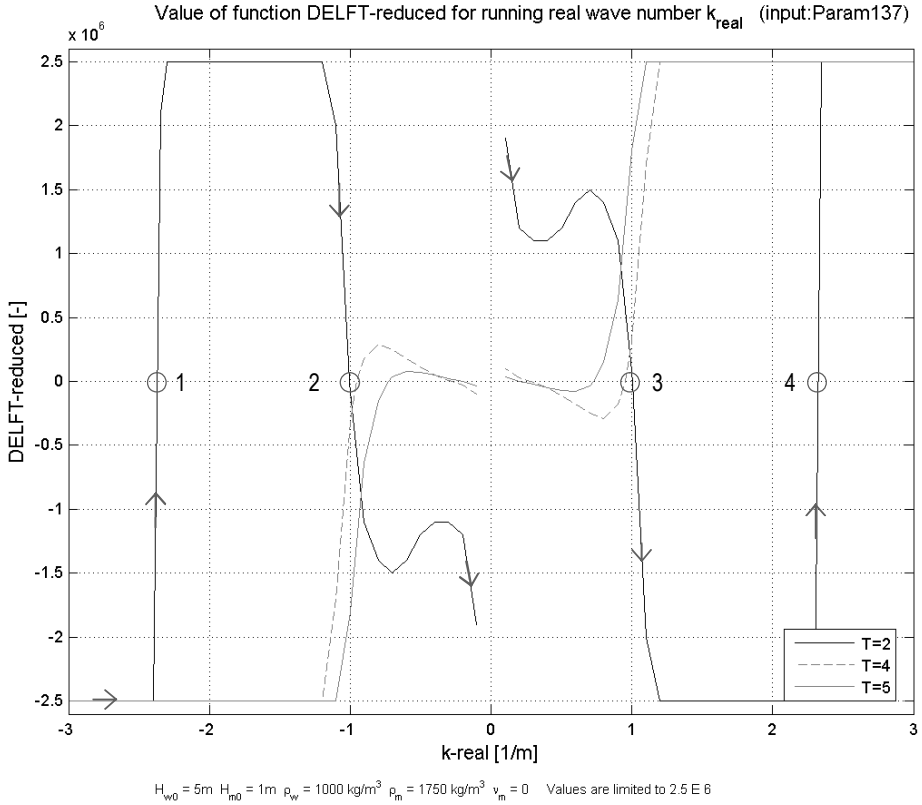

Figure 16 Graphs of the function DELFT-reduced (reduction of DELFT for the situation without damping) as function of the real wave number *k* for three values of the wave period *T*. Walking from left to right along the function (indicated for T=2) the x-axis is passed four times (neglecting the results at *k*=0). The numbers 1 to 4 represent IWneg, EWneg, EWpos IWpos respectively (see Table 1 in section 16)

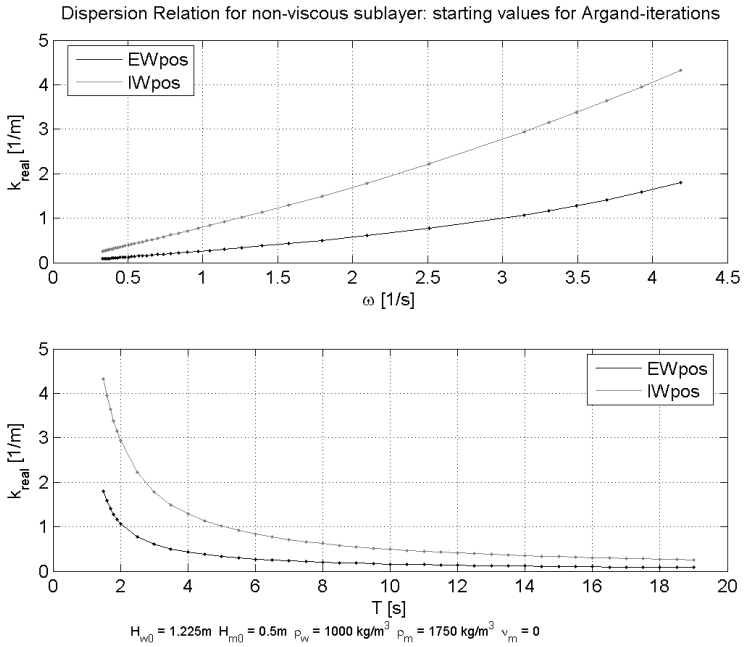

Figure 17 Situation without damping: development of the real wave numbers *k* as function of the wave angular frequency ω (top) and the wave period *T* (bottom)
External wave in positive direction = zero crossing 3 in Figure 16
Internal wave in positive direction = zero crossing 4 in Figure 16

4.5.3 Increasing viscosity

For each combination of parameters an Argand diagram can be drawn for all roots. In Figure 18 Argand diagrams are plotted for various values of T and for all four roots. The viscosity increases from 0 to 0.5 m^2/s.

The roots are presented in Figure 18 in the same order as 1-4 in Figure 16: IWneg, EWneg, EWpos, IWpos.

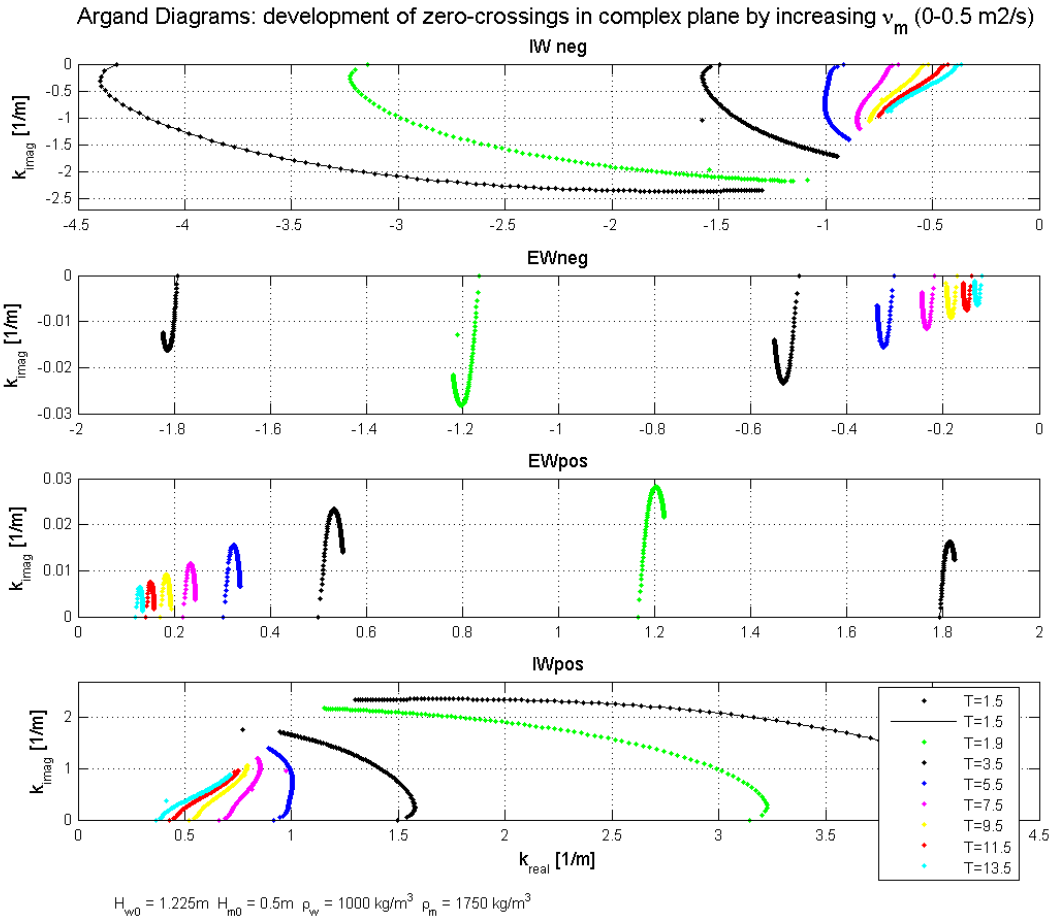

Figure 18 Argand Diagrams; This graph shows the development of the wave number k for increasing values of the mud viscosity ν_m for various values of the wave period T (each presented by a separate sequence of dots)

4.5.4 Maximum viscosity

By plotting the real coordinate and the imaginary coordinate of the last point of each sequence of dots against the wave period (or angular frequency), a graph is obtained of the dispersion relation for a system with a sublayer with ν_m = 0.5 m^2/s and other parameters as indicated. This graph is plotted in Figure 19.

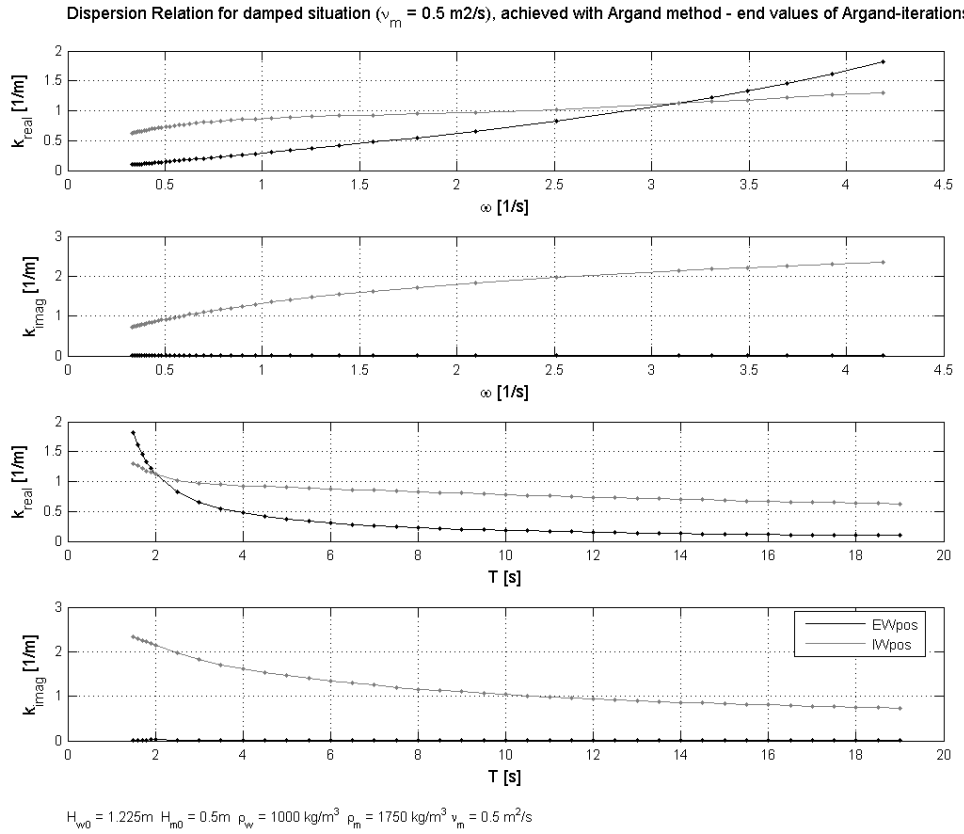

Figure 19 Dispersion relation for the damped situation (ν_m = 0.5 m^2/s). This graph shows the real (1&3) and imaginary (2&4) wave number as function of ω (1&2) and T (3&4).

The results for the DELFT dispersion equation obtained with the solving routine described in 4.2.2 are compared with the results obtained with the Argand method. The latter confirmes the results of the solving routine, as can be seen in Figure 14 where the dots indicate results obtained with the Argand method.

4.5.5 Discussion

Based on the graphs presented in the previous sections, a few conclusions can be drawn:

- Subplot 2&3 of Figure 18 show that for a certain parameter set there can be a value for the viscosity where the damping reaches a maximum. The smaller the wave period, the larger the viscosity value at which this maximum is reached (see e.g. plot 3, the Argand Diagram for T = 1.5 (at the right side): the highest value for k_{imag} is reached just before the maximum viscosity is reached).
- The real wave numbers of the internal waves (subplot 1&4, Figure 18) are very sensitive for the increasing viscosity. The real wave numbers of the external waves (subplot 2&3), are much less sensitive.
- The imaginary wave number of the internal waves (subplot 1&4) are an order 10^2 larger than the imaginary wave number of the external waves (subplot 2&3), which means that the internal waves decay faster than the external waves.
- The real wave numbers of the internal waves (subplot 1&4) can be decreased so much with increasing viscosity that their values come close to or even become smaller than

the real wave numbers of the external waves (subplot 2&3). (Compare also Figure 19, panel 1 and 3 with Figure 17 panel 1 en 2, in Figure 19 the lines cross each other at ω = 3.1 or T = 2).

- The convergence is not always succesful. With other parameter set, jumps were found in the value of k_{imag} of the order 10^2 (probably convergence to another solution) and also Figure 18 shows a few inexplicable outliers.

The crossing of the lines in Figure 19 is remarkable. Attention should be given to this property especially when an iteration method is used that calculates the answer by iteration directly from one starting value for the real wave number to the answer. The imaginary wave number of the internal wave remains an order 10^2 larger than the imaginary wave number of the external wave. So discrimination between roots is remains possible.

The Argand method indicates very well the development of the wave numbers starting from starting values that are easily to compute and have a clear physical meaning. This is a great advantage of this method. The general application of this method can be hindered by the fact that also this method does not always iterate to the proper solution and that this method does consume more computation time, depending on the number of steps while increasing the viscosity and the criteria of the iteration method (maximum error, maximum number of staps).

A remark on the number of solutions for the DELFT dispersion equation:

As indicated in Table 1, section 2.3.1, four solutions are present for a system of two non-viscous layers with different density. Also Gade's dispersion equation (eq. 19), the shallow water limit of the DELFT dispersion equation, has four solutions. So there are good reasons to state that the DELFT dispersion equation has four solutions as well. Verification of this statement using **Cauchy's Argument Principle** indicated the presence of more than four solutions, the exact number depending on the size of the investigated complex domain. The 'extra' solutions appear to be almost completely imaginary. There presence probably could be explained by the fact that an hyperbolic function of a imaginary parameter has infinitely many solutions, e.g.:

$$\cosh(x) = \cos(x/i) = 0, \quad \rightarrow \quad x = i(n+1/2)\pi \qquad \text{where } n = 0,1,2,3,\ldots$$

The physical meaning of these 'extra' solutions is not clear, while the physical meaning of the first four solutions is clear because of the ressemblance with the analytical solutions of the limits. Therefore, these 'extra' solutions are not investigated further.

4.6 Discussion, conclusions and recommendations

This chapter described the DELFT dispersion equation and a solving routine to compute the wave number with this dispersion equation. A starting value is proposed that is assembled from explicit expression for the shallow water and the deep water limit of the DELFT dispersion equation. In the investigation of the results, attention is given to the behaviour of the solving routine and the behaviour of the function itself. Contour plots of the results show that the assembled starting value yields results over the entire domain. Comparison of these results with results for other dispersion equations show that the behaviour of the function is plausible. In case of shallow water, the results coincide with Gade. In case of a large normalized mud layer thickness, the results coincide with Dalrymple and Liu (model 1a). In case of deep water, the real wave number will not be adjusted by the mud.

The method is compared with results obtained with an alternative method: the Argand method. This method gives the same results. It also showed that the imaginary wave number for the internal wave is two orders larger than the imaginary wave number of the external wave. This means that the internal wave is damped very fast and is a justification of the statement in section 2.3.2 that the external wave is the relevant wave for this study.

Although the solving routine gives results over the entire range of kH_{w0}, occasional errors still occur. The routine is also quite time consuming. Depending on the consequences of these disadvantages for implementation into SWAN, it can be worth to improve the solving routine. While improving the routine, it is important to realize that the initial motivation for employing DZANLY (an apparent better convergence to the proper solution from inaccurate initial approximations compared to a Newton method) is not that relevant anymore, because a more accurate starting value is found.

5 Recent implementations of viscous two-layer models into wave models

5.1 Introduction

It is only recently that the development started to implement the viscous two-layer models described in chapter 2 into numerical wave (energy) models. These wave models are not only applicable for the theoretical case of uni-directional and mono-chromatic waves over flat bottoms, but can deal with the more realistic circumstances of wind and swell sea approaching from various directions and propagating over an area of varying bottom geometry.

This chapter discusses three recent implementations of viscous two-layer models into wave models. Prior to the descriptions of these implementations, some attention is given to the principles of the wave energy model SWAN (section 5.2) and to mud in SWAN till 2006 (section 5.3). Section 5.4 discusses the implementation of De Wit into SWAN as described in Winterwerp *et al.* (2007). Section 5.5 discusses the implementation of Ng into SWAN as described in Rogers and Holland (in review). Section 5.6 discusses the implementation of Ng into a phase-resolving wave model as described by Kaihatu *et al.* (2007). This chapter is finalized with a discussion (section 5.7) that gives the foundation for the remaining part of this study by discussing the most important differences between the various implementations, indicating the priorities in further model development and resuming the fundamental questions on the implementation of viscous bottom models into the wave energy model SWAN.

5.2 The SWAN wave model

Section 5.2.1 describes the key equation of the wave model SWAN and the processes it takes into account. Section 5.2.2 describes more generally the classification of SWAN. The sources for these sections are Booij *et al.* (1999), Ris *et al.* (1999), the technical documentation of SWAN (SWAN team, 2007) and Holthuijsen (2007).

5.2.1 Model Set-up

The wave action density balance

The SWAN model is based on the description of waves in a two-dimensional wave action density spectrum for each grid point and timestep: $N(\sigma,\theta; x,y,t)$. The balance equation for the wave action density is:

$$\frac{\partial}{\partial t}N+\frac{\partial}{\partial x}c_{g,x}N+\frac{\partial}{\partial y}c_{g,y}N+\frac{\partial}{\partial \theta}c_{\theta}N+\frac{\partial}{\partial \sigma}c_{\sigma}N=\frac{S_{tot}}{\sigma} \tag{136}$$

where
σ = relative radian frequency in a frame of reference moving with the current velocity
θ = wave direction
$N(\sigma, \theta) = E(\sigma, \theta)/\sigma$.

The wave action density spectrum $N(\sigma, \theta)$ and the relative radian frequency σ are used instead of the energy density spectrum $E(\omega, \theta)$ and the absolute radian frequency ω to account for wave-current interaction. In the presence of ambient currents, action density is conserved, whereas energy density is not conserved. In the absence of ambient currents, σ can be replaced by ω and no frequency shifting by currents is present. In that case equation (136) reduces to:

$$\frac{\partial}{\partial t}E+\frac{\partial}{\partial x}c_{g,x}E+\frac{\partial}{\partial y}c_{g,y}E+\frac{\partial}{\partial \theta}c_{\theta}E=S_{tot} \tag{137}$$

Kinematic terms

The left-hand side of equation (136) is the kinematic part. The first term represents the local rate of change of action density in time. The second and third term denote the propagation of action in two-dimensional geographical space, with the group velocity $c_{g,x}$ and $c_{g,y}$ as the propagation velocities in x and y space. These terms account for shoaling. The fourth term represents depth-induced and current-induced refraction, with propagation velocity c_{θ} in θ space. The fifth term of equation (136) represents the effect of shifting of the relative frequency due to variations in depth and mean currents. In case of external conditions that vary only slowly, the situation can be considered as stationair. In that (quasi-)steady case the first term can be omitted. When also the waves come in at right angles to a shore with straight and parallel depth contours, the situation can be considered as one dimensional and no refraction will occur. In that case only the second term remains on the left-hand side.

Source and sink term

The right-hand side contains the total source and sink term S_{tot} in terms of energy density. This term contains the effects of generation, dissipation and non-linear wave-wave interaction.

$$S_{tot} = \underbrace{S_{wind}}_{\text{Generation}} + \underbrace{S_{wc}+S_{b}+S_{br}}_{\text{Dissipation}} + \underbrace{S_{nl4}+S_{nl3}}_{\text{Wave-wave interactions}} \tag{138}$$

Energy is added to the spectrum by transfer of wind energy to the waves (S_{wind}). Energy is dissipated by white-capping (S_{wc}), bottom induced dissipation (S_b) and depth-induced surf breaking (S_{br}). White-capping can be described as breaking of waves controlled by the wave

steepness. Bottom induced dissipation can be caused by bottom friction, bottom motion, percolation losses or bottom irregularities. For continental shelf seas with sandy bottoms, bottom friction (S_{bfr}) is the dominant term. The nonlinear wave-wave interaction consist of quadruplet wave-wave interactions (S_{nl4}) and triad wave-wave interactions (S_{nl3}). Quadruplet wave-wave interactions are dominant in deep water. This mechanism transfers wave energy from the spectral peak to lower and to higher frequencies. This mechanism is responsible for the evolution of the spectrum from only wind sea to a spectrum containing swell as well. In shallow water, also triad wave-wave interactions occur, transferring energy from lower frequencies to higher frequencies. These mechanisms are nonlinear, but the spatial scale on which these phenomena happen, is a number of wave lenghts (quite long compared to e.g. depth-induced breaking).

5.2.2 Classification

The SWAN model is classified as *a third generation, phase-averaged, Eulerian model for coastal regions*. Without discussing the development from first and second to third generation wave models, we mention that in a **third-generation** wave model the relevant processes are represented explicitly without a priori restrictions on the evolution of the spectrum. The model is called phase-averaged because it considers the **phase-averaged** energy by relating this quantity to the surface wave amplitude via $E = \frac{1}{2}\rho g a^2$. The model does not predict time series of water level elevations, but statistical properties of the waves via the energy spectrum. The fact that the model considers phase averaged properties only, makes the model applicable on a larger scale (compared to e.g. phase-resolving models). The model uses an **Eulerian** approach, on which the wave evolution is formulated on a grid. This is quite common for deep-ocean or shelf-sea wave models. All processes then can be included as sources and sinks in the basic equation. Drawbacks of this approach in coastal waters are the absence of diffraction and the use of linear wave theory for propagation. These are drawbacks because diffraction and nonlinear phenomena become more important in the presence of breakwaters and close to the coast. Compensation of these drawbacks is possible via the other terms. The real important adaption in SWAN compared to third generation deep ocean models is the adaptation of the formulation of various processes for **shallow water**, the addition of bottom dissipation, depth-induced wave breaking and triad wave-wave interactions (typically shallow water phenomena) and the use of **implicit** propagation schemes. Explicit schemes, normaly used for deep ocean models, are not efficient for a coastal wave model. This is caused by the Courant criteria $\Delta t < \Delta x / c_{g,x}$ and $\Delta t < \Delta y / c_{g,y}$, that states that the wave energy may not travel more than one grid cel in one time step, while the grid cells has to be small, because of the strong changes in the seabed topography. But also when using an implicit scheme, Δt still has its limits, namely to be much smaller than the time scales of the phenomena involved. But this (less stringent) criterium is related to accuracy in stead of stability.

5.3 Mud in SWAN till 2006

In case of sandy bottoms the bottom friction S_{bfr} is the dominant term in the bottom-induced wave damping S_b. When fluid mud is present, the bottom-induced wave damping might be dominated by energy dissipation in the viscous mud layer ($S_{b,m}$).

The absence of a mud-related dissipation term in SWAN was often compensated by manipulation of existing bottom friction parameterizations. In the calibration, the bottom friction is increased to get a dissipation in the model that corresponds to the observations in the presence of mud. Numerical experiments by Sheremet and Stone (2003) show that this manipulation results in damping of low-frequency waves, with almost no effect in the high-frequency part of the spectrum, while they report to have observed damping at the high-frequency part as well. These results underline the need for the implementation of a physically correct mechanism for mud-induced dissipation.

5.4 Implementation of De Wit into SWAN by Winterwerp *et al.* (2007)

5.4.1 Introduction

Winterwerp *et al.* (2007) describes the first implementation of a viscous two-layer model in SWAN, the validation of this model against small-scale wave attenuation measurements carried out in a laboratory wave flume and the application of this model to predict wave attenuation in the Guyana coastal system.

This section describes the principles of this model (5.4.2) and shortly discusses the results of the simulations (5.4.3). The constraints of this model are discussed in section 5.4.4.

5.4.2 Principles of the model

Dispersion equation

The dispersion equation used in this model is the dispersion equation of De Wit (see 2.4.3).

Energy dissipation term

The dispersion equations in chapter 2 result in a wave number for uni-directional, mono-chromatic waves over a bed of uniform bathymetry. To implement mud-induced damping into SWAN, a formulation for the energy dissipation $S_{b,m}(\omega,\theta)$ is required, where $S_{b,m}(\omega,\theta)$ is a sink term accounting for viscous dissipation in the mud layer. Winterwerp *et al.* (2007) use the expression for the energy dissipation obtained by Gade (1958, Part II). This expression was obtained by Gade by integrating the work done by the surface waves on the mud layer below over one wave period. This term is implemented in SWAN using the principle that the

equation (139) can be applied for each wave frequency and direction and that superposition of the individual solutions is allowed. This principle follows from linear wave theory, where the various waves are considered independently. Application of this principle is common in spectral wave models, including SWAN. The formula for the energy dissipation is written here in the same symbols as used in the remainder of this report and corrected for the omission of the frequency in Gade (1958)):

$$\frac{S_{b,m}}{E} = -\alpha\omega g H_{w0} R \frac{b}{a} \sin\left(\varphi - \beta\right) \tag{139}$$

where R and β (directly related to amplitude and phase of the complex wave number) result from:

$$Re^{i\beta} = \left(\frac{k}{\omega}\right)^2 \tag{140}$$

and the amplitude ratio b/a and phase difference φ between interface and surface elevation follow from:

$$\frac{b}{a} = \sqrt{\left(1 - gH_{w0}R\cos\left(\beta\right)\right)^2 + \left(gH_{w0}R\sin\left(\beta\right)\right)^2} \tag{141}$$

$$\tan\varphi = \frac{-H_{w0}gR\sin\left(\beta\right)}{1 - H_{w0}gR\cos\left(\beta\right)} \tag{142}$$

The meaning of the symbols are explained in Table 6.

Symbol	Description	[-]
$S_{b,m}$	Energy dissipation caused by viscous mud	Nm/ m^{2}s
E	Present energy per m^2	Nm / m^2
α	Optional calibration coefficient	[-]
H_{w0}	Equilibrium height of water layer, position interface	m
a	Amplitude of water surface displacement	m
b	Amplitude of interface displacement	m
φ	Phase difference between surface and interface displacement	rad
k	Complex wave number	rad / m
ω	Wave (angular) frequency (2π / T)	rad / s

Table 6 Overview of parameters in the expressions for Energy Dissipation by mud

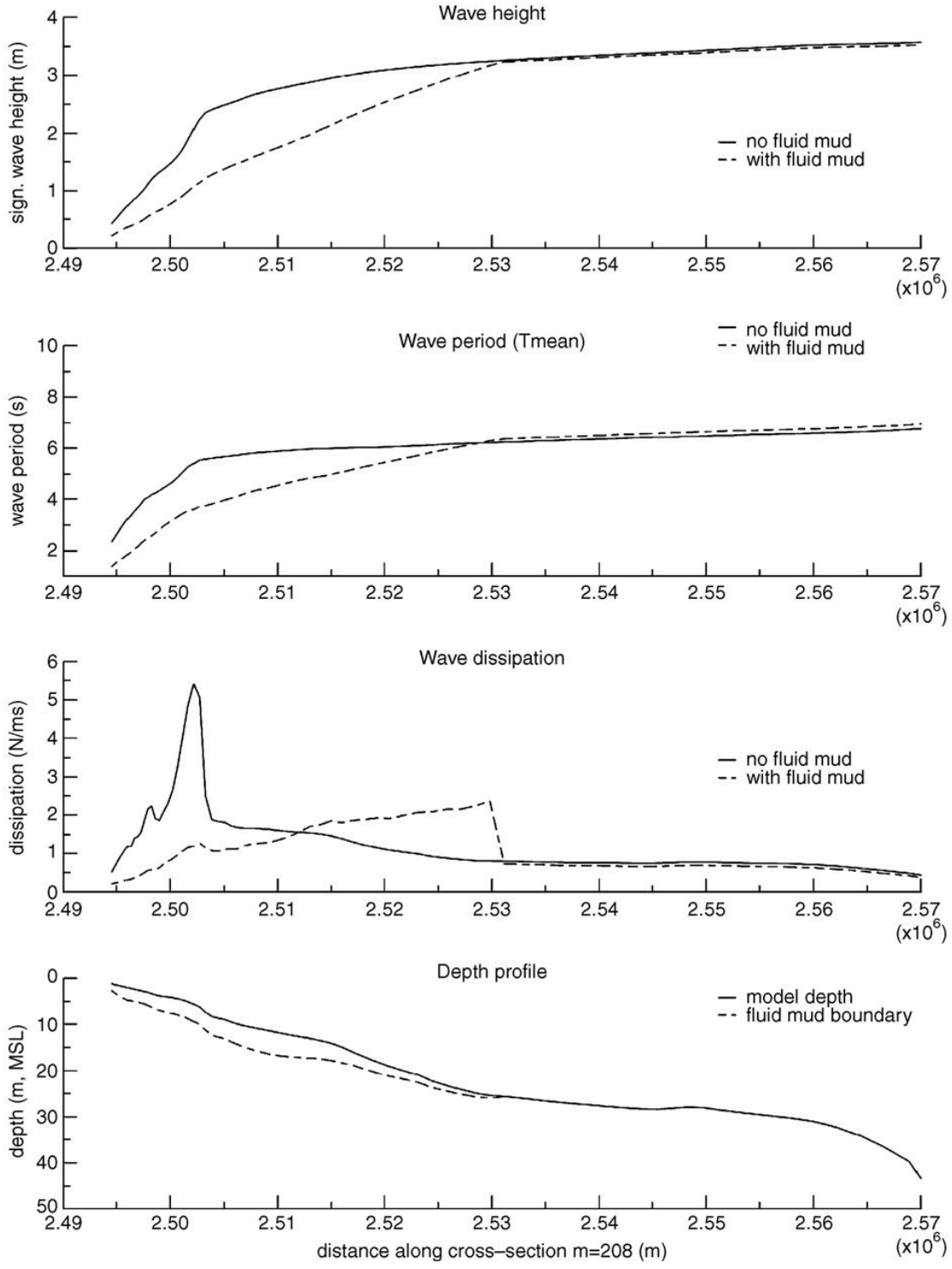

Figure 20 Winterwerp *et al.* (2007) figure 12: Computed cross-shore profiles of significant wave height; mean wave period; wave dissipation; and depth profile together with the thickness of the fluid mud layer as schematised in the SWAN-mud model. Continuous lines: results for simulation without mud. Dashed lines: results for simulations with fluid mud.

5.4.3 Results of simulations

The model of Winterwerp *et al.* (2007) was validated on laboratory experiments by De Wit (1995) and applied on the Guyana coastal system. Direct comparison between nearshore observations and model results was not possible, because of the likely change in the bathymetry since the moment of the wave observations and the moment of the bathymetry observations. But with the model, damping was obtained of the same order of magnitude as in the observations. Comparison between simulations with SWAN-mud and simulations with only a sandy bottom shows much more energy dissipation when mud is taken into account.

It was concluded that *"when including the SWAN mud wave damping model (...), the damping effect of the wave energy is in reasonable agreement with the observations. Wave heights are significantly overestimated in case fluid mud-induced wave damping is not included in the SWAN simulations."* (Winterwerp *et al.*, 2007)

Figure 12 of Winterwerp *et al.* (2007) showes that the dissipation of wave energy starts at the offshore end of the fluid mud layer. From that point on, the wave height decreases gradually. In the simulations with fluid mud, no dissipation by bottom induced wave breaking is present. This agrees with field observations. For the investigated situation, the mean wave period decreases strongly over the fluid mud layers, with a stronger dissipation of the low-frequency waves.

5.4.4 Constraints of the model

The conclusions of Winterwerp *et al.* (2007) clearly show that it is important to implement a separate term into the model representing the mechanism for mud-induced dissipation. In this section constraints of the model are discussed, indicating possibilities for further model development. This evaluation discusses:

1. the used two-layer model
2. the energy dissipation term
3. energy propagation in the model
4. remaining restrictions

The validity of the model is firstly limited by the constrains of the **schematization of De Wit**. The most important restriction is that the schematization of De Wit is only valid for mud layer thicknesses that are small compared to the wave length (see section 2.4.3).

The **implementation of the energy dissipation** into SWAN via the formulation for $S_{b,m}(\omega,\theta)$ obtained by Gade (equation (139)) also introduces a restriction to the model. Gade derived his expression using expressions for the pressure, the amplitude ratio and the phase difference between interface and surface that follow from his shallow water approximation of the two-layer system. Therefore, it is possible that the model will give a erroneous estimation of the energy dissipation at deeper water even though a wave number is used that follows from a dispersion equation that is valid on the concerned domain. If this is the case, the extension of the domain of application to deeper water by using De Wit instead of Gade

is nullified by the use of an energy dissipation term inconsistent with De Wit at deeper water.

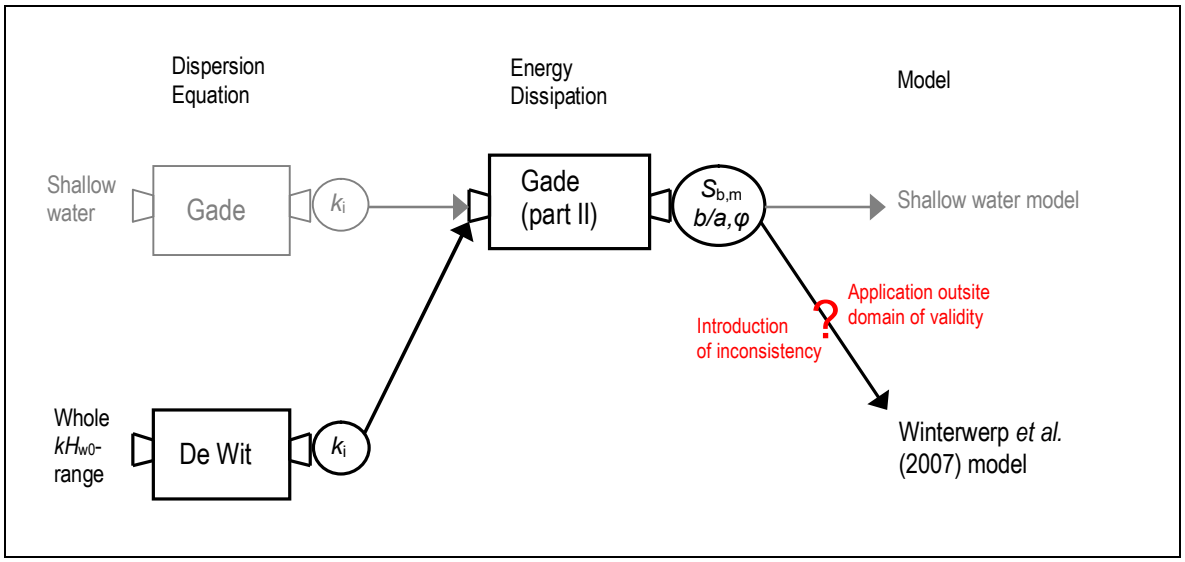

Figure 21 Schematic presentation of the structure of the model of Winterwerp *et al.* (2007) (black lines). The model uses the dispersion equation of De Wit, valid on the whole kH_{w0}-range. The energy dissipation is calculated with the energy dissipation term obtained by Gade (1958, part II), which is derived under the shallow water assumption. The use of this term in the Winterwerp *et al.* model, aimed for the whole kH_{w0}-range, probably introduces an inconsistency in case of application on non-shallow water, in essence reducing the application of the model to shallow water again. The gray chain on top indicates the possible structure of a consistent shallow water model that can be assembled with the equations presented in literature.

(The issue of the consistency between dispersion equation and energy dissipation term is extensively investigated in chapter 6 and 7.)

The **location of the calculation of the wave number** in the code also introduces a restriction in the applicability of (this version of) the model. The mud affected wave number is calculated inside the procedure that determines the mud-induced energy dissipation term. But the modification of the wave number by the fluid mud has influence on other terms of the action balance as well. At first we mention the group velocity, which is of major importance for the calculation of the **propagation of energy** through the domain and the transfer of energy over directions. But also other source and sink terms are affected by the change of the wave number. In fact at all places where the wave number plays a part in the determination of energy changes, propagation or dissipation the mud affected wave number has to be used. It is expected that the influence of mud on energy propagation will be the strongest in cases where high differences in energy propagation velocities can be expected and where they are of influence on for instance refraction patterns and shoaling. Practical situation where this is the case are situations with large variations in bed level, transitions from sandy to muddy bottoms, or patches of mud.

(The inclusion of the influence of fluid mud on energy propagation in the SWAN-mud model is the subject of chapter 8.)

Remaining limitations

Winterwerp *et al.* (2007) mention the constraint formed by the difficulty to establish the mud parameters, especially the mud layer thickness. This is caused by the fact that the thickness of a layer of fluid mud is determined by the wave height, the mud properties, plasticity, transport of mud and probably the stress history. This has severe consequences for a model describing wave damping by fluid mud, because these models are very sensitive for the mud layer thickness. It is proposed to develop a advanced rheological model to model the liquifaction in a proper way.

In the article it is also mentioned that further model calibration is required, but that it is difficult to acquire data on muddy coasts, because of the poor accessibility of the sites.

5.5 Implementation of Ng by Rogers and Holland (in review)

5.5.1 Introduction

Rogers and Holland (under review) also describe the implementation of a viscous two-layer model into SWAN. Their article contains a verification of wave damping implementations in SWAN in which their model is compared to the model described in Winterwerp *et al.* (2007). The model is applied on waves near Cassino Beach, Brazil, and compared to simulations without dissipation by mud, simulations with the model of Winterwerp *et al.* and measurements. Finally the model is used for inverse modelling: a method used to determine the mud characteristics that would yield the observed wave heights.

This section starts with a description of the principles of the model of Rogers and Holland (5.5.2). Thereafter the verification containing the comparison between Winterwerp *et al.* and Rogers and Holland is summarized (5.5.3). The results of the simulations are discussed in 5.5.4. The constraints of the model are discussed in section 5.5.5.

5.5.2 Principles of the model

Dispersion equation

The dispersion equation used in this model is the dispersion equation of Ng (see 2.4.7).

Energy dissipation term

The solution for the wave number is implemented in SWAN via a relative energy dissipation term given by:

$$\frac{S_{b,m}}{E} = -2C_{g,x}k_i \tag{143}$$

This expression has been derived for a mono-chromatic, uni-directional wave train propagating over a flat muddy bottom, with dissipation by mud as only source or sink term. In that case the action density balance reduces to:

$$\frac{\partial C_{g,x} N}{\partial x} = \frac{S_{b,m}}{\omega} \tag{144}$$

The relative energy dissipation term (143) is obtained by substituting (145) into the reduced action density balance (144), calculating the derivative and dividing both sides by N.

$$N = E/\omega, \qquad E = \frac{1}{2}\rho g a^2, \qquad a = a_0 e^{-k_i x} \tag{145}$$

Also in this model it is assumed that the expression for energy dissipation can be applied to calculate the energy dissipation for each bin in the $E(\omega,\theta)$-spectrum seperately.

5.5.3 Verification and comparison

Rogers and Holland verify their wave damping implementation in SWAN with simple tests and compare their implementation with the model described in Winterwerp *et al.* (2007). The first test compares the results obtained for the wave number k_i via the various dispersion equations at various mud layer thicknesses (like in chapter 4). The second test compares the decay rates obtained for the dispersion equation of Ng, the dispersion equation of De Wit, the SWAN-implementation of Rogers and Holland and the SWAN-implementation of Winterwerp *et al.* for a situation with a flat, muddy bottom and all energy contained in a single frequency and direction. Ng, De Wit and Rogers give almost exactly the same result for the wave height, while Winterwerp differs from its corresponding expected decay rate. According to Rogers and Holland, this suggests that the deviation in the dissipation is more likely due to differences in *implementation*, rather than differences in the dispersion equation.

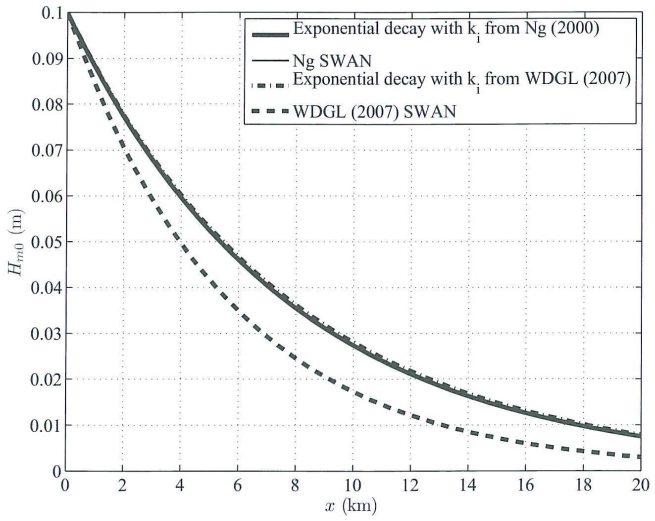

Figure 22 Rogers and Holland, figure 3: comparison of decay rates obtained with the dispersion equation of Ng, the SWAN-implementation of Rogers and Holland, the dispersion equation of De Wit and the SWAN-implementation of Winterwerp *et al.* (mentioned in same order as in legend) for a situation with a flat, muddy bottom and all energy contained in a single frequency and direction.

5.5.4 Results of simulations

Rogers and Holland (under review) applied their model to Cassino Beach, Brazil. This location is characterized by a mild slope of the sea bottom and a wave climate that is dominated by wind sea and relatively young swell. The rheological information used in the model is based on in situ measurements (Holland *et al.*, under review). The model is run for wave data obtained during a storm on 21-23 May 2005, firstly for the Cassino example itself and secondly for a hypothetical scenario, which is the same, except for the mud location. In the latter case the mud is located at or near the surf zone, much closer to the shore as in the original Cassino example. They present an exponential decay rate by showing the distance of propagation at which a wave would be attenuated to 50% or 10% of its original amplitude. This example showed that the dissipation is much faster when the mud is at or near the surf zone.

Rogers and Holland also compared the model for a situation without dissipation by mud and a situation with dissipation caused by mud assumed to be present in a uniform lens of 40 cm with measurements for the wave height obtained for three locations. These tests are aimed to evaluate the necessity of including dissipation by viscous mud in the wave model. The tests with dissipation are carried out with their own model, but also with the model of Winterwerp *et al.* (2007).

These tests showed that for the situation without mud, the wave height was clearly overpredicted. This means that some type of muddy bottom induced dissipation is needed. The overprediction was less for high-energy cases. Rogers and Holland suggest that this is caused by the change in viscosity in situations with high waves: a high level of forcing reduces the viscosity. Therefore the effect of the mud-induced damping would be smaller.

With mud-induced dissipation, the model results and the observations fit much better, especially for the locations closest to the beach. Overprediction of dissipation occurs, especially at the heighest waves at the most offshore measurement point. This could be explained with the same argument of changing viscosity, but Rogers and Holland also give as possible explanation that the true mud distribution in the region might be thinner or patchyer than the uniform lens of 40 cm applied in the simulation.

The model results of Rogers and Holland coincide better with the observations than the results obtained with Winterwerp *et al.* The latter consistently overpredicts the wave damping.

5.5.5 Constraints of the model

This section discusses constraints of the model, focussing on (compare 5.4.4):
1. the used two-layer model
2. the energy dissipation term
3. energy propagation in the model

The validity of the model of Rogers and Holland is firstly limited by the constraints of the **dispersion equation of Ng**, a boundary layer approximation that covers only a part of the domain covered by the schematization of De Wit. This dispersion equation is valid when the mud layer thickness is small compared to the wave length (like De Wit) and small compared to the water layer thickness (see 2.4.7).

The **formulation of the energy dissipation** also yields constraints. In the derivation for the uni-directional wave C_g is considered in the direction of propagation. In case of waves in various directions, the energy dissipation of each directional bin has to be calculated using its own energy propagation velocity. This would require extension of the dissipation term to:

$$\frac{S_{b,m}}{E} = -2C_{g,x}k_i - 2C_{g,y}k_i \tag{146}$$

containing a vectorial summation of $C_{g,x}$ and $C_{g,y}$ to obtian the energy propagation velocity in the direction of propagation. Although not treated in the article, this step does not seem to restrict the application. A question is which $C_{g,x}$ is used in the model to calculate the dissipation according to equation (143). As explained before, $C_{g,x}$ is also affected by the mud.

This problem is equivalent again with the **location of the calculation of *k*** in the SWAN code. When *k* would be calculated on a higher level, it can be made available for calculation of other parameters influenced by mud.

Finally, in comparing their model with the model of Winterwerp *et al.* Rogers and Holland state (section 2.2.3): "*Unlike the implementation of Ng in SWAN, the Winterwerp et al. SWAN implementation uses the mud–adjusted wave number to calculate a mud-adjusted group velocity which is shared with the rest of the model and used in calculation of kinematics.*

For his reason , the Winterwerp et al. implemention can produce "shoaling" and "refraction" effects associated with spatial variation of mud, separate from traditional shoaling and refraction associated with variation of depths or currents." Although this remark clearly appoints the desired model developments, it is not entirely correct concerning the model of Winterwerp *et al.* (2007). So both models encounter the same constraint concerning the influence of mud on other phenomena than the dissipation itself.

5.6 Implementation of Ng by Kaihatu *et al.* (2007)

5.6.1 Introduction

The implementation of a viscous two-layer model into a wave model described by Kaihatu *et al.* (2007) is quite different from the two previously discussed models, because a wave model is used that differs strongly from the wave model SWAN. Kaihatu *et al.* compared their model with laboratory experiments and tested the model on theoretical 1D and 2D cases. This section shortly describes the setup of the model (5.6.2) and the results obtained in the tests (5.6.3).

5.6.2 Principles of the model

Wave model

The wave model used by Kaihatu *et al.* is a model described in Kaihatu and Kirby (1995). This is a '*parabolic frequency-domain mild-slope equation model with second-order nonlinear wave-wave interactions*'. The model belongs to the category of phase-resolving models. The basics of the model are formed by a parabolic version of the mild-slope equation. Characteristics of this kind of models are that the wave condition is computed line-by-line, propagating in a forward direction, that the resolution of the method is a small fraction of the wave length and that these models can deal very well with nonlinear processes, diffraction and rapid variations in the evolution of waves (e.g. breaking). These models are especially suitable for small scale (say ten wave lenghts) calculations on uni-directional waves which characteristics are given by a fully deterministic description. The wave generation by wind is absent in these models.

Here only the principle characteristics of this type of models are mentioned, based on the literature below. For equations and further discussions on the mild slope equation and phase-resolved models, see Holthuijsen (2007, p.6;218;262), Dingemans (1997, section 4.3) and Kaihatu and Kirby (1995).

Dispersion equation

The dispersion equation used to describe mud-induced dissipation is the dispersion equation of Ng (see 2.4.7). The imaginary part of the wave number describes the dissipation effect of the mud, while the real part is considered to describe the effect of mud on the wave

kinematics. Kaihatu investigates the effect of the adjusted real part on energy transfer within the wave spectrum and on the increase of the wave length during propagation over thickening fluid mud. The latter causes an inverse shoaling effect.

Nonlinear wave-wave interaction

Kaihatu *et al.* extensively deal with the nonlinear wave-wave interaction by describing the way this mechanism is implemented in the model. The reason for this is the following: The dissipation mechanism described by the dispersion equation requires direct interaction between wave motion and bottom. Therefore it is in essence a long wave dissipation mechanism. But cohesive sediment coasts in practise turn out to be of dimensions on which also "*indirect wave-sediment energy exchange processes can become important*" (Kaihatu *et al.,* 2007), where dissipation of short-wave energy via nonlinear wave-wave interaction is normally considered as the most important process. This spectrum-wide wave damping was observed in the field experiments of Sheremet and Stone (2003), but was not reproduced in simulations with damping by enhanced bottom friction or observed in measurements for areas with sandy bottoms. Therefore Kaihatu stresses the importance of nonlinear wave-wave interaction in models where dissipation by viscous mud is investigated.

5.6.3 Results of simulations

Kaihatu *et al.* validated their model with the laboratory experiments of De Wit, the same data used by Winterwerp *et al.* (2007). Further testing was done in both one and two spatial dimensions. It was found that the actively-dissipated frequencies were mainly present at shallow and intermediate water depths. By simulations with and without the nonlinear wave-wave interactions it was found that the "*subharmonic interactions are responsible for the dissipation of the high frequencies of the wavefield, even if beyond the deep water limit.*" It was also found that the change of the real part of the wave number by the mud did not much influence the wave-wave interaction.

In case of patches of mud, strong damping inside the patch leads to significant diffraction on the lee side. This diffraction is reproduced well with this wave model.

5.7 Discussion

5.7.1 Introduction

Considering the models described above, this section discusses the most important differences between the models (5.7.2) and indicates the priorities in the further development and testing of an adaptation to SWAN to model the decrease of energy during the propagation of a wave field over fluid mud (5.7.3). Before starting with the model extension in chapter 7, a few fundamental questions on the implementation of viscous two-layer models into the wave energy model SWAN are discussed in section 5.7.4.

5.7.2 Overview

Table 7 resumes some important information concerning the models described in the previous sections.

Name	Wave model	type	two-layer model	Dissipation term	Propagation?
Winterwerp et al.	SWAN	phase averaged	De Wit	Gade (part II)	no
Rogers and Holland	SWAN	phase averaged	Ng	Rogers	no
Kaihatu	Kaihatu&Kirby	phase resolved	Ng	[-]	yes

Table 7 Some important information concerning the models described in literature

Winterwerp *et al.* (2007) and Rogers and Holland (in review) both implemented a viscous two-layer model into SWAN, a phase-averaged wave energy model. Kaihatu *et al.* (2007) use a phase-resolving model. Phase-resolving models are especially suitable for small scale, fully deterministic simulations, diffraction and nonlinear wave-wave interaction. Phase-averaged models are better suited to model statistical properties of the waves on a larger scale.

The type of the wave model also makes a difference concerning the implementation of the influence of mud on dissipation and propagation. In the SWAN-models, a separate energy dissipation term is needed. Winterwerp *et al.* (2007) uses a term derived by Gade, Rogers and Holland (in review) derive their own term. This term has to be added to the source and sink terms of the energy balance. In Kaihatu's model, the influence of mud on dissipation (and propagation) is known as soon as the mud-adjusted wave number is calculated and available in the model. Both Winterwerp *et al.* (2007) and Rogers and Holland (in review) only consider the influence of the mud on the dissipation. The effects of the mud-adjusted wave number on other parameters and phenomena, like the group velocity and energy propagation, are not yet taken into account.

The energy dissipation term used in Winterwerp *et al.* is based on shallow water assumptions. The expectation that the model will give an incorrect estimation of the energy dissipation at deeper water, is supported by the results of the comparison between Winterwerp *et al.* and Rogers and Holland as shown in Figure 22.

The dispersion equations used to implement in the wave models are De Wit in Winterwerp *et al.* (2007) and Ng in Rogers and Holland (in review) and in Kaihatu *et al.* (2007). As discussed before, the schematization of De Wit is less strict concerning the mud layer thickness.

5.7.3 Priorities in model development

Priorities in the further development of an adaptation to SWAN to model the decrease of energy during the propagation of a wave field over fluid mud are the following:

1. Implementation of the DELFT dispersion equation described in chapter 3 and the solving routine to compute the mud-adjusted wave number described in chapter 4
2. Derivation and implementation of a process based energy dissipation term for a phase averaged model, consistent with the DELFT dispersion equation
3. Adaptation of the code to make the mud-adjusted wave number available for calculation of other parameters and processes, allowing for energy propagation being affected by mud

The derivation of a new energy dissipation term is described in chapter 6. The implementation of the DELFT dispersion equation and the newly derived energy dissipation term is described in chapter 7. The adaptation to compute the influence of mud on energy propagation is described in chapter 8.

5.7.4 Remaining constriants

With the elaboration of the priorities formulated in the previous section, important constraints mentioned in the discussion of the separate models are resolved. But other constraints remain and form fundamental restrictions on the SWAN-model adapted for propagation over fluid mud.

Linearity

The first important restriction is imposed by the assumption that the problem is linear. This assumption is important for various steps in the model. It is on the basis of the two-layer model that is used to calculate the mud-affected wave number. But it is also the justification of the superposition of the energy term per wave frequency and direction to compute the total energy dissipation (a basic principle in SWAN itself). This principle is only true when the amount of energy at one frequency or direction does not influence the dissipation at another frequency or direction. The energy at various frequencies is connected in a non-linear way: energy can be transferred from one frequency to another by non-linear wave-wave interaction. But this does not make it impossible to describe the problem as linear. The various energy dissipation and energy transfer terms can be treated separately and linear, especially because the spatial scale of the wave-wave interaction is much larger than the spatial scale of the dissipation by viscous mud.

Small spation variability

A second important restriction concerns the assumed small spatial variability of the water depth and the newly introduced variables in space (mud layer thickness, density, viscosity). As soon as any hard boundary or modification of layer thickness or mud property is encountered, (partial) reflection occurs. In a simple mathematical model, this reflection would be described using not only the external wave traveling in positive directions, but also the other solutions of the dispersion equation. These other solutions are not available in the SWAN-version considering mud-induced damping.

But also this omission does not impose constraints to a SWAN-mud model that are not already present in SWAN itself. Small spatial variability of the variables in space is an assumption in SWAN itself. Therefore the model does not deal with reflection in general. Reflection on hard structures or clear discontinuities can only be taken into account by using a separate reflection module that removes or adds energy from or to the spectrum via extra source and sink terms on the specific location of the structure.

This assumption is already present in the derivation of the regular dispersion equation. The regular dispersion equation is derived under the assumption of a horizontal bottom. Therefore the wave number can be considered independent from x. In third generation wave models for oceans (with explicit scheme) the capacity of the model to deal with spatial variability is limited by the courant criterium and efficiency (small Δx would lead to small Δt, because $\Delta t < \Delta x/c_{g,x}$, see the remarks on ocean models in section 5.2.2). The implicit propagation scheme of SWAN makes the model better capable to deal with the stronger variations in seabed topography in coastal seas. But in this case the assumptions used in the description of the kinematics itself impose limits on the spatial variability the model can deal with.

Conclusions

The conclusion from the preceding considerations is that the implementation of mud into SWAN in principle does not impose restrictions on the model that are not already present in SWAN itself.

6 Derivation of an energy dissipation term

6.1 Introduction

The previous chapter indicates the need for the derivation and implementation of an energy dissipation term that is consistent with the used dispersion equation. This chapter describes step by step the derivation of an energy dissipation term consistent with the DELFT dispersion equation. The derivation follows Gade (1958): the wave period averaged work by the pressure on the interface is used as measure for the energy loss. But in this derivation the DELFT dispersion equation is used to determine the wave number, the pressure fluctuation and the phase and the amplitude of the interface displacement.

The derivation of a new energy dissipation term is one of the main contributions of this project to the development of SWAN-mud models. Therefore it is presented in the main text of this report. The last section of this chapter (6.8) summarizes the conclusions. Those not interested in the derivation can limit themselves to the conclusions without losing the thread of the story.

Section 6.2 explains how the vector of constants can be computed with the coefficients of the matrix. Section 6.3 focusses on the ratio between the (complex) amplitudes of the interface and surface displacement. In section 6.4 the expression for the pressure is investigated. Section 6.5 shows how the work on the interface can be computed, thus giving an expression for the dissipation of energy. The dissipation rate is related to the total amount of energy in section 6.6. This defines a relative energy loss. On various places in this derivation, a comparison is made with expressions by Gade (1958). Numerical computations in section 6.7 illustrate the conclusions about terms that have to be taken into account. Section 6.8 forms the conclusion of this chapter and gives the key equations.

6.2 Calculation of vector of homogeneous solution

Given the coefficient matrix derived in chapter 3, the five unknows of the vector of homogeneous solutions can be expressed in terms of the surface wave amplitude a. As soon as the solution for the wave number k is computed, the unknowns can be computated as well.

$$\begin{bmatrix} \cosh(k\,Htot0) & \sinh(k\,Htot0) & 0 & 0 & -\omega & 0 \\ \sinh(k\,Htot0) & \cosh(k\,Htot0) & 0 & 0 & -\frac{g\,k}{\omega} & 0 \\ \cosh(k\,Hm0) & \sinh(k\,Hm0) & 0 & 0 & 0 & -\omega \\ 0 & 0 & -\frac{k\,(\cosh(m\,Hm0)-1)}{m} & \frac{k\,(-\sinh(m\,Hm0)+m\,Hm0)}{m} & 0 & \omega \\ 0 & 0 & \cosh(m\,Hm0) & \sinh(m\,Hm0) & 0 & 0 \\ \frac{\omega\sinh(k\,Hm0)}{k} & \frac{\omega\cosh(k\,Hm0)}{k} & -\frac{2\,I\,\nu\,\rho 2\,k\sinh(m\,Hm0)}{\rho 1} & -\frac{\rho 2\,(-\omega+2\,I\,\nu\,k^2\cosh(m\,Hm0)-2\,I\,\nu\,k^2)}{k\,\rho 1} & 0 & \frac{g\,(\rho 2-\rho 1)}{\rho 1} \end{bmatrix} \begin{bmatrix} C1 \\ C2 \\ I\,C4 \\ C3 \\ a \\ \xi 0 \end{bmatrix} = \begin{bmatrix} 0 \\ 0 \\ 0 \\ 0 \\ 0 \\ 0 \end{bmatrix} \quad (147)$$

Matrix equation of the system

Using the first and the second row, C1 and C2 can be expressed in terms of a.

$$C1 := \left(- \frac{\sinh(k\ Htot0)\ g\ k}{\omega} + \cosh(k\ Htot0)\ \omega \right) a \tag{148}$$

$$C2 := \left(-\sinh(k\ Htot0)\ \omega + \frac{\cosh(k\ Htot0)\ g\ k}{\omega} \right) a \tag{149}$$

Using the fifth and the fourth row, C3 and C4 can be expressed in terms of ξ_0.

$$C3 := - \frac{\cosh(m\ Hm0)\ \omega\ \xi 0\ m}{k\ (-\sinh(m\ Hm0) + \cosh(m\ Hm0)\ m\ Hm0)} \tag{150}$$

$$C4 := - \frac{I\ \omega\ \xi 0\ m\ \sinh(m\ Hm0)}{k\ (-\sinh(m\ Hm0) + \cosh(m\ Hm0)\ m\ Hm0)} \tag{151}$$

The third or the sixth row can be used to express ξ_0 in terms of a. Substituting the expressions for C1 and C2 in the equation following from the third row and solving for ξ_0 gives:

$$\xi 0 := \left(\cosh(k\ Hm0) \cosh(k\ Htot0) - \frac{\cosh(k\ Hm0) \sinh(k\ Htot0)\ g\ k}{\omega^2} - \sinh(k\ Hm0) \sinh(k\ Htot0) + \frac{\sinh(k\ Hm0) \cosh(k\ Htot0)\ g\ k}{\omega^2} \right) a \tag{152}$$

where ξ_0 is the complex amplitude of the interface displacement and a the real amplitude of the surface displacement.

6.3 Ratio between interface and surface displacement

With the use of:

$$\sinh(x-y) = \sinh(x)\cosh(y) - \cosh(x)\sinh(y) \tag{153}$$

$$\cosh(x-y) = \cosh(x)\cosh(y) - \sinh(x)\sinh(y) \tag{154}$$

$$H_{w0} = H_{tot0} - H_{m0} \tag{155}$$

the complex amplitude of the interface displacement ξ_0 is written in a more convenient way:

$$\xi 0 := \left(\cosh(k\ Hw0) - \frac{\sinh(k\ Hw0)\ g\ k}{\omega^2} \right) a \tag{156}$$

Key equation 1: Relation between (complex) interface and surface amplitude

where the (complex) ratio between ξ_0 and a is given by:

$$rXi0a := \cosh(k\ Hw0) - \frac{\sinh(k\ Hw0)\ g\ k}{\omega^2} \tag{157}$$

$$rXi0a = \frac{\xi 0}{a} = \frac{be^{i\varphi}}{a} \tag{158}$$

The modulus and argument of *rXi0a* give information on the real amplitude ratio and the phase difference between interface and surface displacement.

$$\mathrm{mod}\left(rXi0a\right) = \sqrt{\left(\mathrm{Re}\left(rXi0a\right)\right)^2 + \left(\mathrm{Im}\left(rXi0a\right)\right)^2} = \frac{b}{a} \tag{159}$$

$$\arg\left(rXi0a\right) = \arctan\frac{\mathrm{Im}\left(rXi0a\right)}{\mathrm{Re}\left(rXi0a\right)} = \varphi \tag{160}$$

The analytical expressions for modulus and argument can be obtained with

$$rXi0aReal := \cosh(Hw0\ kr)\cos(Hw0\ ki) - \frac{g\ kr\ \sinh(Hw0\ kr)\cos(Hw0\ ki)}{\omega^2} + \frac{g\ ki\ \cosh(Hw0\ kr)\sin(Hw0\ ki)}{\omega^2} \tag{161}$$

$$rXi0aImag := \sinh(Hw0\ kr)\sin(Hw0\ ki) - \frac{g\ kr\ \cosh(Hw0\ kr)\sin(Hw0\ ki)}{\omega^2} - \frac{g\ ki\ \sinh(Hw0\ kr)\cos(Hw0\ ki)}{\omega^2} \tag{162}$$

These expressions can not be easily reduced to more compact formulations. For that reason the analytical expressions are not given here.

Comparison with Gade

A comparison with Gade is made by expanding *rXi0a* with a Taylor series, with the use of:

$$\sinh\left(x\right) = x + \frac{x^3}{3!} + \frac{x^5}{5!} + \frac{x^7}{7!}\ldots \tag{163}$$

$$\cosh\left(x\right) = 1 + \frac{x^2}{2!} + \frac{x^4}{4!} + \frac{x^6}{6!}\ldots \tag{164}$$

In case of shallow water (Gade), $kH_{w0} << 1$. So we can expand around $kH_{w0} = 0$ and neglect terms of $(kH_{w0})^n$ with $n \geq 2$:

$$rXi0a \approx 1 - \frac{gk}{\omega^2} kH_{w0} = 1 - gH_{w0}Re^{i\beta} \qquad \text{with } Re^{i\beta} = \left(\frac{k}{\omega}\right)^2 \text{ (introduced by Gade)} \tag{165}$$

This is exactly the expression given by Gade and used to compute amplitude ratio and phase difference (see Gade I-16, I-32, I-33, I-41).

6.4 The pressure term

In section 3.3, equation (49), the assumed solution for the pressure was

$$p1(x, z, t) := P1(z)\, \mathbf{e}^{(I\,(k\,x - \omega\,t))} + \rho 1\, g\, (Htot0 - z) \tag{166}$$

The amplitude of the pressure in the upper layer is given in section 3.4, equation (56):

$$P1(z) := \frac{\omega\, \rho 1\, (C1\, \sinh(k\, z) + C2\, \cosh(k\, z))}{k} \tag{167}$$

The expressions for C1 and C2 are known and can be substituted in expression (167). We use

$$\sinh(x - y) = \sinh(x)\cosh(y) - \cosh(x)\sinh(y) \tag{168}$$

$$\cosh(x - y) = \cosh(x)\cosh(y) - \sinh(x)\sinh(y) \tag{169}$$

$$diepte = H_{tot0} - z \quad = \text{position below equivalent water level} \tag{170}$$

to rewrite the amplitude as:

$$P1(diepte) := \rho 1\, a\, g\, \cosh(k\, diepte) - \frac{\rho 1\, a\, \omega^2\, \sinh(k\, diepte)}{k} \tag{171}$$

Key equation 2: Expression for the amplitude of the pressure fluctuation in the upper layer

Why only the real part of the pressure amplitude is relevant

Expression (171) shows that the amplitude of the pressure fluctuation $P_1(diepte)$ is complex due to the presence of the complex wave number k. Only the real part of the amplitude is relevant for the calculation of the energy dissipation. The reasoning is as follows:

1) It is necessary to split the pressure in a real and an imaginary part before multiplication with the (real) interface displacement and integration over a wave period T to obtain the work. This necessity originates from the fact that the real part of the product of two complex functions is not the same as the product of the real part of these functions. In mathematical notation

$$\mathrm{Re}\left(e^{i(kx-\omega t)} * e^{i(kx-\omega t)}\right) \neq \mathrm{Re}\left(e^{i(kx-\omega t)}\right)\mathrm{Re}\left(e^{i(kx-\omega t)}\right) \tag{172}$$

2) If the pressure amplitude is split up, the imaginary part of the pressure amplitude times the imaginary part of the function describing the fluctuation itself does also give a real product:

$$i\,\mathrm{Im}\left(P1\left(diepte\right)\right) * i\sin\left(k_r x - \omega t\right) * e^{-k_i x} \rightarrow \text{real} \tag{173}$$

but this product does not represent the physics involved. The reason for this is the fact that the 'imaginary part of the fluctuation' i*sin(*phase*) is introduced by describing the harmonic wave at the surface with the Eulerian expression $e^{(i\ phase)}$. Here the mathematical describtion does not describe exactly what is physically present, adding an imaginary part. We seek the physically present pressure, therefore the influence of this added imaginary part of the fluctuation domain should be omitted.

3) Another argument is that the fluctuation of the pressure in the upper layer has to have the same form and phase as the water level elevation as long as no viscosity is present in the upper layer. This will not be the case if other harmonics than cos(*phase*) are added.

Based on these arguments, it is stated that only the real part of the pressure amplitude is relevant for the computation of the work.

Determination of real part of the pressure amplitude

When the k-value is determined via the iteration, the real part of the pressure amplitude can be computed, just by taking:

$$\mathrm{Re}\left(P1\left(diepte\right)\right) \tag{174}$$

To get insight in the cause of the differences between the shallow water approximation and this more extended approach, analytical expressions for the real and imaginary part of the pressure amplitude are derived. This derivation, that is presented in appendix E, makes use of:

$$k = k_r + i * k_i \tag{175}$$

$$k = \mathrm{mod}\, k * e^{i \arg k} \tag{176}$$

$$\mathrm{mod}\left(k\right) = \sqrt{k_r^{\,2} + k_i^{\,2}} \tag{177}$$

$$\arg\left(k\right) = \arctan\frac{k_i}{k_r} \tag{178}$$

and results in:

$$Real\_P1(diepte) := \rho 1\ a\ g \cosh(diepte\ kr) \cos(diepte\ ki) - \frac{\rho 1\ a\ \omega^{2} \sinh(diepte\ kr) \cos(diepte\ ki) \cos(ARGk)}{MODk} - \frac{\rho 1\ a\ \omega^{2} \cosh(diepte\ kr) \sin(diepte\ ki) \cos(-0.5\ \pi + ARGk)}{MODk} \tag{179}$$

$$Imag\_P1(diepte) := I\ \rho 1\ a\ g \sinh(diepte\ kr) \sin(diepte\ ki) + \frac{I\ \rho 1\ a\ \omega^{2} \sinh(diepte\ kr) \cos(diepte\ ki) \sin(ARGk)}{MODk} + \frac{I\ \rho 1\ a\ \omega^{2} \cosh(diepte\ kr) \sin(diepte\ ki) \sin(-0.5\ \pi + ARGk)}{MODk} \tag{180}$$

Because the first term of these two equations result from the first term of equation (171) and the second and third terms result from the second term of equation (171), the terms are called respectively:

(for eq. 179)	Real_P1_1	Real_P1_2a	Real_P1_2b
(for eq. 180)	Imag_P1_1	Imag_P1_2a	Imag_P1_2b

The order of magnitude of the various pressure terms

At *diepte* = 0, that is where $z = H_{tot0}$, all the real and imaginary terms of the pressure amplitude except the first real term become zero, due to sinh(0) = 0 and sin(0) = 0. The first real part equals the contribution of the surface level elevation in the second Taylor term (BC II, equation (83)):

$$p_1\left(x, z = H_{tot0}, t\right) + \zeta \frac{\partial p_1}{\partial z}|_{z=H_{tot0}} = 0 \;\Rightarrow\; \rho_1 a g \cosh\left(0 * k_r\right)\cos\left(0 * k_i\right)e^{i(kx-\omega t)} - \rho_1 g a e^{i(kx-\omega t)} = 0 \tag{181}$$

At *diepte* ≠ 0, the other terms are not equal to zero. Although a small numerical investigation shows that the first real term is the dominant term also at larger depths, it is not justified to generalize this statement based on the symbolic notation. Below, the shallow water and deep water limits for the pressure amplitude at diepte = H_{w0} are investigated, using the Taylor series expansions:

$$\sinh\left(x\right) = x + \frac{x^3}{3!} + \frac{x^5}{5!} + \frac{x^7}{7!}... \tag{182}$$

$$\cosh\left(x\right) = 1 + \frac{x^2}{2!} + \frac{x^4}{4!} + \frac{x^6}{6!}... \tag{183}$$

$$\sin\left(x\right) = x - \frac{x^3}{3!} + \frac{x^5}{5!} - \frac{x^7}{7!}... \tag{184}$$

$$\cos\left(x\right) = 1 - \frac{x^2}{2!} + \frac{x^4}{4!} - \frac{x^6}{6!}... \tag{185}$$

At first, we assume that both in shallow and deep water the modulus MOD*k*, the real wave number k_r and the unadjusted wave number k_{nomud} are of similar order of magnitude. Furthermore the real wave number is always larger than the imaginary wave number.

$$O\left\{MODk\right\} = O\left\{k_r\right\} = O\left\{k_{nomud}\right\} \tag{186}$$

$$k_r > k_i \tag{187}$$

For **shallow water** we find:

$$kH_{w0} \ll 1 \qquad \Rightarrow \qquad \omega^2 \approx g\left(k_{nm}\right)^2 H_{w0} \tag{188}$$

The order of magnitude of the terms becomes:

Term		Order ratio	shallow water
Real_P1_1	$\rho_1 ag$	1	
Real_P1_2a	$-\rho_1 ag\left(k_{nm}\right)^2 H_{w0}H_{w0}k_r \cos\left(\arg k\right)/MODk$	$\left(kH_{w0}\right)^2$	$\rightarrow 0$
Real_P1_2b	$\rho_1 ag\left(k_{nm}\right)^2 H_{w0}H_{w0}k_i \sin\left(\arg k\right)/MODk$	$\ll\left(kH_{w0}\right)^2$	$\rightarrow 0$
Imag_P1_1	$\rho_1 agH_{w0}k_r H_{w0}k_i$	$<\left(kH_{w0}\right)^2$	$\rightarrow 0$
Imag_P1_2a	$\rho_1 ag\left(k_{nm}\right)^2 H_{w0}H_{w0}k_r \sin\left(\arg k\right)/MODk$	$<\left(kH_{w0}\right)^2$	$\rightarrow 0$
Imag_P1_2b	$\rho_1 ag\left(k_{nm}\right)^2 H_{w0}H_{w0}k_i \cos\left(\arg k\right)/MODk$	$<\left(kH_{w0}\right)^2$	$\rightarrow 0$

Table 8: Comparison of order of magnitude of the terms of the pressure amplitude in shallow water

The discrimination with the < and << sign is based on the assumption that cos(arg$k$) is close to one. In case of multiplication with sin(arg$k$) or using k_i in stead of k_r, the 'order ratio' becomes < kH_w. If both are the case, the order becomes << kH_{w0}. It can be concluded that in shallow water only Real_P1_1 has to be taken into account. The physical meaning of this is a hydrostatic influence of the water level elevation on the pressure. This is the way how the pressure is taken into consideration in the computation of the Work in Gade (1958).

For completeness the **shallow water** limit of the pressure term (171) is also investigated in the same way as the shallow water limit of the amplitude ratio. The Taylor series expansion of

$$P1(diepte) := \rho 1\ a\ g\ \cosh(k\ diepte) - \frac{\rho 1\ a\ \omega^2\ \sinh(k\ diepte)}{k} \tag{189}$$

around $kH_{w0} = 0$ becomes:

$$P1\left(H_{w0}\right) \approx \rho_1 ag - \rho_1 a\omega^2 H_{w0} = \rho_1 ag - \rho_1 agk_{nm}k_{nm}H_{w0}H_{w0} \approx \rho_1 ag \tag{190}$$

This gives the same result as above.

For **deep water** we find:

$$kH_{w0} > 3 \quad \Rightarrow \quad \omega^2 = gk_{nm} \tag{191}$$

$$k_i \rightarrow 0 \quad \Rightarrow \quad \arg k \rightarrow 0 \tag{192}$$

In that case the order of magnitude of the various terms becomes:

Term		Order ratio	deep water
Real_P1_1	$\rho_1 ag\cosh(H_{w0}k_r)$	1	
Real_P1_2a	$-\rho_1 agk_{nm}\sinh(H_{w0}k_r)/MODk$	1	
Real_P1_2b	$\rho_1 agk_{nm}\cosh(H_{w0}k_r)H_{w0}k_i \arg k/MODk$	$H_{w0}k_i \arg k$	→ 0
Imag_P1_1	$\rho_1 ag\sinh(H_{w0}k_r)H_{w0}k_i$	$H_{w0}k_i$	→ 0
Imag_P1_2a	$\rho_1 agk_{nm}\sinh(H_{w0}k_r)\arg k/MODk$	$\arg k$	→ 0
Imag_P1_2b	$\rho_1 agk_{nm}\cosh(H_{w0}k_r)H_{w0}k_i/MODk$	$H_{w0}k_i$	→ 0

Table 9: Comparison of order of magnitude of the terms of the pressure amplitude in deep water

This analysis shows that the importance of the second real term (2a) increases with increasing relative water depth kH_{w0}. In this case, the amplitude of the pressure as function of depth becomes:

$$P_1(diepte) = \rho_1 ag\cosh(k_r * diepte) - \frac{\rho_1 a\omega^2 \sinh(k_r * diepte)}{MODk} \tag{193}$$

which is (171) with k replaced by k_r, while MODk is approximately equal to k_r for small k_i. In the computation of the work, Gade (1958) only takes into account the first term, $\rho_1 ag$.

6.5 Work on the interface

Gade (1958) expresses the work dW done per unit area in time dt on the lower layer at a given abscissa as:

$$dW = -p\frac{dn}{dt}dt \tag{194}$$

where dn is the infinitesimal displacement normal to the interface of an element of the interface. The slope of the interface is assumed to be very small, based on the assumption that the amplitude a of the surface level is small compared to depth and wavelenght and the fact that the amplitude of the interface for an external wave is smaller than the amplitude of the surface. Therefore we can take the vertical displacement of the interface instead of n. The work dW becomes:

$$dW = -p\frac{d\xi}{dt}dt \tag{195}$$

The total work done per unit area during a whole wave period T at a particular point is found by integration. Division by T results in the average energy transmitted through the interface per unit area and time.

$$Work = -\frac{1}{T}\int_0^T p\frac{d\xi}{dt}dt \tag{196}$$

Dalrymple and Liu (1978) notice that the work in fact consists out of two parts: the pressure in the upper fluid and the shear stress both working on the moving interface. It is only the first part that is taken into account by Gade. As long as the water layer is considered as non-viscous this is justified, because in that case the shear stresses are absent in the water layer. Dalrymple and Liu (1978) argue that also for viscosity in both layers *"in most cases, i.e. when the lower layer is of reasonable thickness with respect tot the boundary layer scale,* $(\omega/2\nu_m)^{1/2} H_{m0} > 1$*, the first of these is of most importance, ..."*. For these reasons, the work by the pressure is considered as the only mechanism of energy transfer from water layer to mud layer.

Using the expression

$$\xi(x, t) := b\cos(kr\,x - \omega\,t + \phi)\,\mathbf{e}^{(-ki\,x)} \tag{197}$$

for the displacement of the interface, and the expression

$$ReDrukInt := Real\_P1\,\mathbf{e}^{(-ki\,x)}\cos(kr\,x - \omega\,t) + \rho 1\,g\,Hw0 - \rho 1\,g\,b\cos(kr\,x - \omega\,t + \phi)\,\mathbf{e}^{(-ki\,x)} \tag{198}$$

for the pressure on the interface (using Taylor, but taking only - $\rho_1 g\xi$ into account, as in BC VI) the product representing dW in an infinitesimal time span dt can be expressed as:

$$\begin{aligned} dW := &-Real\_P1\,(\mathbf{e}^{(-ki\,x)})^2\cos(kr\,x - \omega\,t)\,b\sin(kr\,x - \omega\,t + \phi)\,\omega \\ &- \rho 1\,g\,Hw0\,b\sin(kr\,x - \omega\,t + \phi)\,\omega\,\mathbf{e}^{(-ki\,x)} \\ &+ b^2\cos(kr\,x - \omega\,t + \phi)\,(\mathbf{e}^{(-ki\,x)})^2\,\rho 1\,g\sin(kr\,x - \omega\,t + \phi)\,\omega \end{aligned} \tag{199}$$

where *Real_P1* is the real part of the total amplitude of the pressure fluctuation *P1* at diepte = H_{w0}, that is at the interface.

$$Real\_P1 = \mathrm{Re}\left(P1(H_{w0})\right) = \mathrm{Re}\left(\rho_1 ag\cosh\left(kH_{w0}\right) - \frac{\rho_1 a\omega^2\sinh\left(kH_{w0}\right)}{k}\right) \tag{200}$$

Because

$$\sin(x)\cos(y) = \frac{\sin(x+y)+\sin(x-y)}{2} \tag{201}$$

the first term of dW can be expressed as

$$-Real\_P_1 e^{(-2k_i x)} b\omega \left(\frac{\sin(2k_r x - 2\omega t + \varphi) + \sin(\varphi)}{2} \right) \tag{202}$$

while the third term of dW becomes

$$\rho_1 g b^2 \omega e^{(-2k_i x)} \frac{\sin(2(k_r x - \omega t + \varphi))}{2} \tag{203}$$

Only the sin(φ)-part of the first term contributes to the integral, because all the other terms amount to:

$$\int_0^{2\pi/\omega} A \sin(B - C\omega t) dt = 0 \tag{204}$$

The expression for the average work per unit area and time becomes:

$$AvWork := -\frac{1}{2} \omega \, Real\_P1 \, b \, \mathbf{e}^{(-2\, ki\, x)} \sin(\phi) \tag{205}$$

So only the term explicitely related to the phase shift between surface and interface, the term representing the multiplication of the pressure fluctuation and the interface displacement, contributes to the averaged work. This is a physically sound description.

6.6 Relative energy loss

The energy loss can be related to the total amount of energy. The total wave period averaged energy per unit area is:

$$Energie := \frac{1}{2} \rho 1 \, g \, a^2 \, (\mathbf{e}^{(-ki\, x)})^2 \tag{206}$$

The relative dissipation is obtained by division of the avarage work and the average energy:

$$RelDiss := -\frac{\omega \, Real\_P1 \, b \sin(\phi)}{\rho 1 \, g \, a^2} \tag{207}$$

Key equation 3: Expression for the Relative Energy Dissipation

As explained in 6.4, the real amplitude of the pressure fluctuation at the interface, Real_P1, consists of three terms (Real_P1_1, Real_P1_2a and Real_P1_2b). When these terms are substituted one by one in this expression for the relative dissipation, we obtain also three partial dissipation terms:

Pressure term	Relative dissipation term
Real_P1_1	$RelDiss1 := -\frac{\omega \cosh(Hw0\ kr)\cos(Hw0\ ki)\ b \sin(\phi)}{a}$ (208)
Real_P1_2a	$RelDiss2a := \frac{\omega^3 \sinh(Hw0\ kr)\cos(Hw0\ ki)\cos(ARGk)\ b \sin(\phi)}{a\ MODk\ g}$ (209)
Real_P1_2b	$RelDiss2b := \frac{\omega^3 \cosh(Hw0\ kr)\sin(Hw0\ ki)\cos(-0.5\ \pi + ARGk)\ b \sin(\phi)}{a\ MODk\ g}$ (210)

Table 10: Relative dissipation terms following from the various terms of the pressure amplitude

Computation of the dissipation in this way, enables us to compare the contributions of the various pressure terms to the total dissipation at various water depths. Together, these terms form the total relative dissipation:

$$RelDiss := -\frac{\omega \cosh(Hw0\ kr)\cos(Hw0\ ki)\ b \sin(\phi)}{a} + \frac{\omega^3 \sinh(Hw0\ kr)\cos(Hw0\ ki)\cos(ARGk)\ b \sin(\phi)}{a\ MODk\ g} + \frac{\omega^3 \cosh(Hw0\ kr)\sin(Hw0\ ki)\cos(-0.5\ \pi + ARGk)\ b \sin(\phi)}{a\ MODk\ g} \quad (211)$$

Remember that the ratio b/a is given by the modulus of $rXi0a$ as given in equation (159).

Comparison to Gade

Finally this expression is compared to Gade's expression for the relative energy loss:

$$Work / E = -\omega g H_{w0} R \frac{b}{a} \sin(\varphi - \beta) \quad (212)$$

Note that, compared to formula (II-11) in Gade (1958), ω is added to correct for the typing error and symbols are replaced by their equivalent notation in this report. Hence φ represents the phase difference between surface an interface. R and β result from:

$$Re^{i\beta} = \left(\frac{k}{\omega}\right)^2 \quad (213)$$

and the amplitude ratio b/a and phase difference φ between interface and surface elevation follow from:

$$rXi0a_{\text{acc. to Gade}} = 1 - gH_{w0}Re^{i\beta} \quad (214)$$

$$\text{mod}(rXi0a) = \frac{b}{a} = \sqrt{\left(1 - gH_{w0}R\cos(\beta)\right)^2 + \left(gH_{w0}R\sin(\beta)\right)^2} \quad (215)$$

$$\tan\left(\arg\left(rXi0a\right)\right) = \tan\varphi = \frac{-H_{w0}gR\sin\left(\beta\right)}{1-H_{w0}gR\cos\left(\beta\right)} \tag{216}$$

Gade (1958) used a shallow water limit of the complex ratio of the interface and surface displacement *rXi0a*, ànd a shallow water limit of the amplitude of the pressure fluctuation (*Real_P1*) to compute the dissipation. Gade states that $gH_{w0}R$ is close to one for shallow water conditions and that β is small compared to φ. In the limit case his expression reduces to:

$$Work / E = -\omega\frac{b}{a}\sin\left(\varphi\right) \tag{217}$$

The relative dissipation term for shallow water, consistent with the DELFT dispersion equation, is *RelDiss1*, obtained by substituting the first real term for the pressure amplitude into (207). As became clear while investigating the shallow water limit in section 6.4, only the first pressure term is relevant for shallow water conditions. This gives

$$RelDiss1 = -\frac{\omega\cosh\left(H_{w0}k_r\right)\cos\left(H_{w0}k_i\right)b\sin\left(\varphi\right)}{a} \approx -\omega\frac{b}{a}\sin\left(\varphi\right) \tag{218}$$

Or in table format:

Derivation	Energy Dissipation Term		Reduced for $kH_{w0} << 1$
GADE:	$Work / E = -\omega gH_{w0}R\frac{b}{a}\sin\left(\varphi-\beta\right)$	→	$Work / E = -\omega\frac{b}{a}\sin\left(\varphi\right)$
DELFT:	$RelDiss1 := -\frac{\omega\cosh(Hw0\ kr)\cos(Hw0\ ki)\ b\sin(\phi)}{a}$	→	$RelDiss = -\omega\frac{b}{a}\sin\left(\varphi\right)$

Table 11: Comparison of Relative Energy Dissipation Term for GADE and DELFT in shallow water limit case

So in shallow water, Gade's energy dissipation term and the newly derived energy dissipation term give the same results.

6.7 Numerical example

The conclusions of the analytical investigation above are verified with a numerical example for intermediate water depth. This example is presented in Table 12. For the imput in the left column, the wave number *k* is computed with the iteration method presented in chapter 4. This wave number is used to compute the amplitude ratio, the phase difference and the contribution of the various pressure terms to the relative energy dissipation.

Input	Output
$T := 5.000$	with dispersion equation:
$\omega := 1.256637062$	$kr := 0.285128$
$Hw0 := 2.0000$	$ki := 0.0159164$
$Hm0 := 1.00$	$MODk := 0.2855718967$
$Htot0 := 3.0000$	$ARGk := 0.05576407273$
$\rho 1 := \rho 1$	with vector of homogeneous solutions / *rXi0a*:
$\rho 2 := 1750.00$	$b := 0.1492343882a$
$\nu := 0.500$	$\phi := -0.7909079906$
$g := 9.81$	with pressure terms and integral:
	$RelDiss1 := 0.1555295798$
	$RelDiss2a := -0.04512748593$
	$RelDiss2b := -0.0001555962776$

Table 12 Numerical verification of conclusions of the previous sections

The conclusions about the importance of the second real term of the pressure amplitude are supported by this numerical example. In this case, omitting the contribution of the second term, leads to an overestimation of the damping of 40%:

$$\frac{\text{RelDiss1}}{\text{RelDiss}} = \frac{0.155}{0.155 - 0.045} = 0.407 \tag{219}$$

Another important result is that the phase difference φ has a negative value. Because the elevation of surface and interface are described by:

$$\zeta(x,t) = \text{Re}\left(ae^{i(kx-\omega t)}\right) \tag{220}$$

$$\xi(x,t) = \text{Re}\left(\xi_0 e^{i(kx-\omega t)}\right) = \text{Re}\left(be^{i\varphi}e^{i(kx-\omega t)}\right) = b\cos\left(kx-\omega t+\varphi\right) \tag{221}$$

a negative value for φ means that the interface wave is ahead of the surface wave (see section 2.4.1).

A more extended example of a numerical computation is given in Figure 23. This figure shows the three terms (*RelDiss1, RelDiss2a, RelDiss2b*) that contribute to the energy dissipation term derived in this chapter (*RelDiss*). It illustrates the increasing importance of taking into account the *RelDiss2a* for increasing values of kH_{w0}. The dissipation term according to Gade coincides with the newly derived energy dissipation term where kH_{w0} is small, but considerably overestimates the dissipation at higher values of kH_{w0}. (Note that the various computation all have the same input, including the wave number k, computed with the DELFT dispersion equation and the solution procedure of described before.)

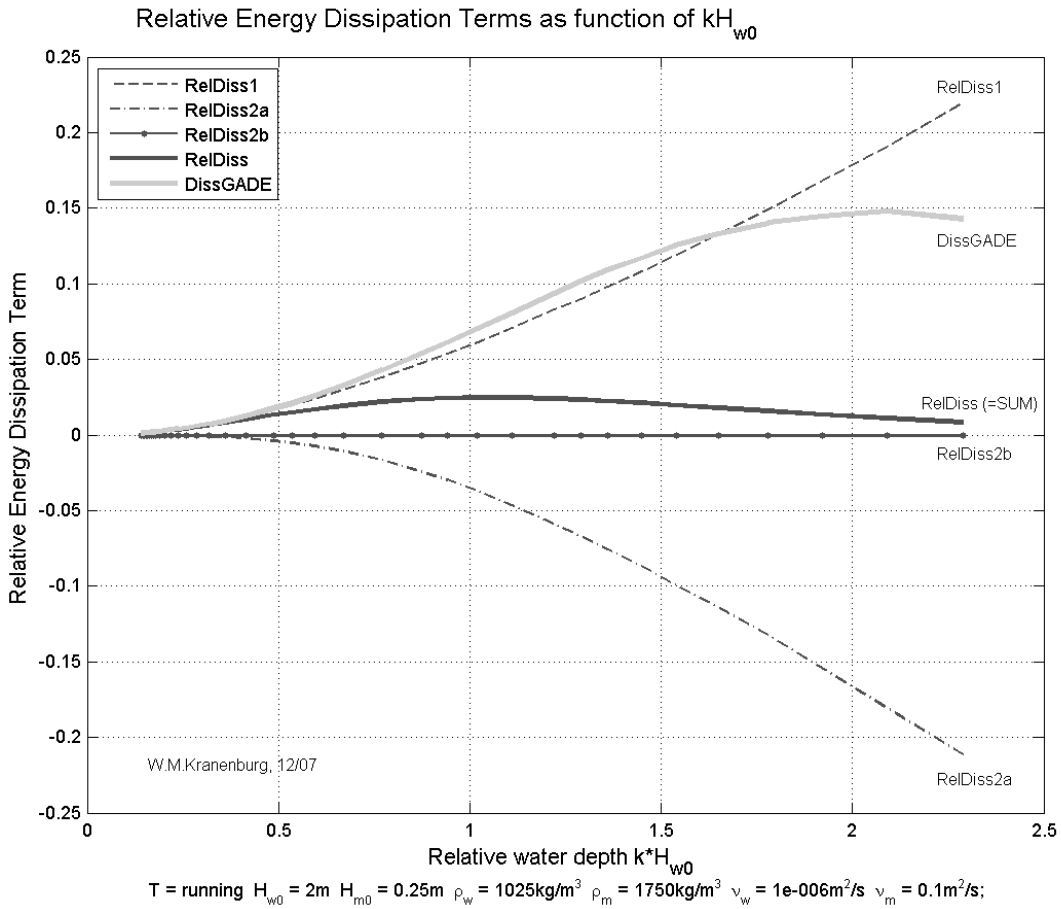

Figure 23 Graph of the Relative Energy Dissipation Terms as function of the relative water depth kH_{w0}. This graph shows the three terms (*RelDiss1, RelDiss2a, RelDiss2b*) that contribute to the total energy dissipation term derived in this chapter (*RelDiss,* thick dark gray line). The thick light gray line shows the energy dissipation term according to Gade (1958). The thick lines coincides at low values of kH_{w0}. The importance of *RelDiss2a* increases with increasing kH_{w0}. The dissipation term according to Gade stays close to *RelDiss1* over the main part of the domain.

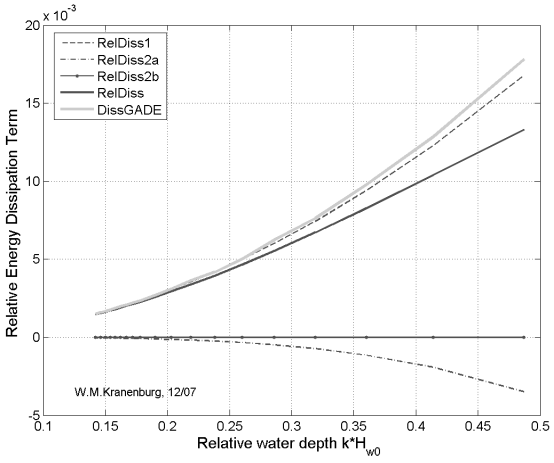

Figure 24 Detail ofFigure 23 for low values of kH_{w0}

This agrees with the remarks made on the limits of the various pressure terms in section 6.4, especially Table 8 and Table 9:

- For shallow water (kH_{w0}< 1/3), both *Real_P1_2a* and *Real_P1_2b*, and therefore the connected dissipation terms, approach zero. The dissipation term *RelDiss1*, connected to the pressure term *Real_P1_1* is the only term contributing to *RelDiss* and gives the same results as the dissipation term according to Gade.
- For intermediate water depths (1 < kH_{w0}< 3), *Real_P1_2b*, and therefore the connected dissipation term, stays very small. Both *Real_P1_1* and *Real_P1_2a* contribute to the total energy dissipation RelDiss.
- For deep water (3 < kH_{w0}), *Real_P1_2b*, and therefore the connected dissipation term, approaches zero again. *Real_P1_1* and *Real_P1_2a* approach to the same value, except for the minus sign. Therefore the energy dissipation term *RelDiss*, which is the sum of the contributions of the dissipation terms connected to these pressure terms, approaches zero, while the dissipation term according to Gade keeps a high and positive value. *RelDiss* approaching zero for deep water conditions is in agreement with the expectation: deep water means no influence of the bottom resulting in no mud-induced wave damping.

6.8 Conclusions

This chapter described the derivation of an energy dissipation term consistent with the DELFT dispersion equation. The same method is followed that has been applied by Gade (1958). However, here expressions are used for the amplitude ratio, the phase difference between interface and surface and the amplitude of the pressure fluctuation that are valid on the whole kH_{w0}-domain. The main assumption of the method is that the energy dissipation in the second layer equals the energy transport through the interface. The transfer of energy over the interface is induced by the work of the pressure on the fluctuating interface. A mean energy dissipation term is obtained by taking the integral of the work over a wave period. When this term is divided by a wave period and by the total amount of present energy, a relative energy dissipation term is. This relative energy dissipation is given by:

$$RelDiss := -\frac{\omega \sin(\phi)\, Real\_P1\, b}{\rho 1\, g\, a^2} \tag{222}$$

where:

$$\frac{b}{a} = \mathrm{mod}\left(rXi0a\right) \tag{223}$$

$$\varphi = \arg\left(rXi0a\right) \tag{224}$$

$$rXi0a := \cosh(k\, Hw0) - \frac{\sinh(k\, Hw0)\, g\, k}{\omega^2} \tag{225}$$

$$Real\_P1 = \mathrm{Re}\left(P1(H_{w0})\right) = \mathrm{Re}\left(\rho_1 a g \cosh\left(kH_{w0}\right) - \frac{\rho_1 a \omega^2 \sinh\left(kH_{w0}\right)}{k}\right) \tag{226}$$

with:

Symbol	Description	[-]
a	Amplitude of water surface displacement	m
b	Amplitude of interface displacement	m
φ	Phase difference between surface and interface displacement	rad
ρ_1	Density of water	kg / m^3
Real_P1	Real amplitude of pressure fluctuation	N / m^2
diepte	$H_{tot} - z$, position below equivalent water level	m
ω	Wave (angular) frequency (2π / T)	rad / s
rXi0a	Complex ratio of interface and surface displacement	[-]
H_{w0}	Equilibrium height of water layer, depth of interface	m
k	Wave number	rad / m

Table 13 Overview of parameters in the expression for the Relative Energy Dissipation by mud

This expression is valid for the same parameter domain as the associated DELFT dispersion equation. At shallow water conditions, this expression reduces to Gade's (1958) expression for the energy difference. This can be demonstrated by substituting the shallow water limits of *rXi0a* and *Real_P1* in equation (222). The results for Gade's expression and the newly derived energy dissipation term start to diverge considerably with increasing relative water depth kH_{w0}. This leads to the conclusion that Gade's expression is not applicable for intermediate and deep water conditions. Another conclusion is that the displacement of the interface is ahead of the displacement of the surface.

Although the amplitude of the surface wave a is present in the expressions above, the energy dissipation term is independent of the value of a (because both *Real_P1* and b are a function of a). This is consistent with the assumption that the wave amplitude is considered small compared with depth and that therefore the problem can be considered as linear.

The implementation of the relative energy dissipation term derived in this chapter into the wave model SWAN is described in the next chapter.

7 Implementation of 'DELFT' into SWAN (1): Energy dissipation

7.1 Introduction

In chapter 2 various viscous two-layer models have been discussed. In chapter 3 a dispersion equation (DELFT) has been derived for a schematization compatible with the conditions of the majority of practical field study cases. A method to compute the wave number from this equation is presented in chapter 4. An overview of the recent implementation of viscous bed models into wave models has been given in chapter 5, mainly focussing on implementations into the wave model SWAN. A new energy dissipation term, consistent with the DELFT dispersion equation, has been presented in chapter 6. This chapter describes the first step in the implementation of the DELFT dispersion equation and the newly derived energy dissipation term into the wave model SWAN.

Section 7.2 describes how and where dispersion equation and energy dissipation term are implemented in the code of SWAN. Section 7.3 describes various validation tests executed with SWAN-mud. Finally, section 7.4 discusses conclusions and suggestions for further improvement.

7.2 Implementation into SWAN

With the newly derived dissipation term that is consistent with and valid for the same domain as the DELFT dispersion equation, a model can be set up which is valid on the whole kH_{w0}-range. The content of the model is shown in the picture below.

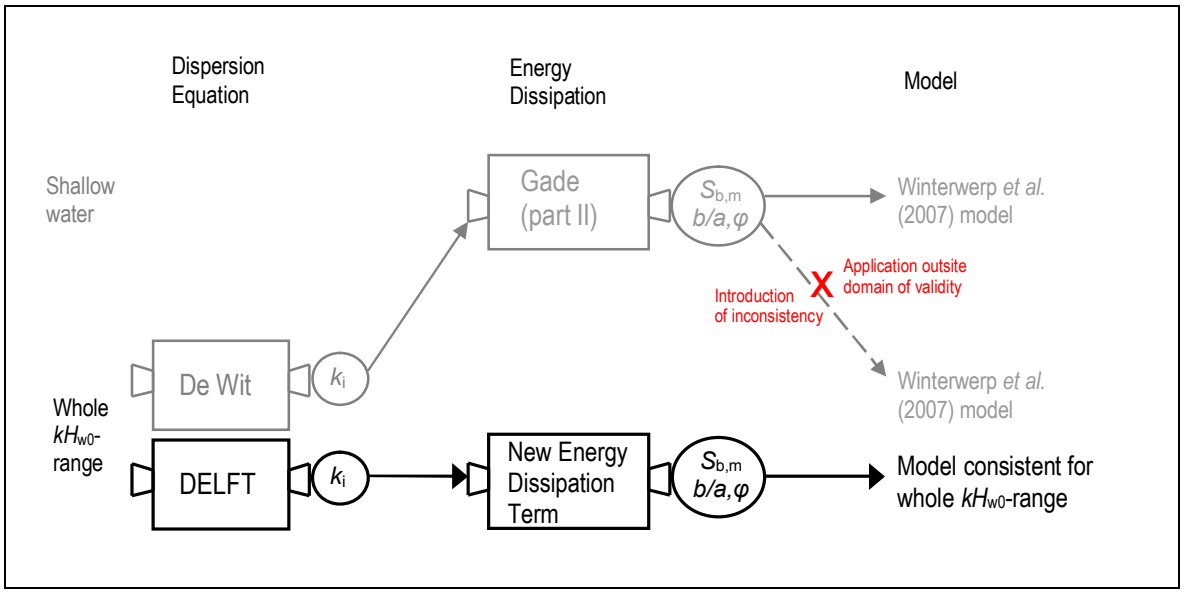

Figure 25 Schematic presentation of the content of the new model (black lines), compared to the model of Winterwerp *et al.* (2007) (gray lines). The model uses the dispersion equation DELFT and the

newly derived energy dissipation term, both valid on the whole kH_{w0}-domain. Proven the fact that the energy dissipation term obtained by Gade (1958, part II) is a shallow water reduction of the newly derived energy dissipation term (see appendix E), the domain of validity of the Winterwerp *et al.* model reduces to shallow water.

The first step in the implementation of the mud-adjusted wave number k and the newly derived energy dissipation term $S_{b,m}$ consists of adding these parameters to the existing SWAN infrastructure. This implementation is suitable to carry out some simple validation tests, but is inefficient and not complete. The next step in the development of the model contains the adaptation of the location where the wave number k is computed. This makes the model more efficient and makes it possible to compute the influence of mud on energy propagation. This next stap is the subject of chapter 8.

The structure of the adapted SWAN model (first step of implementation, called here SWAN-mud (I)), is illustrated with a Program Structure Diagram (Figure 26). The Program Structure Diagram in Figure 27 is a more detailed elaboration of the subroutine used to calculate the mud-induced dissipation term $S_{b,m}$. These two tables show at which level the wave number k is calculated. It is shown that the mud-adjusted wave number is not available outside the $S_{b,m}$-calculation and is calculated inside the general SWAN-iteration loop and the directional sweeps.

SWAN-mud (I), stationair

Initialisations			
Boundary Conditions			
	Four directional sweeps		
		Grid loop (x,y)	
			calculation propagation velocities of energy (x,y)
			calculation propagation velocities of energy (σ,θ)
			calculation SOURCE and sink terms:
			S_{bfr}
			$S_{b,m}$
			S_{wc}
			S_{br}
			S_{nl3}
			S_{nl4}
			S_{wind}
			calculation left-hand side terms in ACTION balance:
			$\delta C_x N/\delta x$
			$\delta C_y N/\delta y$
			$\delta C_\sigma N/\delta \sigma$
			$\delta C_\theta N/\delta \theta$
			solve matrix filled in SOURCE and ACTION $\rightarrow N(x,y,\sigma,\theta)$
Iterate until iteration criterium is fulfilled			

Figure 26 Program Structure Diagram of the SWAN-mud (I), with the mud-induced dissipation term $S_{b,m}$ as one of the source and sink terms.

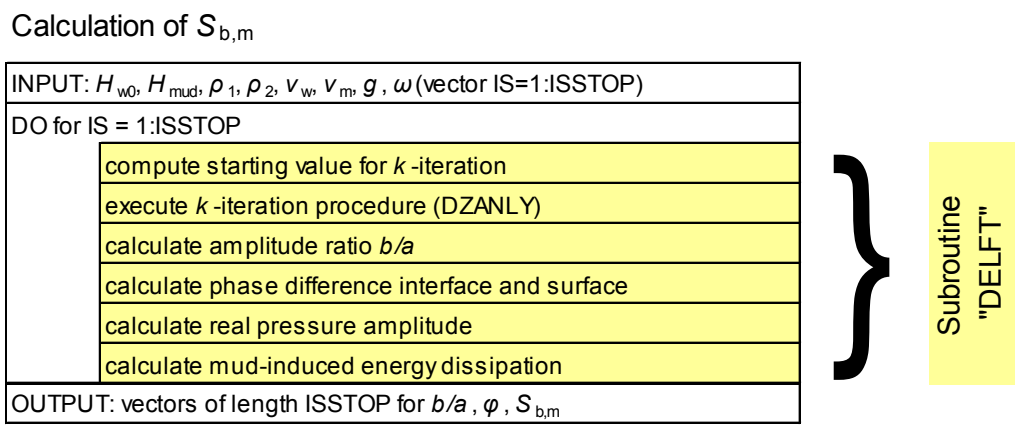

Figure 27 Program Structure Diagram of the calculation of the mud-induced dissipation term $S_{b,m}$ in the SWAN-mud (I) model. The computation takes place in the subroutine DELFT. The mud affected wave number is calculated within this subroutine with the iteration procedure discussed in chapter 4.

Like in Winterwerp *et al.* (section 5.4) and Rogers and Holland (section 5.5) the calculation of the mud-adjusted wave number k is implemented at a low level in the wave model SWAN, where it is only used to calculate the mud-induced energy dissipation term $S_{b,m}$ (ω,θ). At all the other locations in the program where the wave number k is needed, the unadjusted and real wave number is used. Therefore no influence of the mud is present in the calculation of the energy propagation velocities $c_{g,x}$, $c_{g,y}$ or c_θ. This means that the presence of mud does not have any influence on the processes of refraction and shoaling. Also for the calculation of the other source and sink terms, the unadjusted wave number is used. This means that no influence of the mud is present in the calculation of generation, dissipation and wave-wave interaction processes via the wave number. These processes are influenced by the total amount of energy. Obviously influence of mud is present in this way.

Strictly speaking, the omission of the influence of mud on the propagation of energy restricts the applicability of the SWAN-mud (I) model to cases without shoaling or refraction. Kaihatu *et al.* (2007) state that the influence of the change of the wave number by fluid mud on the wave-wave interaction is small, so this is not expected to impose limits on the applicability. In practice, this means that the applicability of the model is limitted to cases where energy propagates along straight lines over flat bottoms with equally distributed mud of constant properties.

7.3 Validation with simple dissipation tests

7.3.1 Test 1: Monochromatic, one-directional waves over a flat bottom with a mud layer of constant thickness

Description test lay-out

In this test a monochromatic wave is constructed by concentrating a pack of energy at an infinitesimal frequency and directional range. This sharply peaked spectrum is prescribed at

the boundary of a one dimensional domain, representing a straight flume with a layer of fluid mud of constant thickness at constant water depth (see Figure 28).

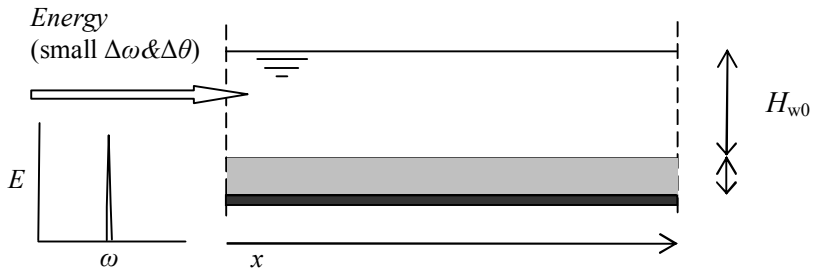

Figure 28 Schematic presentation of the lay-out of test 1: monochromatic, one-directional wave over a flat bottom (indicated by the dark gray volume) with a mud layer of constant thickness (indicated by the light gray volume).

Test objective and expected results

The decrease of energy during the propagation over the mud layer is calculated in SWAN-mud (I). When the energy at location x is calculated, also the significant wave height H_s can be calculated via:

$$H_s \approx 4\sqrt{m_0} \qquad \text{with} \qquad m_0 = \iint E(\omega,\theta)\, d\omega d\theta \tag{227}$$

where m_0 is the zero-th order moment of the energy spectrum.

The results of this computation will be compared with the results for the decay of the wave height H_s calculated directly from the imaginary wave number with:

$$H_s = H_{s0} e^{-k_i x} \tag{228}$$

where k_i is the same imaginary wave number as calculated in SWAN and used to determine the energy dissipation term $S_{b,m}$. Comparison with this (analytical) method is possible because k_i has the same value in the whole domain in case of uniform bottom geometry and properties.

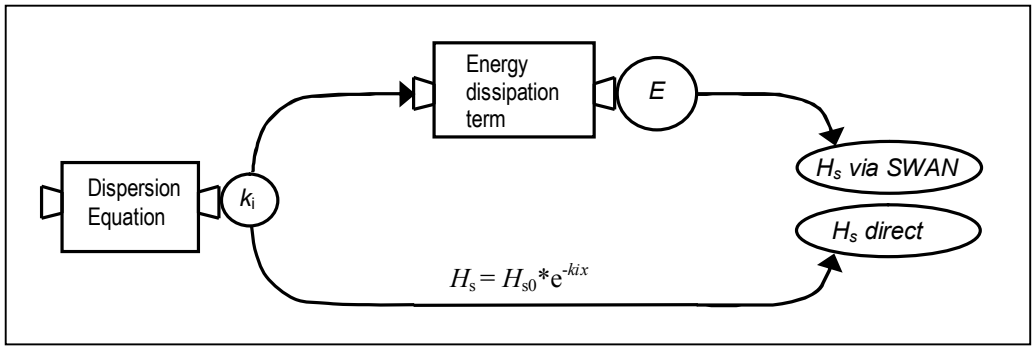

Figure 29 Schematic presentation of the two methods used to calculate H_s in test 1: the first method (top) calculates H_s with the use of the energy dissipation term in SWAN, the second method calculates H_s directly with the analytical expression $H_s=H_{s0}e^{-ki}$.

If the mud-induced dissipation term correctly represents the energy loss, the two graphs should coincide, both for shallow water and intermediate water depths.

Results

The results obtained with this test are shown in graphs of the significant wave height H_s as function of the travelled distance over the mud.

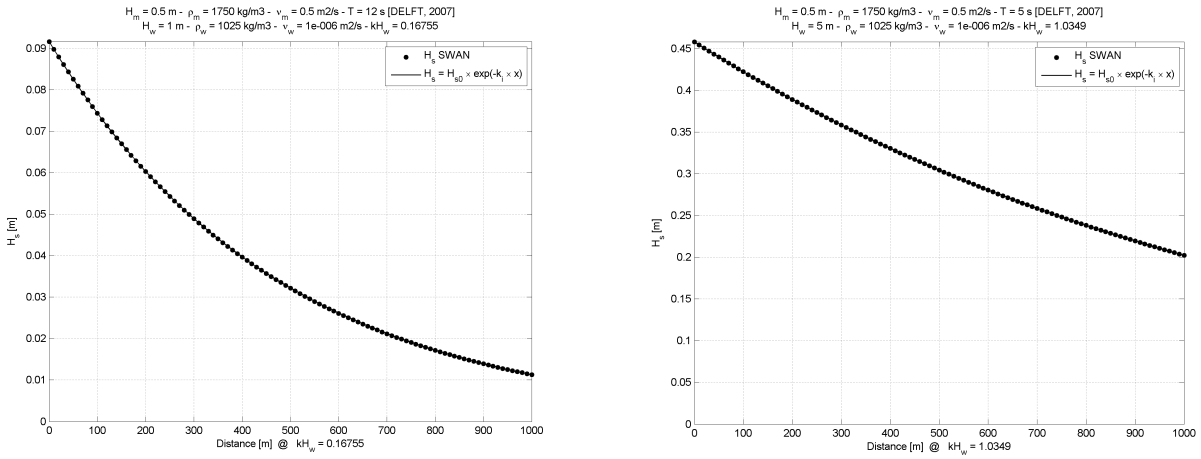

Figure 30 Test 1: Significant wave height H_s calculated via the newly derived energy dissipation term implemented in SWAN-mud (I) (dots) and directly with the analytical expression $H_s=H_{s0}e^{-kix}$ (continous line) for shallow water (left) and intermediate water depth. The kH_{w0}-values are indicated in the pictures. The wave number k is calculated with the dispersion equation DELFT.

The two lines coincide exactly, which is the case for all tested cases. This result shows that the newly derived energy dissipation term correctly represents the mud-induced energy loss. It also shows that the dispersion equation and the dissipation term are now consistent with each other both for shallow water as for intermediate water depths.

Test 1b: Comparison with other models

The results are compared to the models of Winterwerp *et al.*(2007), the model of Rogers and Holland (in review) and a shallow water model using both the dispersion equation and the energy dissipation term of Gade.

Name model	Reference	Dispersion Equation	Energy Dissipation	Domain of validity
Gade complete	Figure 21 (gray)	Gade	Gade (part II)	shallow water
Winterwerp *et al.*	section 5.4 & Figure 25 (gray)	De Wit	Gade (part II)	shallow water
Rogers and Holland	section 5.5	Ng	Rogers and Holland	all kH_{w0}-values
SWAN-mud (I)	section 7.2 & Figure 25 (black)	DELFT	new dissipation term	all kH_{w0}-values

Table 14 The new SWAN-mud (I) model (row 4) has been compared with the models in row 1, 2 and 3.

The energy dissipation term obtained by Gade (part II) is the shallow water limit of the newly derived energy dissipation term. The dispersion equations of Gade, De Wit and DELFT do give the same results for the wave number k for shallow water. Therefore, Gade complete and Winterwerp *et al.* (2007) are expected to give the same results for small values of kH_{w0}. Comparison of Figure 31 with the left panel of Figure 30 shows that this indeed the case.

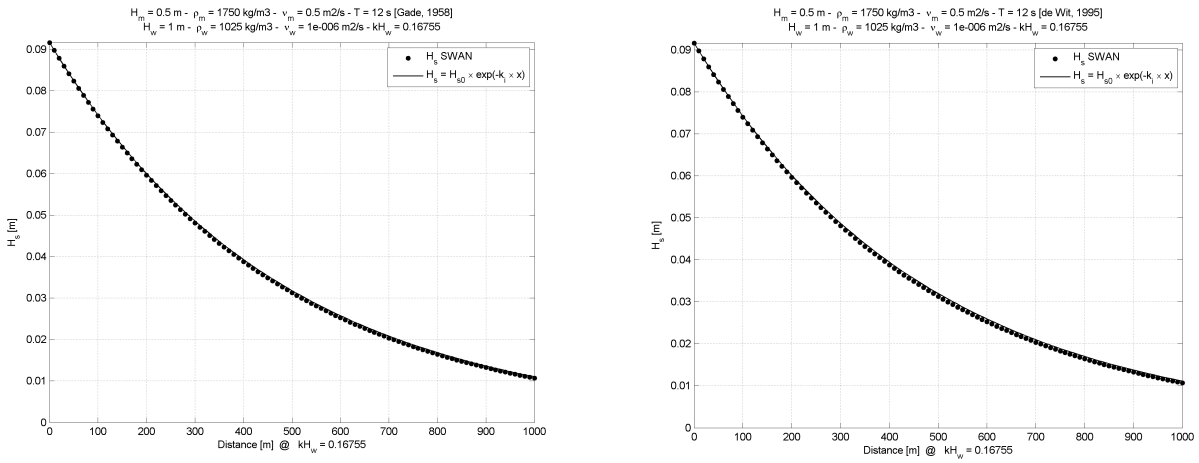

Figure 31 Test 1b, comparison for shallow water: The significant wave height calculated via energy dissipation implemented in SWAN (dots) and directly with the analytical expression $H_s=H_{s0}e^{-kix}$ (continous line). The left panel shows Gade complete, the right one shows Winterwerp *et al.* (2007)

At intermediate water depths ($kH_{w0} \approx 1$), two kinds of deviations are expected. Firstly we expect that k_i will be overpredicted by the dispersion equation of Gade, leading to too strong dissipation. Secondly we expect that computations with the energy dissipation term of Gade (part II) will also cause overprediction of the damping (compared to calculations with $H_s=H_{s0}e^{-kix}$). The results shown in Figure 32 are obtained for the same settings used in Figure 30, right panel. The results confirm the expectations, confirming the observation that Winterwerp *et al.* (2007) is in fact a shallow water model.

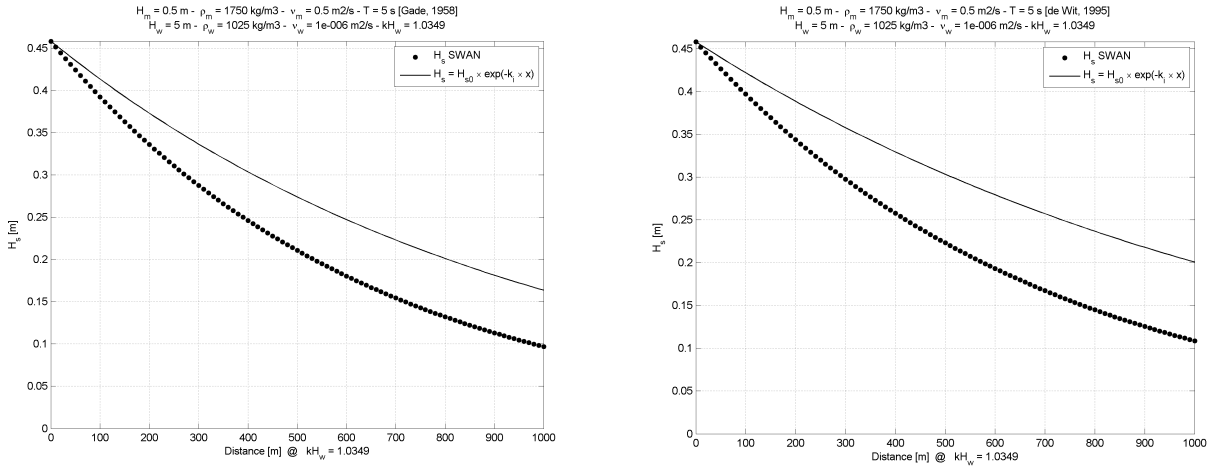

Figure 32 Test 1b, comparison for intermediate water depth: The significant wave height is computed from the energy dissipation according to Gade implemented in SWAN (dots) and directly from the analytical expression $H_s=H_{s0}e^{-kix}$ (continous line). The left panel shows Gade complete, the right one shows Winterwerp *et al.*(2007).

The SWAN-mud (I) model is compared with the model of Rogers and Holland by running the same test case as executed by Rogers and Holland (discussed in section 5.5.3, shown again in Figure 33.b). Figure 33 shows that the SWAN-mud (I) model and the model of Rogers and Holland give the same results.

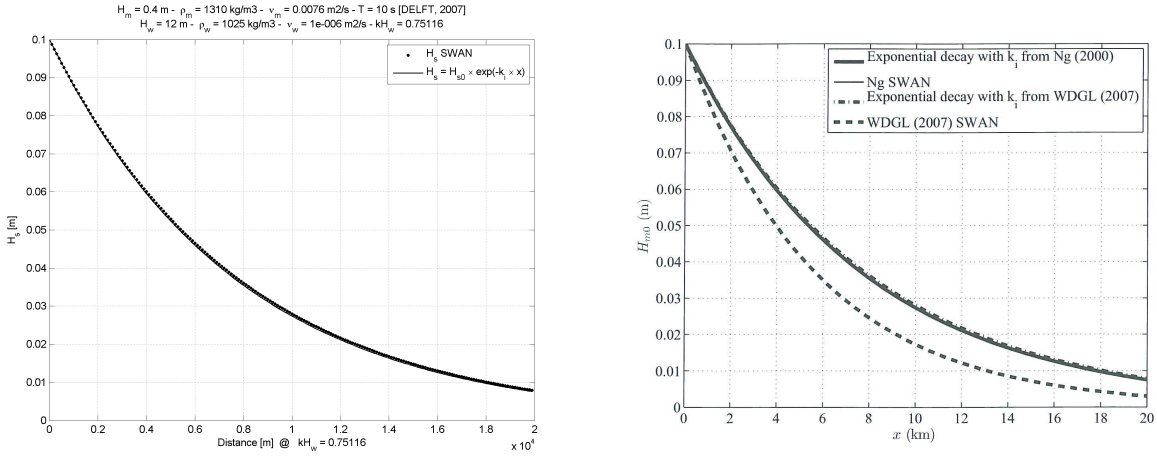

Figure 33 Test 1b, comparison of SWAN-mud (I) (left) with the test case of Rogers and Holland (right) showing results for their own model and for Winterwerp *et al.* (2007). The graphs show the significant wave height computed from the energy dissipation implemented in SWAN and directly from the analytical expression $H_s=H_{s0}e^{-kix}$ (see Figure 22 for a more extensive explanation).

7.3.2 Test 2: A spectrum of uni-directional waves over a flat bottom with a mud layer of constant thickness

Description test lay-out

Test 1 is extended by using a spectrum of waves as forcing of the system. The energy is spread over a broader frequency range but is still concentrated in a single directional bin. The bottom is flat and the mud layer is of constant thickness.

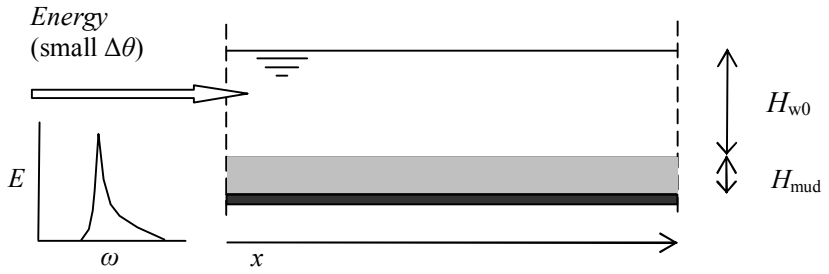

Figure 34 Schematic presentation of the lay-out of test 2: a spectrum of waves over a flat bottom with a mud layer of constant thickness.

Test objectives and expected results

This test investigates whether the model deals correctly with a full spectrum as well. The statement in literature (Sheremet and Stone, 2003) that the longer waves are more affected by the presence of fluid is investigated. The shape of the spectrum and the mean frequency are the discriminating parameters in this investigation. If the longer waves are more affected, it can be expected that the energy is reduced more at the lower frequencies and that the mean frequency shifts to a higher value.

Explanation of graphical presentation

The results are presented in a series of graphs (starting from Figure 35). The central graph is a contourplot of the variance density spectrum as function of the travelled distance x. The interpretation of this graph is facilitated by a second graph showing the variance density spectrum at a few distances (bottom left) and a résumé of some important spectral characteristics at x = 0 m and x = 300 m. The central graph also shows the development of the mean frequency of the waves as function of the travelled distance (thick black line). The mean frequency is computed from:

$$f_{mean} = \frac{\int fE(f,\theta)\mathrm{d}f}{\int E(f,\theta)\mathrm{d}f} \tag{229}$$

The top graph shows the significant wave height H_s as a function of the travelled distance, where H_s is computed directly from the variance density spectrum through equation (227). This graph gives the clearest insight in the influence of damping by fluid mud. In the bottom-right graph, the imaginary part of the wave number k_i is plotted as a function of the frequency. In case of one directional waves over a horizontal flat bottom with a mud layer of constant thickness, $k_i(f)$is the same at every grid point.

Results

Figure 35 and Figure 36 clearly show the wave damping by fluid mud. The significant wave height (top graph) and the variance density (center and bottom-left) decrease with travelled distance.

Comparison of the bottom-right graph in Figure 35 and in Figure 36 shows that the $k_i(f)$-funtion differs strongly for these two cases. Figure 35 shows the highest value for k_i at high frequencies. Figure 36 shows a peak value for k_i at a lower frequency. In the first case, the high frequency waves are damped the most. Therefore the mean frequency decreases with travelled distance (center graph). In the latter case, the peak of the damping is in the middle if the spectrum, resulting in a slight increase of the mean frequency with travelled distance. The different frequency of maximum damping is also visible in the shape of the spectra (bottom-left). In the first case the shape of the spectrum is mainly affected in the high frequency part of the spectrum. In the latter case, the spectral shape is mostly affected close to the peak frequency. In Figure 36 the spectrum is dented just right of the peak, around 0.20Hz.

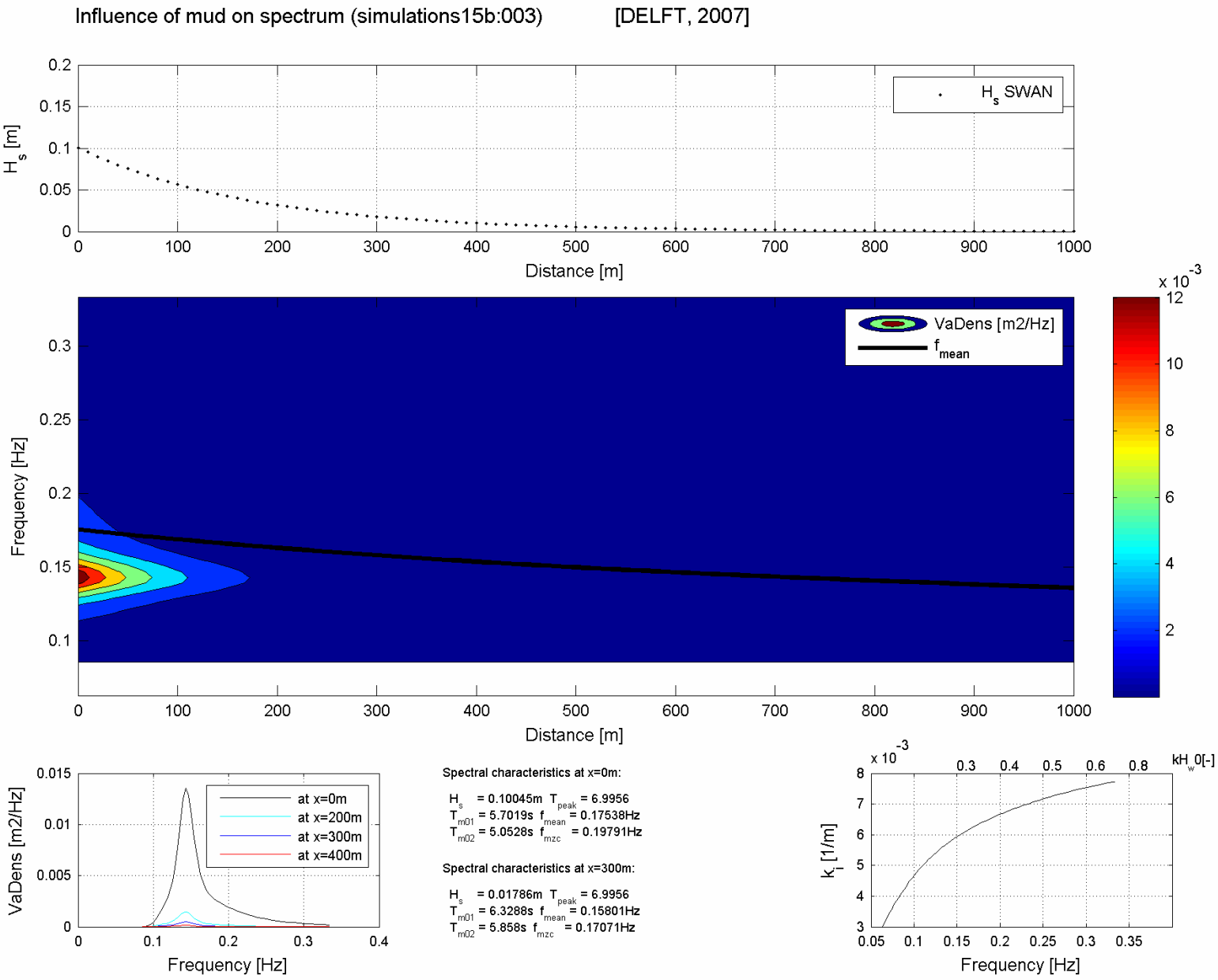

Figure 35: Graphs of the significant wave height H_s as function of the travelled distance x (top), the variance density spectrum as function of x with the mean frequency (central graph), the various density spectrum at x=0m, x=200m, x=300m and x=400m (bottom left), and the imaginary wave number k_i as function of the frequency (bottom right)

Conclusions

The graphs of the imaginary wave number as a function of frequency show that the peak of the damping can occur over the whole frequency domain (period 3-16 s), when using the currently investigated parameter domain. Therefore it is not possible to conclude that only the low frequency waves will be affected by the mud or that the mean frequency will increase. The frequency that receives the strongest damping depends on the local conditions concerning layer thicknesses and mud properties.

7.3.3 Test 3: the consequences of insufficient iterations

Description test lay-out

The lay-out of test 3 is exactly the same as the lay-out of test 2. The only difference is that the maximum number of iterations used to calculate the wave number with the DZANLY numerical iteration procedure is limited to 20 instead of 500 in the simulations before (as criterium next to a very stingent stopping criterium that was almost never reached). Such a reduction would make the procedure much faster.

Test objectives and expected results

The aim of this test is to investigate the sensitivity of the SWAN-calculations for deviations or errors in the computation of the wave number. It is expected that with less iterations, more cases will occur where the iteration has not yet converged to a proper solution. Values for the imaginary wave number that are too high are expected to result in energy loss. This is expected to be the case especially when wave-wave interaction will be taken into account. Values for the imaginary wave number that are too low will yield an underestimation of the damping as long as the value will not become negative. It is expected that negative values for the imaginary wave number will result in 'energy generation' and an increase of the wave height.

Results

Both phenomena are visible in the graphs presented. Figure 38 shows a positive peak in the $k_i(f)$-graph (bottom-right) with extra dissipation at one single frequency (center and bottom-left). (Wave-wave interaction is not activated here.) Figure 39 shows a peak resulting in a *negative* value for the imaginary wave number (bottom-right), causing a huge energy increase at one single frequency (center and bottom-left). The effect is an increase of the significant wave height over the travelled distance (top graph).

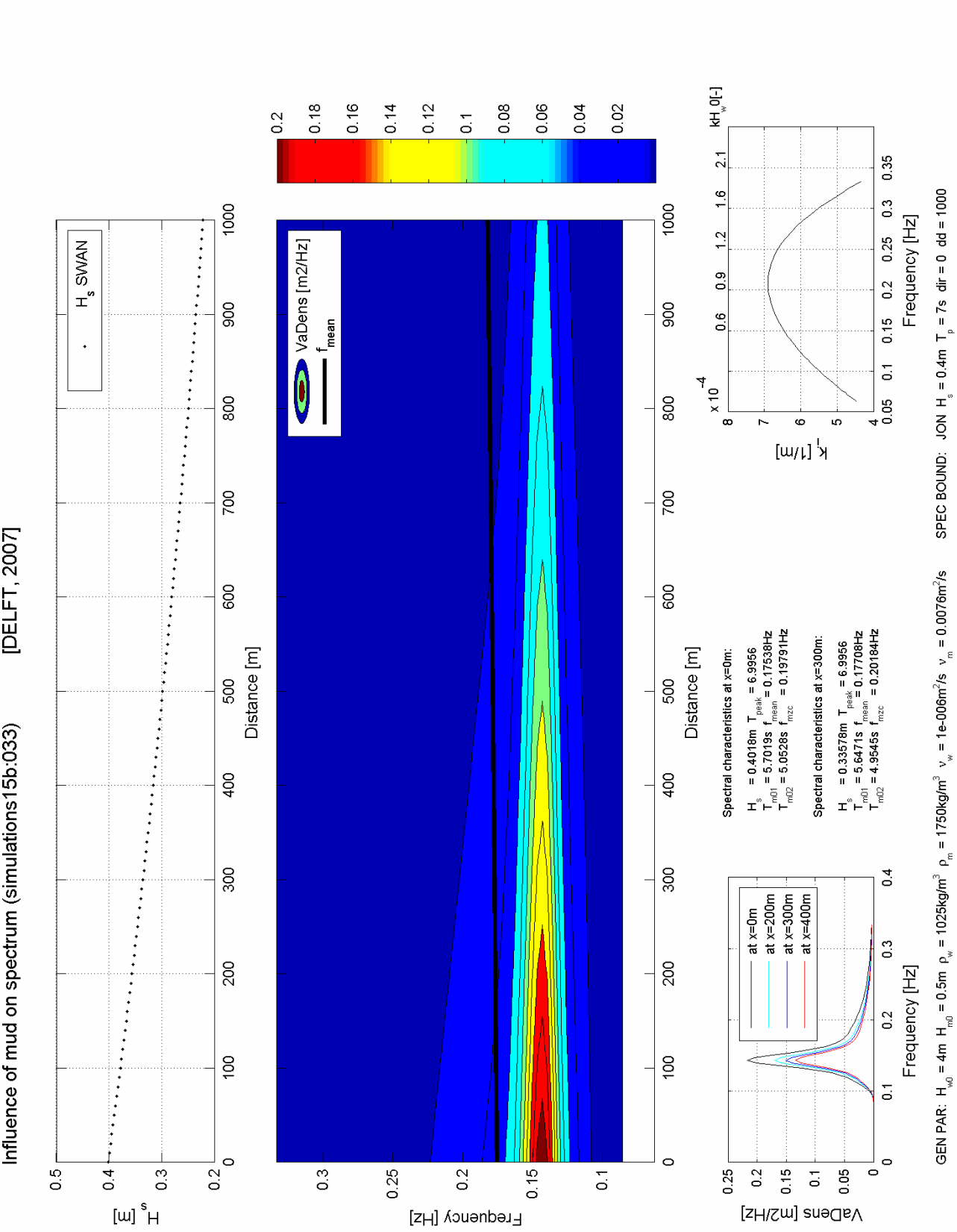

Figure 36: Graphs of the significant wave height H_s as function of the travelled distance x (top), the variance density spectrum as function of x with the mean frequency (central graph), the various density spectrum at x=0m, x=200m, x=300m and x=400m (bottom left), and the imaginary wave number k_i as function of the frequency (bottom right)

Discussion and conclusions

This test makes clear that one single erroneous value for the wave number can totally corrupt the results. Especially the influence of a negative value for the imaginary wave number is far-reaching. As long as the possibility exists that energy is generated by the model and that the significant wave height increases, the model functions insufficiently.

There are reasons to ease this statement. Firstly, the investigations till now show that erroneous results for the iteration are rare and isolated: only a single peak in the frequency spectrum for one specific set of parameters. Secondly, it is only in this test case with constant parameters over het whole area that an erroneous iteration can distort the result cell after cell. In practical cases, the next cell will yield new parameters, thus limiting the influence of errors in the iteration.

However, generation of energy would yield an unstable model. This has to be avoided at all cost. Therefore measures have to be taken to avoid generation of energy. The model achievement can be improved with the following adaptations:

1) Setting the value of the imaginary wave number k_i to zero when a negative value is computed. This adaptation would exclude instabilities, but is not very accurate.

2) Calculation of the wave number k outside the procedure which calculates $S_{b,m}$ (see Figure 26 and Figure 27). This adaptation, aimed to enable the model to take into account refraction and shoaling via the energy propagation velocities, also reduces the number of times that the wave number k is computed for each grid point to one. When less computations are needed, the time consumption of the iteration procedure is less problematic. In that case, application of more iteration staps and more strict criteria is not a problem.

3) Overruling the dissipation term in case dissipation by mud is less than dissipation by sand. This adaptation is needed to deal with gradually transition from sand to mud. It is expected that in case of a very thin mud layer, the damping will not be governed by the mud-induced damping, but by the normal bottom friction. Otherwise bottom induced damping would almost vanish when the first thin mud patches are encoutered by the waves. The details of this transition are not studied within the scope of this thesis. For the time being, the largest bottom dissipation term is set to be dominant via:

$$\begin{aligned} &S_{b,m} \geq S_{bfr} \rightarrow \quad S_{b,m} = S_{b,m} \quad \& \quad S_{bfr} = 0 \\ &S_{b,m} < S_{bfr} \rightarrow \quad S_{b,m} = 0 \quad \& \quad S_{bfr} = S_{bfr} \\ &S_{bottom} = S_{b,m} + S_{bfr} \end{aligned} \tag{230}$$

Where $S_{b,m}$ is the mud-induced dissipation term, S_{bfr} is the dissipation by bottom friction on a sandy bottom and S_{bottom} is the total bottom-induced damping.

With this measure negative peaks for the wave number are overruled and the erroneous generation of energy is prevented, because regular bottom friction will be dominant in case of peaks with negative values for the imaginary wave number.

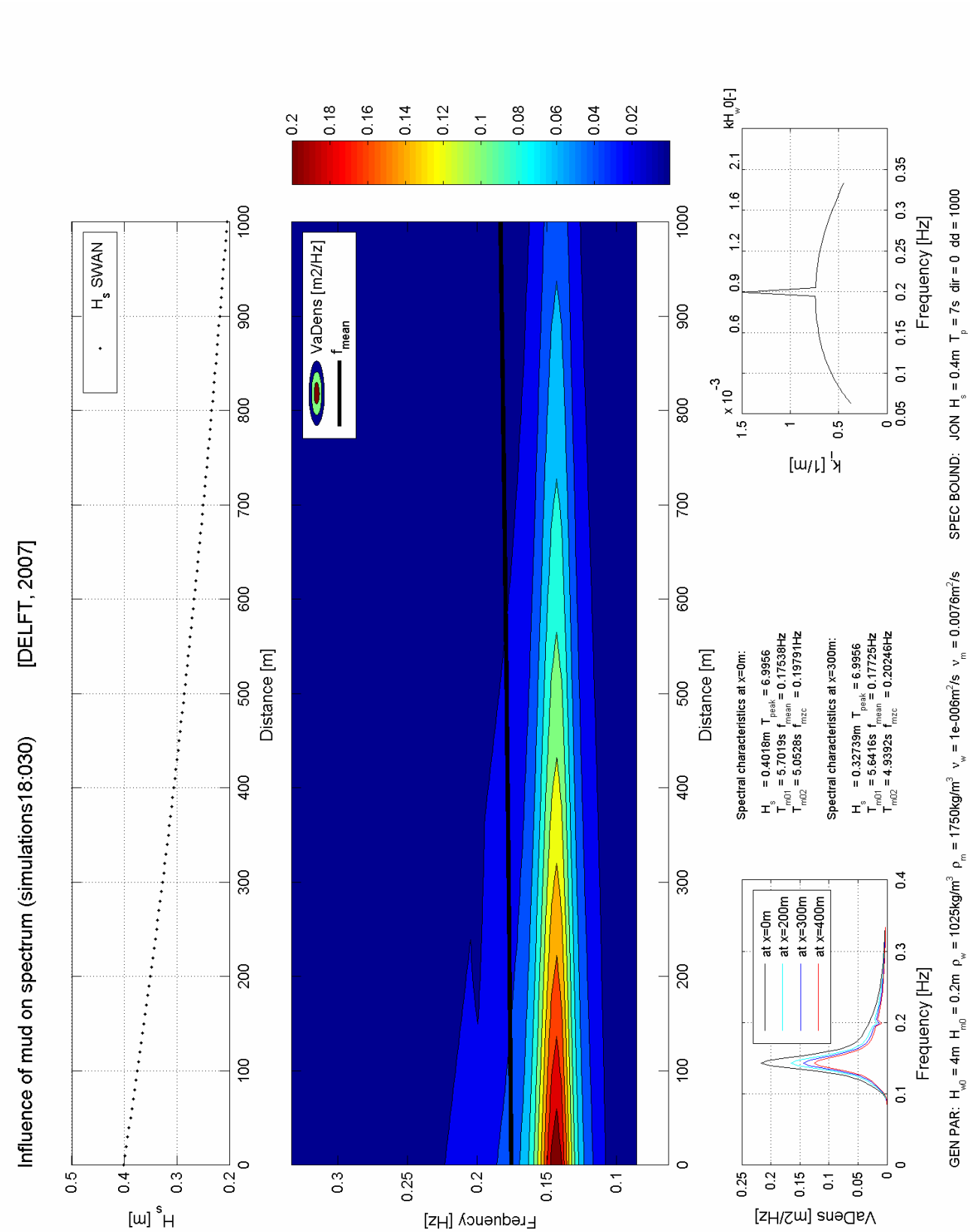

Figure 37: Graphs of the significant wave height H_s as function of the travelled distance x (top), the variance density spectrum as function of x with the mean frequency (central graph), the various density spectrum at x=0m, x=200m, x=300m and x=400m (bottom left), and the imaginary wave number k_i as function of the frequency (bottom right)

The positive peak in the imaginary wave number resulting from an incomplete iteration implies overestimation of the damping. This is visible in the variance density spectrum via an indent at 0.2Hz.

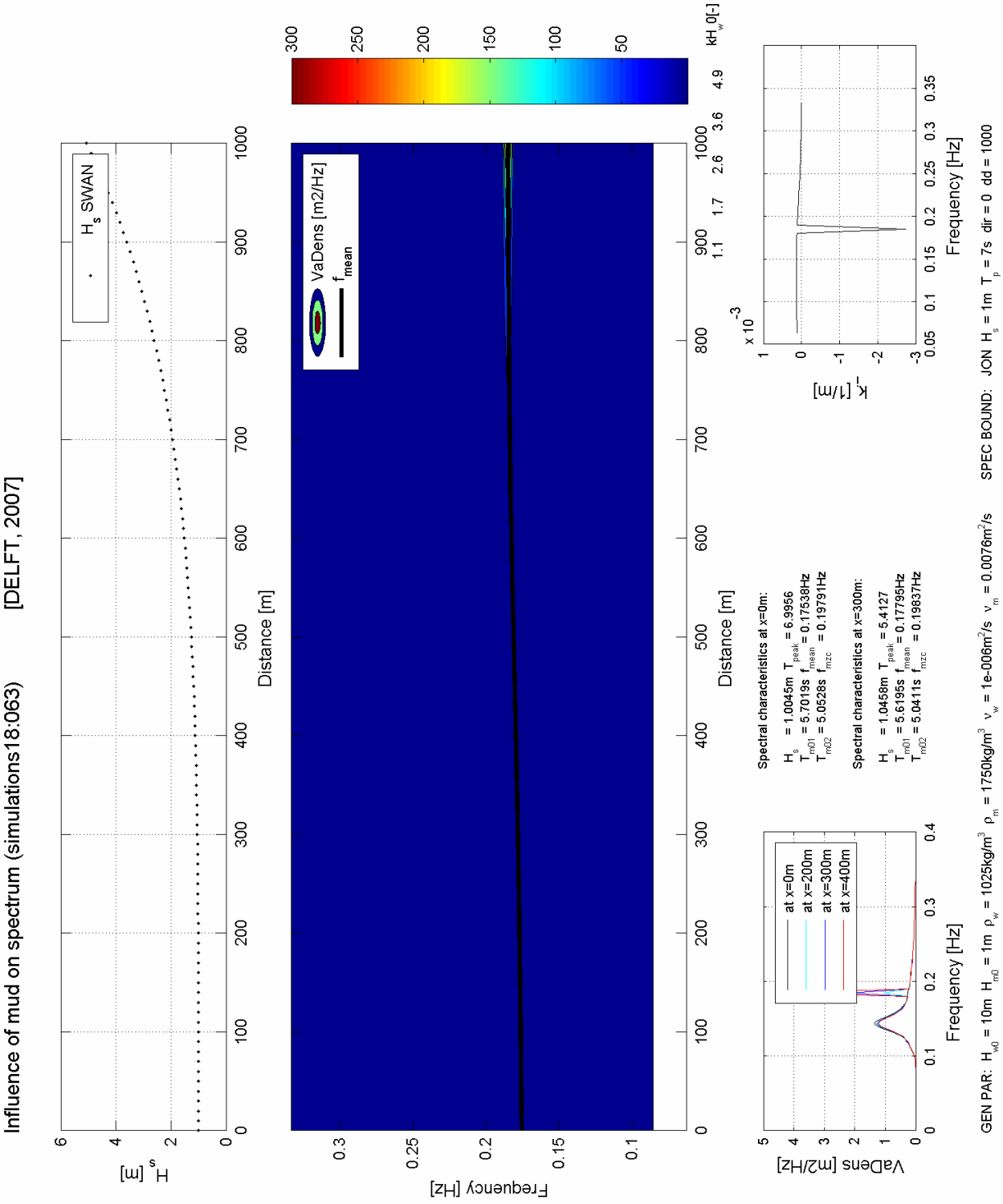

Figure 39: Graphs of the significant wave height H_s as function of the travelled distance x (top), the variance density spectrum as function of x with the mean frequency (central graph), the various density spectrum at x=0m, x=200m, x=300m and x=400m (bottom left), and the imaginary wave number k_i as function of the frequency (bottom right)

The negative value for the imaginary wave number resulting from an incomplete iteration implies generation of energy. This is visible in the variance density spectrum via a peak at 0.18Hz increasing with travelled distance and via the increas of the significant wave height.

4) Correction of the wave number via comparison with neighbouring frequencies (and gridpoints). A physically more sound and probably more accurate improvement would be to identify the peaks by comparing the value for the wave number with results for neighbouring frequencies (and possibly gridpoints) and neutralize them by interpolation between or extrapolation of proper results. Disadvantage is that such a procedure is only possible in case of occasional errors in the iteration and certainty about the values used for inter- or extrapolation. An advantage is that in this way the real part of the wave number can be improved as well.

5) Application of a more reliable iteration procedure. This implies extension of the work done in chapter 4. A more extended investigation could focus on the iteration procedure itself, by comparing the performance of the DZANLY iteration procedure with other procedures available.

Finally, it is also possible to pre-calculate the wave number for a high number of parameter sets and to store the results in a look-up table (LUT). The computations for this table could be carried out very accurately and checked manually. When this table is accessible during the run of SWAN, the wave number can be achieved by interpolation of the results for the nearest parameter sets. However, this approach is rejected, because of the large numbers of parameters involved in the schematization, leading to a huge LUT when the LUT is generated by going through the domain in appropriate small steps.

7.4 Discussion and conclusions

This chapter described the implementation of the DELFT dispersion equation into the wave model SWAN, focussing on energy dissipation. A newly derived energy dissipation term has been implemented and tested. Tests for the case of mono-chromatic, uni-directional waves over a flat bottom with a mud layer of constant thickness prove the consistency between dispersion equation and energy dissipation term. This implies that the SWAN-mud (I) model is valid both for shallow water and water of intermediate water depths. Tests with a spectrum of waves as forcing of the system show that the SWAN-mud (I) model deals well with spectra. It was also shown that it is not possible to conclude that only the low frequency waves will be affected, because the frequency of the highest damping depends on the layer thicknesses and mud properties and can be in the high frequency range. Tests with a strongly reduced number of iterations show that the results of the SWAN-mud (I) model can be distorted heavily in case of erroneous values for the imaginary wave number.

Based on the last test, four suggestions are given for model improvement:

1. set negative values of the wave number to zero to avoid instability
2. reduce the number of times the iteration procedure has to be carried out. This can be achieved by computation of the wave number only once for each grid point and frequency.
3. avoid the negative peaks in the damping by overruling the mud-induced dissipation term in case this dissipation is less than the normal bottom dissipation.
4. correct the erroneous values for the wave number via comparison with values for neighbouring frequencies and gridpoints.
5. investigate the application of other iteration procedures instead of the DZANLY routine

The first three improvements are applied in SWAN-mud (II), described in chapter 8. Suggestion three and four are not studied further within this project.

8 Implementation of 'DELFT' into SWAN (2): Energy propagation

8.1 Introduction

Chapter 7 described the first step in the implementation of the mud-adjusted wave number k and the newly derived energy dissipation term $S_{b,m}$ into SWAN, focussing on the energy dissipation by fluid mud. This chapter describes the next step in the development of the model. It contains the displacement of the location where the wave number k is computed. This makes the model more efficient and makes it possible to compute the influence of mud on energy propagation.

Because the presence of mud affects the wave number k, it will also affect the group velocity c_g ($c_g = \partial\omega/\partial k$). This group velocity is the propagation velocity of energy. Therefore the presence of mud also affects the propagation of energy and the propagation phenomena of shoaling and refraction. This is illustrated in the picture below.

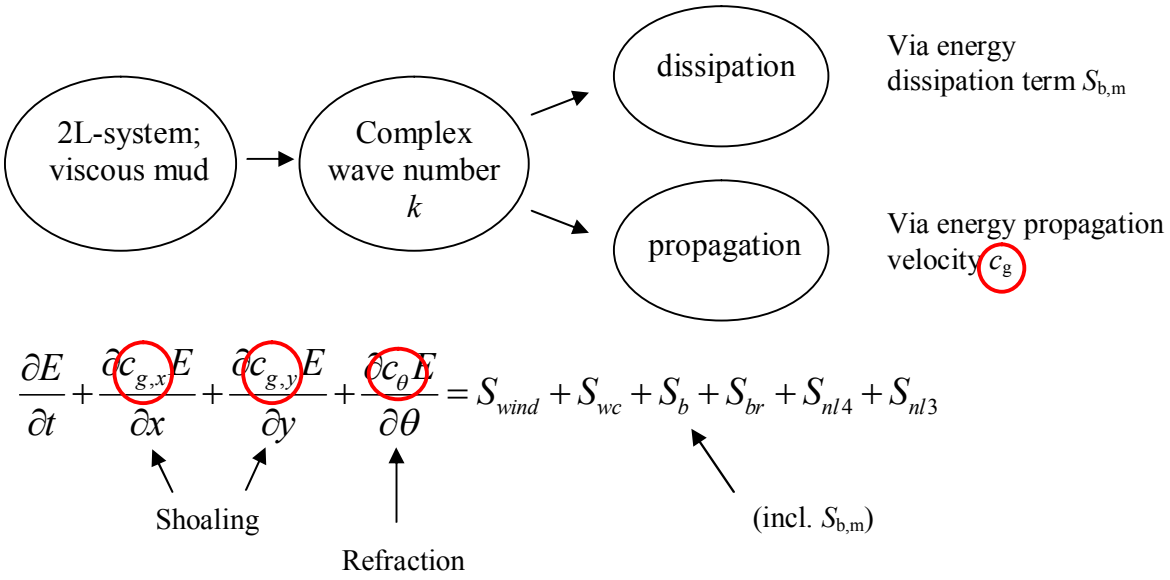

Figure 40 Illustration of the influence of the mud adjusted wave number on both dissipation and propagation of energy

Chapter 8 discusses the inclusion of the influence of fluid mud on energy propagation in the SWAN-mud model. Section 8.2 describes the changes in the implementation compared to chapter 7. Section 8.3 describes a validation with various propagation tests on shoaling and refraction. Finally, section 8.4 discusses conclusions and suggestions for further improvement.

8.2 Consequences for implementation into SWAN

To take into account the effect of mud on the propagation of energy, the mud affected wave number k has to be used to calculate the propagation speed of energy c_g. This means that the iteration procedure to calculate the wave number k has to be carried out on a higher level in the program compared to the implementation described in chapter 7. Figure 26 and Figure 27 in chapter 7 illustrated the structure of SWAN-mud (I). The Program Structure Diagrams in Figure 41 and Figure 42 illustrate the structure of the extended implementation.

SWAN stationair

Initialisations
Boundary Conditions
Four directional sweeps
Grid loop (x,y)
calculation mud affected wave number *(x,y)* (only once)
calculation propagation velocities of energy (*x,y*)
calculation propagation velocities of energy (σ,θ)
calculation SOURCE and sink terms: S_{bfr} $S_{b,m}$ S_{wc} S_{br} S_{nl3} S_{nl4} S_{wind}
calculation left-hand side terms in ACTION balance: $\delta C_x N/\delta x$ $\delta C_y N/\delta y$ $\delta C_\sigma N/\delta\sigma$ $\delta C_\theta N/\delta\theta$
solve matrix filled in SOURCE and ACTION → $N(x,y,\sigma,\theta)$
Iterate until iteration criterium is fulfilled

Figure 41 Program Structure Diagram of the SWAN-mud (II) model (including propagation). The wave number k is calculated before the propagation velocities of energy. This calculation is executed only once for each grid point (compare to Figure 26, chapter 7)

Calculation of $S_{b,m}$

INPUT: H_{w0}, H_{mud}, ρ_1, ρ_2, v_w, v_m, g, ω, $\boldsymbol{k}$ (ω&k vector IS=1:ISSTOP)
DO for IS = 1:ISSTOP
calculate amplitude ratio *b/a*
calculate phase difference interface and surface
calculate real pressure amplitude
calculate mud-induced energy dissipation
OUTPUT: vectors of length ISSTOP for b/a, φ, $S_{b,m}$

Subroutine "DISDELFT"

Figure 42 Program Structure Diagram of the calculation of the mud-induced dissipation term $S_{b,m}$ in the SWAN-mud (II) model (including propagation). The wave number k is an input parameter for this subroutine (compare to Figure 27, chapter 7).

The calculation of the mud-induced dissipation term is simplified. Now the wave number is an input parameter to the calculation of $S_{b,m}$ (see Figure 42). Also the other generation, dissipation and interaction mechanisms make use of the adjusted wave number. However, these effects are considered to be small (Kaihatu *et al.*, 2007).

As long as layer thicknesses and water and mud properties do not change in time, the wave number can be considered as a fixed property to each grid point. Therefore the iteration procedure is executed only once for each grid point. So also in non-stationary SWAN calculations **without coupling** to other models giving feedback on layer thicknesses (flow) or water and mud properties, one calculation per grid point is sufficient.

The present version of the code contains a number of test configurations. The first is the possibillity to choose a dispersion relation to calculate the wave number (1:Gade; 2:DeWit; 3:DELFT). The second is the possibility to choose the energy dissipation term (0:off; 1:Gade; 3:DELFT). Finally it is possible to choose to run the program with or without influence of mud on propagation (0:without; all other values:with). These configurations make it possible to test dissipation and propagation phenomena seperately.

8.3 Validation with simple propagation tests

The objective of the tests in this section is to validate the implementation of DELFT into SWAN for energy propagation. Therefore, the energy dissipation by fluid mud is switched off.

8.3.1 Test 1: A Sloping bottom covered with a thin mud layer

Description test lay-out

A monochromatic, uni-directional wave is sent over a mildly sloping bottom covered with a thin mud layer of constant thickness.

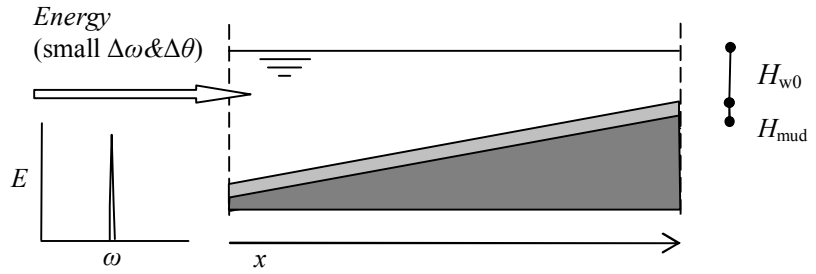

Figure 43 Schematic presentation of the lay-out of test 1: monochromatic, uni-direction wave over a mildly sloping bottom covered with a mud layer of constant thickness

Test objective and expected results

The objective of this test is to check whether shoaling can be reproduced with the use of the mud affected wave number. Because the mud layer is of constant thickness and because dissipation is turned off, the simulation is expected to show a development of the significant wave height H_s comparable to normal shoaling.

Results

The results of the test are shown in Figure 44.

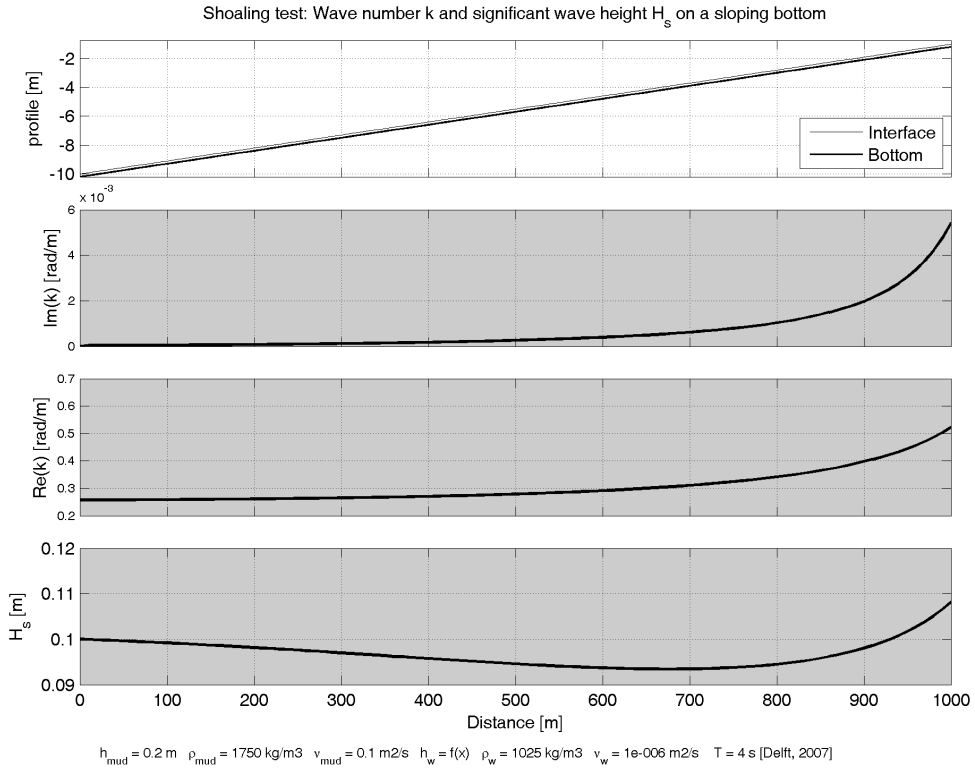

Figure 44 Propagation Test 1: Significant wave height H_s calculated with SWAN-mud (II). Panel 1 shows the used profile, panel 2 & 3 show the imaginary and real part of the wave number respectively. Panel 4 shows the significant wave height H_s.

The development of the significant wave height H_s while propagating over the slope is shown in Figure 44, panel 4. It shows the same behaviour as known for normal shoaling on a sloping bottom: initialy the amplitude decreases, followed by an increase in the shallowest part (see e.g. Holthuijssen 2007).

This result shows that shoaling can be determined using the dispersion relation DELFT and that in the current implementation the mud adjusted wave number is influencing the group velocity.

8.3.2 Test 2: A shallow water layer on top of a mud layer of varying thickness

Description test lay-out

The bathymetry consists of a shallow water layer of constant thickness on top of a fluid mud layer of varying thickness. The energy comes in concentrated in a single frequency and directional bin.

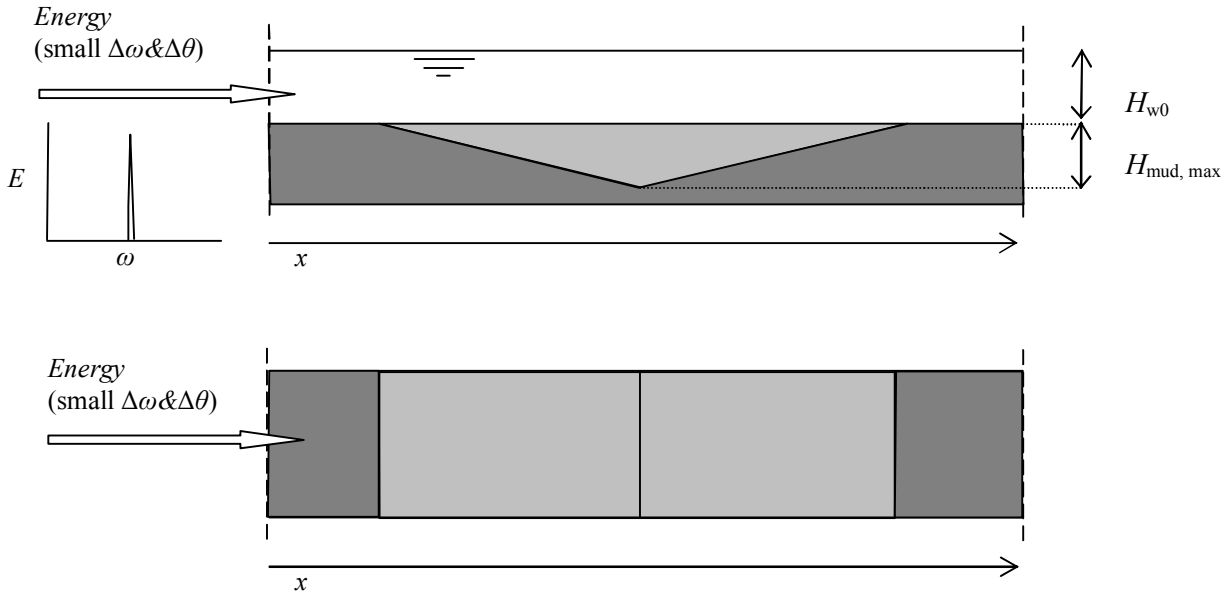

Figure 45 Schematic presentation of the lay-out of test 2: monochromatic, uni-direction wave in a shallow water layer of constant thickness and a mud layer that at first increases and subsequently decreases

Test objective, method and expected results

The objective of this test is twofold: to check for the reversibility of mud-induced shoaling and to compare the results with results obtained analytically.

Shoaling can be considered as horizontal compacting or stretching of wave energy. No energy is dissipated in this phenomenon. When the mud layer thickness varies while the water layer keeps the same thickness, mud-induced shoaling can be expected. In the same way as waves can be compacted or stretched on a certain slope, they will be stretched or compacted again on the reverse slope, finally resulting in the same significant wave height. So the process is reversible. The results of the model are expected to show this reversible behaviour.

The comparison with analytical results has the aim to check the numerical calculations and implementation in the code in a quantitative way. An analytical expression is derived for the shoaling coefficient. This represents the ratio between the significant wave height at location

x and at the beginning of the domain. To do this, the group velocity c_g at both locations is needed. The group velocities are calculated via differentiation of Gade's dispersion equation (see equation 19).

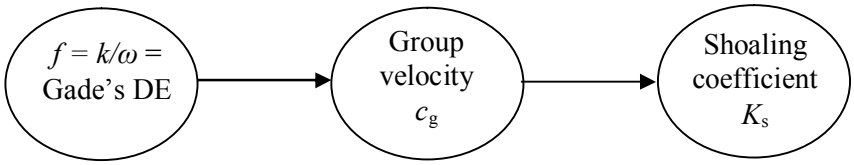

Figure 46 Illustration of the analytical way to calculate the influence of the mud affected wave number on the propagation phenomenon of shoaling

This procedure is described with the following formulae:

$$K_s = \frac{H_s(x)}{H_s(x_0)} = \sqrt{\frac{c_{g,x0}}{c_{g,x}}} \tag{231}$$

$$c_g = \left(\frac{\partial k}{\partial \omega}\right)^{-1} \tag{232}$$

$$\frac{\partial k}{\partial \omega} = \frac{\partial f}{\partial \omega}\omega + f \qquad \text{with } \frac{\partial f}{\partial \omega} = \frac{\partial f}{\partial \Gamma}\frac{\partial \Gamma}{\partial m}\frac{\partial m}{\partial \omega} \quad \text{and} \quad \Gamma, m \text{ see eq. (20)} \tag{233}$$

An important condition for this test is that the choosen parameters represent shallow water conditions, because only at shallow water conditions, Gade's dispersion equation gives the same results for the wave number. Under this condition, also the same results are expected for shoaling.

Results

The results of these tests are shown in Figure 47 and Figure 48.

Figure 47 combines the results of the computation with SWAN-mud (II) (continuous lines) and the analytical computations using Gade (dots). The continuous line clearly shows that the reversible character of shoaling is reproduced by the model. It also shows that the reduction of the wave height for the choosen parameters is more than 10%. Comparison of the results obtained with SWAN and the analytical results shows that SWAN gives the same results as the analytical computation. (The very small differences that exist can be explained by the fact that in this simulation kH_{w0}=0.168, which is close to, but not the same as the shallow water limit).

Figure 48 shows the results for c_g and K_s from the analytical computation using Gade (so these graphs belong to the dots in Figure 47). It illustrates that the propagation velocity of energy is higher in case of propagation over mud. This results in a $K_s < 1$ and in a reduction of the significant wave height H_s (Figure 47, panel 4). The analytical computations are carried out only for half the domain.

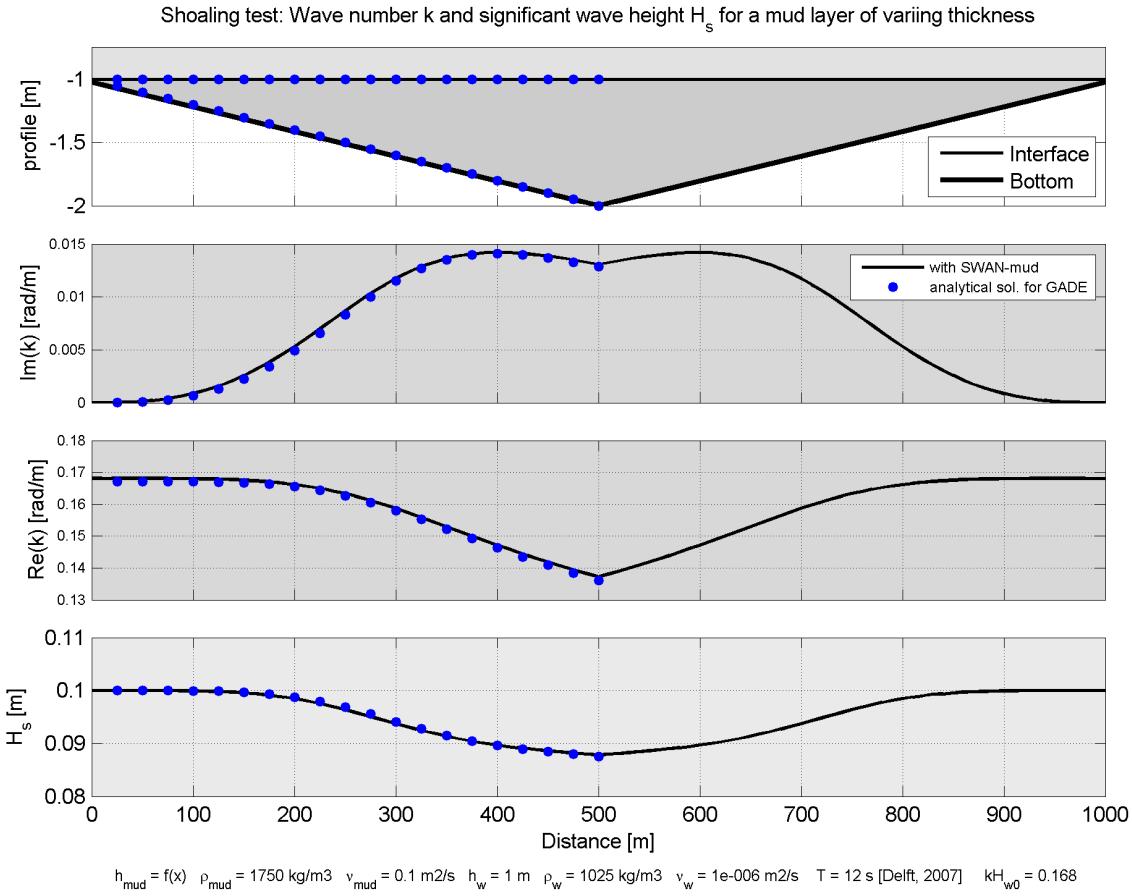

Figure 47 Propagation Test 2: Significant wave height H_s calculated with SWAN-mud (II) using Dispersion Equation 'DELFT'. (continuous line) and in an analytical way using Gade (dots). Panel 1 shows the used profile, panel 2 & 3 show the imaginary and real part of the wave number respectively. Panel 4 shows the significant wave height H_s.

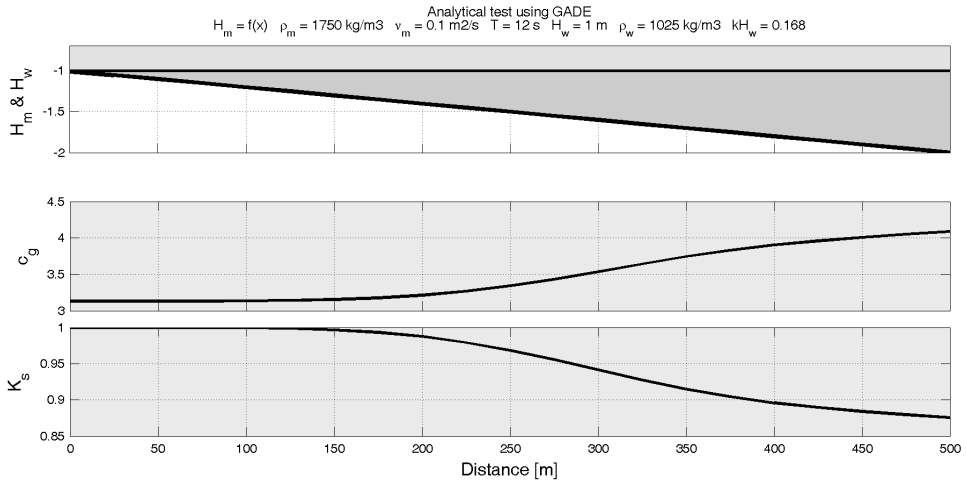

Figure 48 Propagation Test 2: Group velocity c_g and shoaling coefficient K_s as computed in an analytical way from GADE. Panel 1 shows the used profile, panel 2 shows the group velocity c_g and panel 3 the shoaling coefficient K_s representing the ratio of the significant wave height at distance x and at the beginning of the domain.

8.3.3 Test 3: Obliquely incident waves over a mud layer of varying thickness

Description test lay-out

The bathymetry in this test is the same as in the previous test: a shallow water layer of constant thickness on top of a fluid mud layer of varying thickness. Again, the energy comes in concentrated in a single frequency and directional bin, but this time the waves approach obliquely. The depth contours of the mud are assumed to be parallel (which comes with the 1D-approach). The angle between the normal to the contours and the direction of propagation of the incoming waves is 20^{O}.

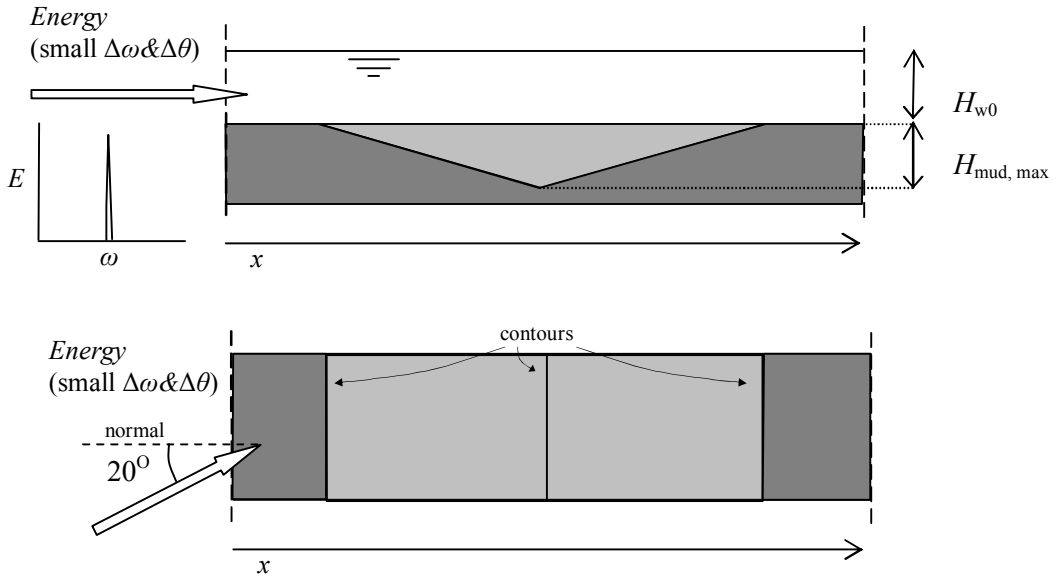

Figure 49 Schematic presentation of the lay-out of test 3: monochromatic, obliquely incident wave in a shallow water layer of constant thickness and a mud layer that at first increases and subsequently decreases

Test objective, method and expected results

The objective of this test is to validate the model for mud-induced refraction. It is expected that the presence of mud under a water layer of constant thickness causes a (reverse) refraction: the real wave number is expected to decrease. In that case the phase speed of the incoming waves will increase (just as in the shoaling test). For obliquely incident waves, this should cause an increase of the angle between 'normal' and direction of propagation. Furthermore, refraction is expected to have influence on the significant wave height (additional to shoaling).

Results

The results of these tests are shown in Figure 50.

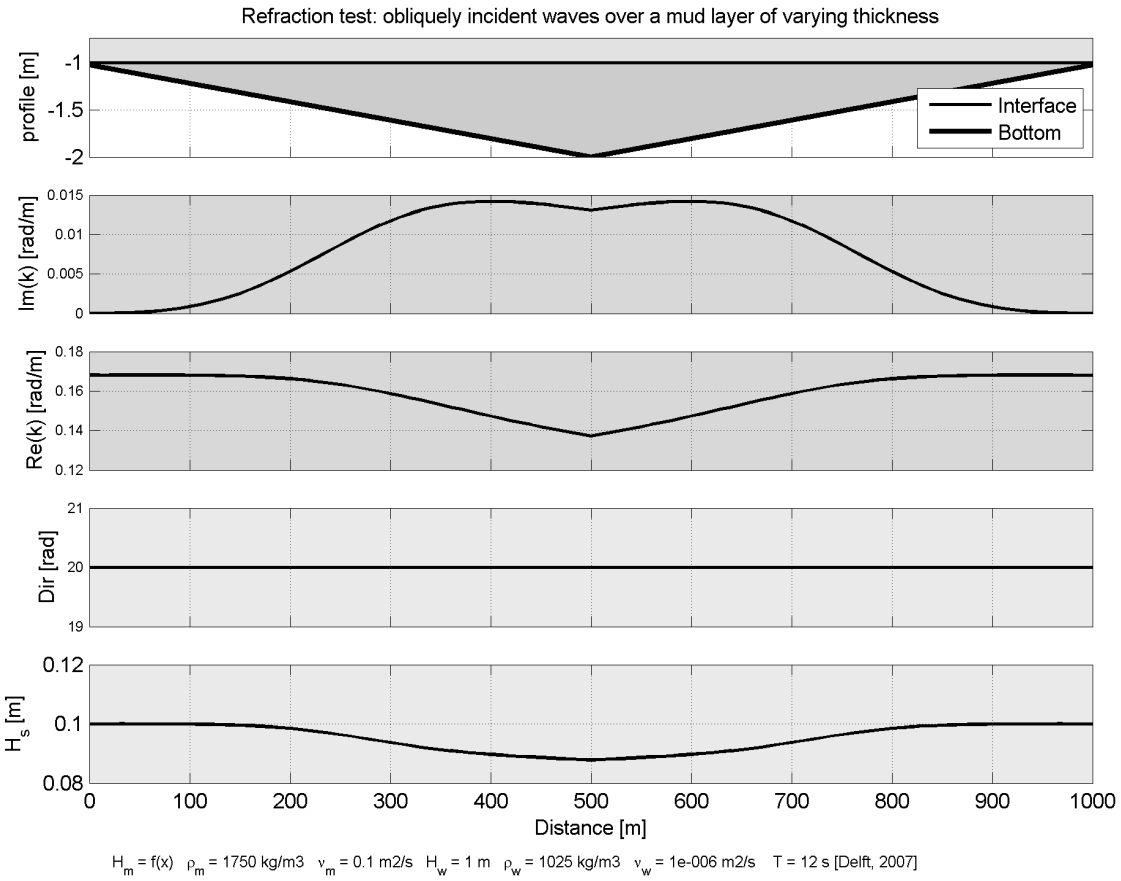

Figure 50 Propagation Test 3: Wave direction *Dir* and Significant wave height H_s calculated with SWAN-mud (II) using Dispersion Equation 'DELFT'. Panel 1 shows the used profile, panel 2 & 3 show the imaginary and real part of the wave number respectively. Panel 4 shows the direction of propagation. Panel 5 shows the significant wave height H_s.

Panel 4 of Figure 50 does not show any effect of mud on the propagation. This is in contradiction with the expectations. Although the mud-adjusted wave number is available in SWAN-mud (II) throughout the whole code and is used to compute the propagation speed of energy in *x*- and *y*-direction ($c_{g,x}$ and $c_{g,y}$), its effect on the propagation speed of energy over frequency and direction (c_σ and c_θ) is apparently not yet accounted for in SWAN in a correct way. The reason for the absence of mud-induced refraction is identified and explained below.

A general formulation to compute c_θ for the situation without current is given in equation (234) (for derivation, see Holthuijsen, p. 204):

$$\frac{d\theta}{dt} = c_{\theta,ref} = -\frac{c_g}{c}\frac{\partial c}{\partial m} \tag{234}$$

where

m is a coordinate axis along an iso-phase line (e.g. the wave crest),

$c_{\theta,\mathrm{ref}}$ the turning rate in time in a frame of reference moving with the wave energy

Using $c = \omega/k$ and $c_g = \partial\omega/\partial k$, this expression can be written as:

$$\frac{d\theta}{dt} = c_{\theta,ref} = \frac{1}{k}\frac{\partial\omega}{\partial k}\frac{\partial k}{\partial m} \tag{235}$$

In the SWAN code, $c_{\theta,\mathrm{ref}}$ is computed with:

$$\frac{d\theta}{dt} = c_{\theta,ref} = -\frac{1}{k}\frac{\omega k}{\sinh\left(2kH_{w0}\right)}\frac{\partial H_{w0}}{\partial m} \tag{236}$$

This expression is obtained from equation (235) using the fact that in the absence of an ambient current, the frequency is constant along the wave crest and that for the regular dispersion equation the frequency can be seen as a function of (only) the wave number k and the water depth H_{w0}, resulting in the equation:

$$\frac{d\omega}{dm} = \frac{\partial\omega}{\partial k}\frac{\partial k}{\partial m} + \frac{\partial\omega}{\partial H_{w0}}\frac{\partial H_{w0}}{\partial m} = 0 \qquad \rightarrow \qquad \frac{\partial\omega}{\partial k}\frac{\partial k}{\partial m} = -\frac{\partial\omega}{\partial H_{w0}}\frac{\partial H_{w0}}{\partial m} \tag{237}$$

Furthermore, the term $\partial\omega/\partial H_{w0}$ is in the code directly subsituted with an expression that is derived using the regular dispersion equation:

$$\frac{\partial\omega}{\partial H_{w0}} = \frac{1}{2\omega}\frac{\partial\omega^2}{\partial H_{w0}} = \frac{1}{2\omega}\frac{\partial\left(gk\tanh\left(kH_{w0}\right)\right)}{\partial H_{w0}} = \frac{\omega k}{\sinh\left(2kH_{w0}\right)} \tag{238}$$

The use of the regular dispersion equation (twice) in the derivation of equation (236), makes this expression not valid in the presence of fluid mud, also not when the mud-adjusted wave number is used to compute $c_{\theta,\mathrm{ref}}$ with this equation. Therefore it is recommended to use the more general equation (235) to compute $c_{\theta,\mathrm{ref}}$ in the presence of fluid mud. To determine the partial derivative of the wave number k with respect to (the direction) m, a proper discretization has to be introduced and information has to be available in the subroutine concerning the wave number k on the locations around the location for which $c_{\theta,\mathrm{ref}}$ is calculated. This recommended adaptation of the code is not yet carried out during this project.

8.4 Discussion and conclusions

This chapter described the inclusion of the influence of fluid mud on energy propagation in SWAN-mud (II). The main characteristic of this implementation is that the mud affected wave number is made available to be used at all places in the model where a wave number is needed. The implementation is tested for various cases. These tests showed that the model

represents the (reversible) shoaling phenomenon as expected. For shallow water the model results are the same as results of analytical computations for this limit case.

Mud-induced refraction is not yet properly represented, because the formula used in SWAN to compute the turning rate in time of wave energy over directions (c_θ) has been derived using the regular dispersion equation (which is not valid in the presence of fluid mud). To account for mud-induced refraction, this formula has to be replaced by a more general applicable formula.

The shallow water test for straightly incoming waves (Figure 47) showed that the reduction of the significant wave height by shoaling can be more than 10%. For this specific case, the damping would be very strong, as illustrated in Figure 51.

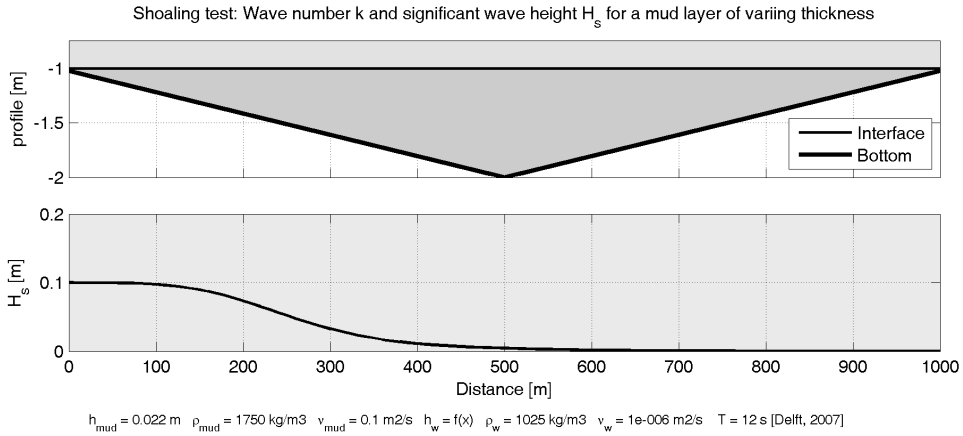

Figure 51 Propagation Test 2 with damping: Significant wave height H_s calculated with SWAN via Dispersion Equation 'DELFT'. Panel 1 shows the used profile. Panel 4 shows the significant wave height H_s.

To assess the importance of the incorporation of mud on wave energy propagation, it will be useful to investigate for various cases the ratio between the reduction of the wave height by propagation and dissipation phenomena. This ratio will not be a 'property' of the location, because it depends on the distance between the locations of varying layer thicknesses.

9 Conclusions and recommendations

9.1 Recapitulation of project objectives

The main objective of this MSc. Thesis project was the development and testing of a modified SWAN-version with which it is possible to model the decrease of energy during the propagation of a wave field over fluid mud.

Additional requirements on the application were formulated. The application has to be:
- applicable for shallow and non-shallow water
- consistent
- efficient
- reliable
- validated

Several sub objectives were distinguished.
1. Study of the short-wave energy dissipation mechanism in two layer systems and comparison of the dispersion relations belonging to the various schematizations in literature
2. Search for an efficient and reliable solving routine to determine the wave number out of the dispersion relation
3. Determination of a mud-induced energy dissipation term that can be used in SWAN, implementation of this term and testing of the model for a simple 1D case
4. Extension of the model with influence of mud on the propagation velocity of energy, testing of the implementation with simple propagation tests (1D/2D)
5. Calibration of the model by application on a practical case: Cassino Beach, Brazil

9.2 Conclusions

Concerning dispersion equations, it can be concluded from this study that:
- The schematization of De Wit (1995) covers the most relevant parameter domain: thin mud layers and shallow and non-shallow water.
- The DELFT dispersion equation, that has been derived in this thesis using the schematization of De Wit, is valid for thin mud layers and all water depths. The equation shows explicable behaviour and forms a sound description of the physics in the domain of validity.
- The DELFT dispersion equation reduces to the original expression of De Wit upon extra assumptions concerning the order of magnitude of the mud-adjusted wave number.
- Viscous two-layer models are suitable for implementation into practical applicable wave energy models to model the influence of fluid mud on progressive waves.

Concerning the solving routine it can be concluded that:

- An iteration procedure using a starting value determined with a function that depends on the relative water depth kH_{w0}, can be used to compute the wave number from the DELFT dispersion equation.
- The solving routine gives results for the wave number over the entire range of kH_{w0}, but occasional erroneous evolutions still occur.

Concerning the energy dissipation terms it can be concluded from this study that:
- The newly derived energy dissipation term is fully consistent with the DELFT dispersion equation.
- This energy dissipation term is valid for all relative water depths and reduces to Gade's expression for energy dissipation under shallow water conditions.
- Gade's expression for energy dissipation, and the Winterwerp *et al.* (2007) model that uses this expression, consistently overestimates the damping at intermediate and deep water. It's validity is limited for shallow water conditions.

Concerning the modification of the wave energy model SWAN, it can be concluded that:
- Implementation of the DELFT dispersion equation to compute the wave number and the newly derived energy dissipation term as extra sink term into SWAN, results in a model that is consistent and valid for all water depths. This consistency is tested with simple sanity checks, as shown in Figure 52.
- Issues of efficiency, consistency and physically sound representation of the influence of mud on other processes than damping, require the computation of the mud-adjusted wave number on a higher level in the Fortran code of SWAN than in the subroutine determining the energy dissipation term itself.

With respect to the influence of the mud on energy dissipation, it can be concluded that:
- The modified SWAN model represents the mud-induced dissipation phenomenon well. This is shown in the validation of the model on mono-chromatic waves and spectra of waves over a flat bottom with mud layers of constant thickness.
- The occasional erroneous evoluations in the iteration procedure lead to erroneous results for the wave properties in SWAN. Considerable overestimation or underestimation of the damping can occur, sometimes resulting in artificial energy generation. The latter has to be prevented at all cost. A simple yet effective measure is taken to avoid this deviation, so the SWAN-mud model is unconditionally stable, but not free of occasional inaccuracies.
- The presence of mud can cause both increase as decrease of the mean frequency, depending on the parameter settings. So not only the low frequency waves will be affected by the mud.

With respect to the influence of the mud on energy propagation, it can be concluded that:
- The modified SWAN model represents the (reversible) mud-induced shoaling phenomenon well, as shown in the validation of the model on mud layers of varying thickness.
- The influence of mud-induced shoaling on the significant wave height can be considerable, but is under circumstances of gradually changing bottom bathymetry probably less important than the influence of dissipation on the significant wave height.

- A modification of the SWAN-subroutine to compute the turning rate of energy in time (c_θ, the propagation speed of energy over the directions) is needed to account for mud-induced refraction.

Concerning the testing of the model by application on a practical case, it can be concluded that:

- the testing of the model on Cassino Beach is not discussed in this report and still has to be completed.

Considering the preceding conclusions, we come to following **general conclusion**:

An extension of SWAN is developed which enables modelling the dissipation of energy during the propagation of a wave field over fluid mud. The implemented dispersion equation and energy dissipation term are mutually consistent and both valid for shallow and non-shallow water. In the Fortran code of SWAN, the wave number is not computed in the subroutine determining the energy dissipation term itself, but on a higher level. In this way the influence of mud on other phenomena, like propagation of energy, is included in the model as well. At the same time, this considerably reduces the number of times the wave number has to be computated. The computation of the wave number itself may need some improvement. At this moment, the model is ready for judicious use by specialists.

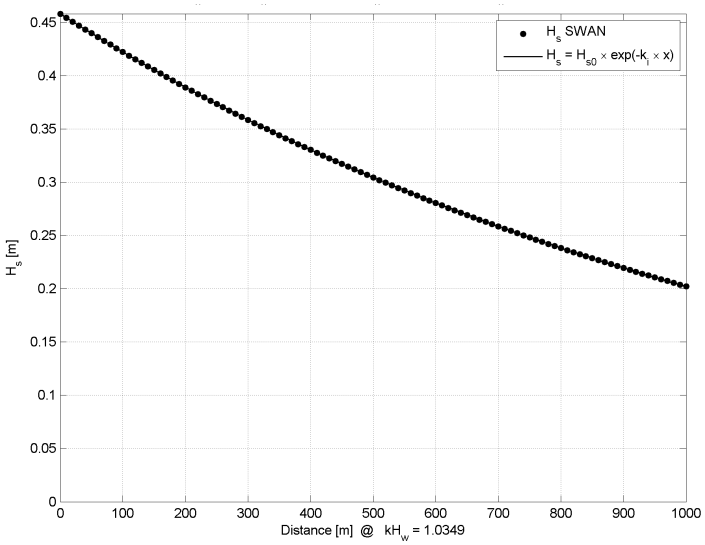

Figure 52

Comparison of the significant wave height H_s calculated with the newly derived energy dissipation term implemented in SWAN (dots) and directly with the analytical expression $H_s = H_{s0}*e^{-kix}$ (continuous line) for intermediate water depth ($kH_{w0} \approx 1$). This figure demonstrates the mutual consistency of the DELFT dispersion equation and the newly derived energy dissipation term

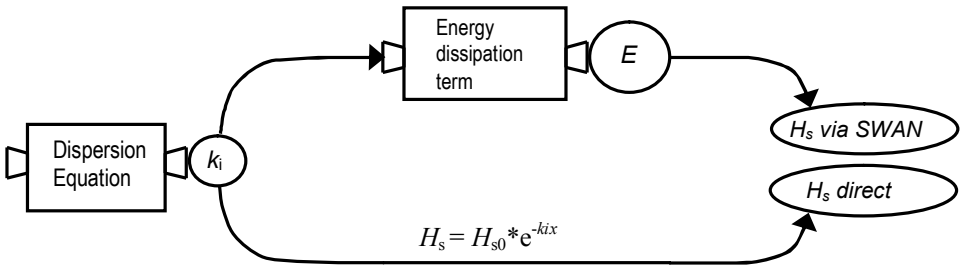

9.3 Recommendations

A number of recommendations for further development of the model is given below.

Suggestions for improvement of the solving routine are:

- To try another iteration method. The original motivation for employing the DZANLY method was an apparent better convergence to the proper solution starting from inaccurate initial approximations compared to a Newton method. This motivation is not relevant anymore when an approprioate starting value is applied. Applying another iteration method could make the model more simple.
- To check the formulated function for the starting value for various sets of parameters, especially with respect to the mud density ρ_m. The coefficients (a and c) of the present function (eq. 116 & 117) are predetermined values, determined by fitting this function by trial and error through the results of previous iterations for various parameter sets. But ρ_m was kept constant during this process. A varying ρ_m may yield a function describing the value of the coefficients a and c.
- To build in a procedure which automatically detects and corrects erroneous solutions for the wave number. Suggestions for an automatic correction procedure are:
  - to set the value of the imaginary wave number k_i to zero when a negative value is computed
  - to detect and correct the erroneous results of the iteration procedure by comparing the results to neighbouring frequencies or gridpoints
  - to compute the wave number with various procedures, resulting in a warning when two different results are given (disadvantage: time consumption)

  One correction procedure has already been implemented in the program. In this procedure, the correction takes place at the level of the dissipation term instead of the wave number. Negative and very low values of mud-induced damping are overruled by the normal bottom dissipation, when the first one is smaller than the latter. It is recommended to test this correction procedure more extensively.

Concerning propagation of energy in the SWAN-mud model, it is recommended to:

- Replace the formula that is currently used to compute the turning rate of energy in time (c_θ) and whose validity is limited to situations where the regular dispersion equation applies, with a more general applicable formala to account properly for mud-induced refraction

Concerning validation of the model, it is recommended to carry out at least the following additional tests:

- Damping at sand-mud transition. A gradually transition of the seabed from sand to fluid mud is a suitable configuration to test the procedure that has to overrule negative dissipation. At the same time it is possible to investigate the influence of the transition on the propagation of energy.
- Interaction between mud-induced dissipation and wave-wave interactions. It is expected that the wave-wave interaction changes because of changing wave lenghts. It is also expected that energy is transferred to the frequency where the mud-induced dissipation is the strongest. Depending on the length scale of the phenomena involved, the frequency of the highest dissipation can start to function as an energy leak. It would be

interesting to investigate the development of various spectral forms. Also comparison of the results with Kaihatu *et al.* (2007) could give more insight.

Concerning calibration of the model, recommendations are:

- To calibrate the model against Cassino Beach observations. This can be carried out in the same way as done by Rogers and Holland (in review) (data 2005) to make it possible to compare the results.
- To do a sensitivity analysis of the model to indicate the relative importance of accurate measurements of the various parameters. Sensitivity analysis like this can be helpful in the preparation of coming measurement campaign. It is suggested to start with conditions such as used by Rogers and Holland, to vary the constant mud layer thickness, and to run the model for a mud layer thickness changing over the profile. This recommendation is based on the suspection that the model is especially sensitive for changes in the mud layer thickness.

Finally it is recommended to set the default parameter values in SWAN in such a way that the model is employed with the consistent combination of dispersion relation and dissipation term that has been derived in this study. The various test configurations present in the code should be available for administrators and specialists only. This concerns the possibility to choose seperately the dispersion equation used to calculate the wave number (Gade, De Wit, DELFT), the energy dissipation term (off, Gade, newly derived term), and the activation of the influence of mud on the group velocity (on, off). These default settings would make it impossible for the user to disregard ignorantly the major contribution of this study to the development of SWAN-mud: the formulation and implementation of a consistent combination of dispersion equation and energy dissipation term.

References

Burden, R.L. and Faires, J.D., 2001. Numerical Analysis, seventh edition. Brooks/Cole, Pacific Grove, USA, 841 pp.

Cornelisse, J.M. and Verbeek, H., 1994. Modellering van erosie door golven, rapport 47, Waterloopkundig Laboratorium, Delft.

Dalrymple, R.A. and Liu, P.L., 1978. Waves over soft mud beds: a two-layer fluid mud model. Journal of Physical Oceanography, 8: 1121-1131.

De Wit, P.J., 1995. Liquefaction of cohesive sediments caused by waves, Delft University of Technology, Delft, 194 pp.

Fenton, J.D., 2006. A note on two approximations to the linear dispersion relation for surface gravity water waves, Universitat Karlsruhe, Karlsruhe, Germany, 2 pp.

Finlayson, B.A., Davis, J.F., Westerberg, A.W. and Yamashita, Y., 1997. Mathematics; Dimensional Analysis. In: R.H. Perry, D.W. Green and J.O. Maloney (Editors), Perry's Chemical Engineers' Handbook, Seventh Edition. McGraw-Hill, New York.

Gade, H.G., 1958. Effects of a nonrigid, impermeable bottom on plane surface waves in shallow water. Journal of Marine Research, 16(2): 61-82.

Guo, J., 2002. Simple and explicit solution of wave dispersion equation. Coastal Engineering, 45: 71-74.

Holthuijsen, L.H., 2007. Waves in oceanic and coastal waters. Cambridge University Press, Cambridge, 387 pp.

Kaihatu, J.M., Sheremet, A. and Holland, K.T., 2007. A model for the propagation of nonlinear surface waves over viscous muds. Coastal Engineering, 54(10): 752-764.

Kranenburg, C., 1998. Dichtheidsstromen, Handleiding college CTwa5302, Delft University of Technology, Delft.

Mei, C.C. and Liu, F.P.L., 1987. A Bingham- plastic model for a muddy seabed under long waves Journal of Geophysical Research, 92(C13): 14581 - 14594.

Ng, C.-O., 2000. Water waves over a muddy bed: a two-layer Stokes' boundary layer model. Coastal Engineering, 40(3): 221-242.

Paidoussis, M.P., 1998. Fluid-structure interactions: slender structures and axial flow, vol.1. Academic Press, London.

Rogers, E. and Holland, K.T., A study of dissipation of wind-waves by viscous mud at Cassino Beach, Brazil: prediction and inversion. Naval Research Laboratory (NRL), Oceanography Division.

Sheremet, A. and Stone, G.W., 2003. Observations of nearshore wave dissipation over muddy sea beds. Journal of Geophysical Research, 108(C11): 3357.

SWAN Team, 2007. Technical Documentation SWAN Cycle III version 40.51AB, Delft University of Technology, Delft.

Visual Numerics Inc., 1997. IMSL, Fortran subroutines for mathematical applications, Volume II.

Winterwerp, J.C., Graaff, R.F.d., Groeneweg, J. and Luijendijk, A.P., 2007. Modelling of wave damping at Guyana mud coast. Coastal Engineering, 54(3): 249-261.

List of symbols

The most important of the symbols used in this MSc-thesis are explained in the list below. When in a particular section the meaning of a symbol deviates from the definitions given below, the local meaning is described explicitely in the section concerned.

Roman letters in alphabetic order:

a	Amplitude of water surface displacement	[m]
b	Amplitude of interface displacement	[m]
c	Phase speed	[m / s]
c_g	Group velocity	[m / s]
c_θ	Turning rate in time of the wave energy over directions	[◦ / s]
E	Wave energy	[J / m^2]
g	Gravitational acceleration	[m / s^2]
h_m	Height of mud layer	[m]
H_{m0}	Equilibrium height of mud layer	[m]
h_{tot}	Height of total system	[m]
H_{tot0}	Equilibrium height of total system	[m]
h_w	Height of water layer	[m]
H_{w0}	Equilibrium height of water layer	[m]
i (I)	Imaginary unit	[-]
k	Wave number	[rad / m]
k_{nm}	Wave number acc. to regular dispersion relation	[rad / m]
L	Wave length	[m]
m	Coordinate along the wave crest	[-]
m	Auxiliary parameter, see eq. 20	[m^{-1}]
N	Wave action density	[J s / m^2]
p	Pressure	[N / m^2]
P	Amplitude of pressure variation	[N / m^2]
$rXi0a$	Complex ratio between ξ_0 and a	[-]
S_b	Sink term of bottom induced dissipation	[J / m^2 / s]
$S_{b,mud}$ $(S_{b,m})$	Sink term of mud-induced dissipation	[J / m^2 / s]
S_{bfr}	Sink term of dissipation by bottom friction	[J / m^2 / s]
S_{br}	Sink term of dissipation by wave breaking	[J / m^2 / s]
S_{nl}	Source & Sink term of nonlinear wave-wave interactions	[J / m^2 / s]
S_{tot}	Total source and sink term in wave energy balance	[J / m^2 / s]
S_{wc}	Sink term of energy dissipation by whitecapping	[J / m^2 / s]
S_{wind}	Source term of wave energy generation by wind	[J / m^2 / s]
t	Time	[s]
T	Wave period	[s]
u	Horizontal orbital velocity in x-direction	[m / s]
Ur	Ursell number	[-]
w	Vertical orbital velocity in z-direction	[m / s]
W	Work	[J / m^2]
(x,z)	Coordinates in horizontal and vertical direction	[-]

Greek letters in alphabetic order:

δ_{BL}	Viscous boundary layer thickness	[m]
ε	Relative density difference	[-]
ζ	Displacement of water surface	[m]
θ	Wave direction	[◦]
ν_w	Kinematic viscosity of water	[m^2 / s]
ν	Kinematic viscosity of mud	[m^2 / s]
ν_m	Kinematic viscosity of mud	[m^2 / s]
ξ	Displacement of interface	[m]
ξ_0	(complex) Amplitude of interface displacement	[m, rad]
ρ_w	Density of water	[kg / m^3]
ρ_m	Density of mud	[kg / m^3]
σ	Normal stress	[N / m^2]
σ	Relative (angular) frequency in a frame of reference moving with the current velocity	[rad / s]
τ	Shear stress	[N / m^2]
φ	Phase difference between surface and interface	[rad]
ω	Wave (angular) frequency (2π / T)	[rad / s]

Appendices

A Solving the ODE for *U2*(z) by hand

This appendix belongs to the derivation of the DELFT dispersion equation in chapter 3.

In equation (59), section 3.4, an ODE for *U2*(*z*) is given:

$$ODE\_U2 := \frac{I\,\mathbf{e}^{(I(k\,x - \omega\,t))}\,(-U2(z)\,\omega\,\rho 2 + E\,k)}{\rho 2} = \nu\left(\frac{d^2}{dz^2}\,U2(z)\right)\mathbf{e}^{(I(k\,x - \omega\,t))} \tag{A239}$$

The solution of this ODE in equation (60) was obtained via MAPLE. This step is elaborated here by hand.

The ODE can be written as:

$$-i\omega U_2(z) + \frac{ikE}{\rho_2} - \nu\frac{\partial^2 U_2(z)}{\partial z^2} = 0 \Rightarrow \frac{\partial^2 U_2(z)}{\partial z^2} + \frac{i\omega}{\nu}U_2(z) = \frac{ikE}{\nu\rho_2} \tag{A240}$$

A solution is assumed in the most general form of:

$$U_2(z) = A\exp(Xz) + F \tag{A241}$$

Substitution of the assumed solution in the ODE gives:

$$\left(X^2 + \frac{i\omega}{\nu}\right)A\exp(Xz) + \frac{i\omega}{\nu}F = \frac{ikE}{\nu\rho_2} \tag{A242}$$

This can only be true if:

$$F = \frac{\nu}{i\omega}\frac{ikE}{\nu\rho_2} = \frac{kE}{\omega\rho_2} \quad \text{en} \quad X^2 = -\frac{i\omega}{\nu} \tag{A243}$$

By using *i* in a practical way, this can be written as:

$$X^2 = (iY)^2 = -\frac{i\omega}{\nu} \Rightarrow Y^2 = \frac{(1+i)^2}{2}\frac{\omega}{\nu} \Rightarrow Y = \pm(1+i)\sqrt{\frac{\omega}{2\nu}} \tag{A244}$$

When we assign the name *Y* to the positive root we obtain for *U2*(*z*):

$$U_2(z) = A_3\exp(iYz) + A_4\exp(-iYz) + \frac{Ek}{\omega\rho_2} \tag{A245}$$

This linear combination of a positive and a negative power of *e* can be written as:

$$U_2(z) = B_3 \cosh(iYz) + B_4 \sinh(iYz) + \frac{Ek}{\omega\rho_2} \tag{A246}$$

where:

$$A_3 = \frac{B_3 + B_4}{2} \quad \text{en} \quad A_4 = \frac{B_3 - B_4}{2} \quad \Rightarrow \quad B_3 = A_3 + A_4 \quad B_4 = A_3 - A_4 \tag{A247}$$

Using ***sinh(ix) = i sin(x)*** and ***cosh(ix) = cos(x)***, $U2(z)$ can be written as:

$$U_2(z) = B_3 \cos(Yz) + iB_4 \sin(Yz) + \frac{Ek}{\omega\rho_2} \tag{A248}$$

Substituting:

$$B_3 = C_3 \ , \qquad iB_4 = C_4 \tag{A249}$$

and filling in again the complete expression for Y, $U2(z)$ reads:

$$U2(z) := \sin\left(\frac{\left(\frac{1}{2}+\frac{1}{2}I\right)\sqrt{2}\sqrt{\omega}\,z}{\sqrt{\nu}}\right) C4 + \cos\left(\frac{\left(\frac{1}{2}+\frac{1}{2}I\right)\sqrt{2}\sqrt{\omega}\,z}{\sqrt{\nu}}\right) C3 + \frac{E\,k}{\omega\,\rho 2} \tag{A250}$$

which is the solution given in equation (60), section 3.4.

B Comparison of the dispersion equations DELFT and DeWit

The dispersion equation DELFT has been derived in appendix A. De dispersion equation of De Wit is given in De Wit (1995). In this appendix the expressions are compared in an analytical way.

The DELFT dispersion equation is given by:

$$\begin{aligned} Disprel := & \left(\frac{\cosh(m\,Hm0)\,\rho 2\cosh(k\,Hw0)}{k} - \frac{\rho 1\sinh(k\,Hw0)\sinh(m\,Hm0)}{m} + \rho 1\sinh(k\,Hw0)\cosh(m\,Hm0)\,Hm0 \right)\omega^4 \\ & + (-2\,I\,k\,\rho 2\,\nu\cosh(m\,Hm0)^2\cosh(k\,Hw0) + 2\,I\,k\,\nu\,\rho 2\sinh(m\,Hm0)^2\cosh(k\,Hw0) + 2\,I\,k\,\rho 2\,\nu\cosh(m\,Hm0)\cosh(k\,Hw0))\,\omega^3 \\ & + \left(\frac{\rho 2\,g\,k\cosh(k\,Hw0)\sinh(m\,Hm0)}{m} - \rho 2\,g\,k\cosh(k\,Hw0)\cosh(m\,Hm0)\,Hm0 - \rho 2\,g\cosh(m\,Hm0)\sinh(k\,Hw0) \right)\omega^2 \\ & + (2\,I\,k^2\,\rho 2\,\nu\,g\sinh(k\,Hw0)\cosh(m\,Hm0)^2 - 2\,I\,k^2\,\rho 2\,\nu\,g\sinh(k\,Hw0)\sinh(m\,Hm0)^2 - 2\,I\,k^2\,\rho 2\,\nu\,g\sinh(k\,Hw0)\cosh(m\,Hm0))\,\omega \\ & + \frac{k^2\,g^2\sinh(k\,Hw0)\sinh(m\,Hm0)\,\rho 1}{m} - k^2\,g^2\sinh(k\,Hw0)\,\rho 1\cosh(m\,Hm0)\,Hm0 + k^2\,g^2\sinh(k\,Hw0)\cosh(m\,Hm0)\,Hm0\,\rho 2 \\ & - \frac{k^2\,g^2\sinh(k\,Hw0)\sinh(m\,Hm0)\,\rho 2}{m} = 0 \end{aligned} \tag{B251}$$

The dispersion equation of De Wit is given by:

$$DEWIT := \left(-1. + \frac{\left(1. - \frac{\rho 1}{\rho 2}\right) g\,k\left(k\,Hm0 - \frac{k\tanh(m\,Hm0)}{m}\right)}{\omega^2} \right)\left(\frac{g\,k\tanh(k\,Hw0)}{\omega^2} - 1. \right) - \frac{\rho 1\left(k\,Hm0 - \frac{k\tanh(m\,Hm0)}{m}\right)\left(\frac{g\,k}{\omega^2} - \tanh(k\,Hw0)\right)}{\rho 2} = 0 \tag{B252}$$

B.1 Rewriting De Wit

At first we expand the expression of De Wit to get an expression with separate terms:

$$\begin{aligned} DEWIT := & -\frac{1.\,g\,k\tanh(k\,Hw0)}{\omega^2} + 1. + \frac{1.\,g^2\,k^3\,Hm0\tanh(k\,Hw0)}{\omega^4} - \frac{1.\,g\,k^2\,Hm0}{\omega^2} \\ & - \frac{1.\,g^2\,k^3\tanh(m\,Hm0)\tanh(k\,Hw0)}{\omega^4\,m} + \frac{1.\,g\,k^2\tanh(m\,Hm0)}{\omega^2\,m} - \frac{g^2\,k^3\,\rho 1\,Hm0\tanh(k\,Hw0)}{\omega^4\,\rho 2} \end{aligned} \tag{B253}$$

$$+\frac{g^2\,k^3\,\rho1\tanh(m\,Hm0)\tanh(k\,Hw0)}{\omega^4\,\rho2\,m}+\frac{\rho1\,k\,Hm0\tanh(k\,Hw0)}{\rho2}-\frac{\rho1\,k\tanh(m\,Hm0)\tanh(k\,Hw0)}{\rho2\,m}=0$$

This expression shows that only even terms of ω are present in De Wit. To make it possible to compare the two dispersion equations, the expression above is multiplied with the factor $\boldsymbol{\omega^4\rho_2\cosh(mH_{m0})\cosh(kH_{w0})/k}$. (This does not have any consequences for the solution of the roots.) The expression that arises can be written as a polynomial for ω:

$$DEWITnew:=\left(\frac{1.\cosh(m\,Hm0)\,\rho2\cosh(k\,Hw0)}{k}+\rho1\sinh(k\,Hw0)\cosh(m\,Hm0)\,Hm0-\frac{1.\,\rho1\sinh(k\,Hw0)\sinh(m\,Hm0)}{m}\right)\omega^4 \tag{B254}$$

$$+\left(\frac{1.\,g\,\rho2\,k\cosh(k\,Hw0)\sinh(m\,Hm0)}{m}-1.\,g\,\rho2\cosh(m\,Hm0)\sinh(k\,Hw0)-1.\,g\,\rho2\,k\cosh(k\,Hw0)\cosh(m\,Hm0)\,Hm0\right)\omega^2$$

$$-\frac{1.\,k^2\,g^2\sinh(k\,Hw0)\sinh(m\,Hm0)\,\rho2}{m}+1.\,k^2\,g^2\sinh(k\,Hw0)\cosh(m\,Hm0)\,Hm0\,\rho2+\frac{k^2\,g^2\sinh(k\,Hw0)\sinh(m\,Hm0)\,\rho1}{m}$$

$$-1.\,k^2\,g^2\sinh(k\,Hw0)\cosh(m\,Hm0)\,Hm0\,\rho1=0$$

B.2 Investigating the difference

When we subtract the newly obtained expression for De Wit from the dispersion equation DELFT, only the odd ω-terms of DELFT remain.

$$+(-2\,I\,k\,\rho2\,\nu\cosh(m\,Hm0)^2\cosh(k\,Hw0)+2\,I\,k\,\nu\,\rho2\sinh(m\,Hm0)^2\cosh(k\,Hw0)+2\,I\,k\,\rho2\,\nu\cosh(m\,Hm0)\cosh(k\,Hw0))\,\omega^3 \tag{B255}$$

$$+(2\,I\,k^2\,\rho2\,\nu\,g\sinh(k\,Hw0)\cosh(m\,Hm0)^2-2\,I\,k^2\,\rho2\,\nu\,g\sinh(k\,Hw0)\sinh(m\,Hm0)^2-2\,I\,k^2\,\rho2\,\nu\,g\sinh(k\,Hw0)\cosh(m\,Hm0))\,\omega$$

The term for ω^3 can be rewritten as:

$$Om3t:=A\,(\cosh(m\,Hm0)+\sinh(m\,Hm0)^2-\cosh(m\,Hm0)^2) \tag{B256}$$

With

$$A:=2\,I\cosh(k\,Hw0)\,\omega^3\,k\,\rho2\,\nu \tag{B257}$$

The term for ω^1 can be rewritten as:

$$Om1t:=(\cosh(m\,Hm0)^2-\sinh(m\,Hm0)^2-\cosh(m\,Hm0))\,B \tag{B258}$$

With

$$B:=2\,I\sinh(k\,Hw0)\,\omega\,k^2\,g\,\rho2\,\nu \tag{B259}$$

The question is whether these terms can be neglected or counterbalance each other. If that is the case, the dispersion equation of De Wit and DELFT amount to the same.

First we look whether the parts within the brackets equal zero. We make use of

$$\cosh^2(x) - \sinh^2(x) = 1 \tag{B260}$$

to rewrite *Om3t* en *Om1t* as:

$$Om3t := A\,(\cosh(m\ Hm0) - 1) \tag{B261}$$

$$Om1t := B\,(1 - \cosh(m\ Hm0)) \tag{B262}$$

The parts within the brackets will only be zero when $mH_{m0} << 1$. Although the mud layer is small compared to the wave length, m can easily be equal to $(1\text{-}i)$ or larger. Therefore it is not justified to use a limit of $\cosh(mH_{m0})$ to neglect these terms.

Now we look to A and B. When we substitute the 'normal' dispersion relation into A, A becomes equal to B:

$$\omega^2 = gk\tanh(kH_{w0}) \tag{B263}$$

$$A := 2\ I\ \sinh(k\ Hw0)\ k^2\ \rho 2\ \nu\ g\ \omega \tag{B264}$$

By doing this, *Om3t* and *Om1t* counterbalance each other. In that case the dispersion equation DELFT reduces to the dispersion equation of De Wit.

It is questionable whether it is correct to substitute the normal dispersion equation into A. The higher the value of kH_{w0}, the more this substitution is justified. This is caused by the fact that the influence of the muddy bottom decreases with growing water depth. So at high water depths the difference between the mud-adjusted ω-k-relation and the unadjusted ω-k-relation becomes smaller. But for more shallow water, the relation between ω and k is more strongly affected by the presence of the mud. Therefore it can be expected that there will be a difference between DELFT and De Wit at lower values of kH_{w0}.

De DELFT dispersion equation is a more general formulation. Therefore this equation is the one that is numerically investigated and implemented in SWAN in this project.

C Reduction of the DELFT dispersion equation for a non-viscous mud layer

The dispersion equation derived in appendix A is reduced for the situation in which ν_m is zero, which represents the case of a non-viscous mud layer. This reduction will be used to calculate a starting value for the iterations with the Argand method. The reduction is necessary because calculations with the dispersion equation with the value of ν_m set to zero do not give results. This is imputed to divisions to zero that will arise when ν_m is set to zero. Therefore the DELFT dispersion equation is reduced to a real function belonging to the situation without damping by elimination of the terms related to damping.

C.1 Reduction

The terms connected to ω^1 and ω^3 are cancelled immediately, because of the multiplication with ν_m. What remaines of the dispersion relation is:

$$\left(\frac{\cosh(m\,Hm0)\,\rho2\,\cosh(k\,Hw0)}{k} - \frac{\rho1\,\sinh(k\,Hw0)\,\sinh(m\,Hm0)}{m} + \rho1\,\sinh(k\,Hw0)\,\cosh(m\,Hm0)\,Hm0 \right) \omega^4$$
$$+ \left(\frac{\rho2\,g\,k\,\cosh(k\,Hw0)\,\sinh(m\,Hm0)}{m} - \rho2\,g\,k\,\cosh(k\,Hw0)\,\cosh(m\,Hm0)\,Hm0 - \rho2\,g\,\cosh(m\,Hm0)\,\sinh(k\,Hw0) \right) \omega^2$$
$$+ \frac{k^2\,g^2\,\sinh(k\,Hw0)\,\sinh(m\,Hm0)\,\rho1}{m} + k^2\,g^2\,\sinh(k\,Hw0)\,\cosh(m\,Hm0)\,Hm0\,\rho2 - k^2\,g^2\,\sinh(k\,Hw0)\,\rho1\,\cosh(m\,Hm0)\,Hm0$$
$$- \frac{k^2\,g^2\,\sinh(k\,Hw0)\,\sinh(m\,Hm0)\,\rho2}{m} = 0 \qquad \text{(C265)}$$

To get some insight in the importance of the various terms in the remaining expression, the expression is divided by $\cosh(mH_{m0})$. This does not have any consequences for the zero crossing points of the equation. At first, the division is applied to the ω^4-term.

$$T4 := \frac{\rho2\,\cosh(k\,Hw0)}{k} - \frac{\rho1\,\sinh(k\,Hw0)\,\sinh(m\,Hm0)}{\cosh(m\,Hm0)\,m} + \rho1\,\sinh(k\,Hw0)\,Hm0 \qquad \text{(C266)}$$

In this term, like in the ω^2-term and ω^0-term term, we get some useful terms not affected by the limit and terms of which it is still not clear if they will contribute to the solution. The latter are the terms with a division by m. To determine their influence we have to investigate the limit of:

$$T42 := \frac{\sinh(m\,Hm0)}{\cosh(m\,Hm0)\,m} \qquad \text{(C267)}$$

Examining this equation it is expected that the limit will be zero when ν_m is zero, because m is expected to become infinite when ν_m becomes zero. But the fact that m is a complex number requires a closer investigation of the limit. This is done by substituting for m:

$$(1-I)\frac{\sqrt{\omega}}{\sqrt{2\nu}} = m = (1-I)\theta \tag{C268}$$

which gives:

$$\frac{\left(\frac{1}{2}+\frac{1}{2}I\right)\sinh((1-I)\,\theta\,Hm0)}{\cosh((1-I)\,\theta\,Hm0)\,\theta} \tag{C269}$$

This term can be expanded in four terms:

$$T42expanded := \frac{\sinh(\theta\,Hm0)\cos(\theta\,Hm0)}{2\,(\cosh(\theta\,Hm0)\cos(\theta\,Hm0) - I\sinh(\theta\,Hm0)\sin(\theta\,Hm0))\,\theta} \tag{C270}$$

$$+\frac{\frac{1}{2}I\sinh(\theta\,Hm0)\cos(\theta\,Hm0)}{(\cosh(\theta\,Hm0)\cos(\theta\,Hm0) - I\sinh(\theta\,Hm0)\sin(\theta\,Hm0))\,\theta}$$

$$-\frac{\frac{1}{2}I\cosh(\theta\,Hm0)\sin(\theta\,Hm0)}{(\cosh(\theta\,Hm0)\cos(\theta\,Hm0) - I\sinh(\theta\,Hm0)\sin(\theta\,Hm0))\,\theta}$$

$$+\frac{\cosh(\theta\,Hm0)\sin(\theta\,Hm0)}{2\,(\cosh(\theta\,Hm0)\cos(\theta\,Hm0) - I\sinh(\theta\,Hm0)\sin(\theta\,Hm0))\,\theta}$$

The expanded inverses of these four terms all look more or less the same. They are given below:

$$invT421 := \frac{2\,\theta\cosh(\theta\,Hm0)}{\sinh(\theta\,Hm0)} - \frac{2\,I\,\theta\sin(\theta\,Hm0)}{\cos(\theta\,Hm0)} \tag{C271}$$

$$invT422 := -\frac{2\,I\,\theta\cosh(\theta\,Hm0)}{\sinh(\theta\,Hm0)} - \frac{2\,\theta\sin(\theta\,Hm0)}{\cos(\theta\,Hm0)}$$

$$invT423 := \frac{2\,I\,\theta\cos(\theta\,Hm0)}{\sin(\theta\,Hm0)} + \frac{2\,\theta\sinh(\theta\,Hm0)}{\cosh(\theta\,Hm0)}$$

$$invT424 := \frac{2\,\theta\cos(\theta\,Hm0)}{\sin(\theta\,Hm0)} - \frac{2\,I\,\theta\sinh(\theta\,Hm0)}{\cosh(\theta\,Hm0)}$$

In all these inverses, a multiplication with θ is in the counter, which means that these inverses become infinite in the case $\nu_m = 0$ (θ = infinite). This gives enough justification to neglect all terms containing

$$\frac{\sinh(m\ Hm0)}{\cosh(m\ Hm0)\ m} \tag{C272}$$

for the case of $\nu_m = 0$.

Then the dispersion equation becomes:

$$Disprelnum0 := \left(\frac{\rho2 \cosh(k\ Hw0)}{k} + \rho1 \sinh(k\ Hw0)\ Hm0 \right) \omega^4 + (-\rho2\ g\ k \cosh(k\ Hw0)\ Hm0 - \rho2\ g \sinh(k\ Hw0))\ \omega^2 + k^2\ g^2 \sinh(k\ Hw0)\ Hm0\ \rho2 - k^2\ g^2 \sinh(k\ Hw0)\ \rho1\ Hm0 \tag{C273}$$

This expression can be used to find initial approximations for the Argand iteration.

C.2 Basic checks

For the situation without a mud layer, the solution still reduces to the normal dispersion relation.

For the situation where only a sublayer is present (H_{w0}=0)with $\nu_m = 0$, the equation reduces to:

$$DispRel\_nonviscsublayeronly := \frac{\rho2\ \omega^4}{k} - \rho2\ g\ k\ Hm0\ \omega^2 \tag{C274}$$

This is the equation for the shallow water wave number k.

$$g\ k^2\ Hm0 = \omega^2 \tag{C275}$$

This is consistent with a basic assumption of this dispersion equation, that assumes the sublayer to be thin compared to the wave length.

D Determination of real and imaginary part of the pressure amplitude

This apppendix belongs to the derivation of the energy dissipation term in chapter 6. To get insight in the cause of the differences between the shallow water approximation and the more extended approach, analytical expressions for the real and imaginary part of the pressure amplitude are derived. This derivation is presented here.

The complex expression for the amplitude of the pressure fluctuation $P_1(diepte)$ is:

$$P1(diepte) := \rho 1\ a\ g \cosh(k\ diepte) - \frac{\rho 1\ a\ \omega^2 \sinh(k\ diepte)}{k} \tag{D276}$$

The real part of the amplitude of the pressure can be determined by substitution of $k = k_r+i*k_i$:

$$P1(diepte) := \rho 1\ a\ g \cosh(diepte(kr + I\ ki)) - \frac{\rho 1\ a\ \omega^2 \sinh(diepte(kr + I\ ki))}{k} \tag{D277}$$

The first term becomes:

$$P1\_1eterm := \rho 1\ a\ g \cosh(diepte\,kr) \cos(diepte\,ki) + I\ \rho 1\ a\ g \sinh(diepte\,kr) \sin(diepte\,ki) \tag{D278}$$

The second term multiplied by k becomes:

$$kP1\_2eterm := -\rho 1\ a\ \omega^2 \sinh(diepte\,kr) \cos(diepte\,ki) - I\ \rho 1\ a\ \omega^2 \cosh(diepte\,kr) \sin(diepte\,ki) \tag{D279}$$

When this is divided again by k, where

$$k = \mathrm{mod}\,k * e^{i \arg k} \tag{D280}$$

$$\mathrm{mod}(k) = \sqrt{k_r^2 + k_i^2} \tag{D281}$$

$$\arg(k) = \arctan\frac{k_i}{k_r} \tag{D282}$$

part a and b of the second term become

$$P1\_term2a := -\frac{\rho 1\ a\ \omega^2 \sinh(diepte\,kr) \cos(diepte\,ki)\ \mathbf{e}^{(-I\ ARGk)}}{MODk} \tag{D283}$$

$$P1\_term2b := -\frac{\rho 1\ a\ \omega^2 \cosh(diepte\,kr) \sin(diepte\,ki)\ \mathbf{e}^{(0.5\ I\ \pi)}\ \mathbf{e}^{(-I\ ARGk)}}{MODk} \tag{D284}$$

Both part *a* and *b* can be splitted up in a real and an imaginary part:

$$Real\_P1\_2a := -\frac{\rho 1\ a\ \omega^2 \sinh(diepte\,kr)\cos(diepte\,ki)\cos(ARGk)}{MODk} \quad \text{(D285)}$$

$$Imag\_P1\_2a := \frac{I\,\rho 1\ a\ \omega^2 \sinh(diepte\,kr)\cos(diepte\,ki)\sin(ARGk)}{MODk} \quad \text{(D286)}$$

$$Real\_P1\_2b := -\frac{\rho 1\ a\ \omega^2 \cosh(diepte\,kr)\sin(diepte\,ki)\cos(-0.5\,\pi + ARGk)}{MODk} \quad \text{(D287)}$$

$$Imag\_P1\_2b := \frac{I\,\rho 1\ a\ \omega^2 \cosh(diepte\,kr)\sin(diepte\,ki)\sin(-0.5\,\pi + ARGk)}{MODk} \quad \text{(D288)}$$

The real and imaginary parts of the pressure amplitude $P_1(diepte)$ consist of the summation of the various real and imaginary parts respectively:

$$Real\_P1(diepte) := \rho 1\ a\ g\cosh(diepte\,kr)\cos(diepte\,ki) - \frac{\rho 1\ a\ \omega^2 \sinh(diepte\,kr)\cos(diepte\,ki)\cos(ARGk)}{MODk} - \frac{\rho 1\ a\ \omega^2 \cosh(diepte\,kr)\sin(diepte\,ki)\cos(-0.5\,\pi + ARGk)}{MODk} \quad \text{(D289)}$$

$$Imag\_P1(diepte) := I\,\rho 1\ a\ g\sinh(diepte\,kr)\sin(diepte\,ki) + \frac{I\,\rho 1\ a\ \omega^2 \sinh(diepte\,kr)\cos(diepte\,ki)\sin(ARGk)}{MODk} + \frac{I\,\rho 1\ a\ \omega^2 \cosh(diepte\,kr)\sin(diepte\,ki)\sin(-0.5\,\pi + ARGk)}{MODk} \quad \text{(D290)}$$